Development of new membrane-tethered toxins as genetic tools for *in vitro* and *in vivo* silencing of ion channels

Inaugural-Dissertation to obtain the academic degree
Doctor rerum naturalium (Dr. rer. nat.)

Submitted to the Department of Biology, Chemistry and Pharmacy
of Freie Universität Berlin

by

Sebastian Auer

from Munich

February, 2010

This work was carried out in the period of Oct. 2006 to Feb. 2010 under the supervision of Dr. Inés Ibañez-Tallon and Prof. Dr. Fritz Rathjen at the Max-Delbrück Center for Molecular Medicine (MDC) in Berlin-Buch.

1st Reviewer: <u>Prof. Dr. Fritz Rathjen</u>

2nd Reviewer: <u>Prof. Dr. Constance Scharff</u>

Date of defence: <u>04.05.2010</u>

Scientific Acknowledgments

I would like to thank my group leader Dr. Inés Ibañez-Tallon for giving me the opportunity to work on this project, for her advices, support and supervision throughout the years.

I also thank the people I have been working with: Silke Frahm, Leiron Ferrarese, Mandë Holford, Branka Kampfrath, Daniela Kurzhals, Martin Laqua, Beate Liehl, Julio Santos-Torres, Marta Slimak, Annika Stürzebecher and Susanne Wojtke. You made this lab a nice place to work in.

Furthermore, I would like to thank colleagues of other labs for helpful discussions, technical support and providing lab resources: René Jüttner (Group Prof. Rathjen, MDC), Prof. Jochen Meier, Caro Bernert and Sabrina Eichler (Group Prof. Meier, MDC), Susann Winter (Group Dr. Lipp, MDC), Hagen Wende (Group Prof. C. Birchmeier, MDC), Carsten Pfeffer (Group Prof. Jentsch, MDC) and Jana Petri & Iris Adam (Group Prof. Scharff, FU Berlin).

Special thanks go to René Jüttner (Developmental Neurobiology group, MDC), Julio Santos-Torres, Martin Laqua and Inés Ibañez-Tallon for carrying out the electrophysiological recordings in HEK cells and neurons (R. J., J. S.-T.), and in *Xenopus laevis* oocytes (M. L., I. I.-T.) in this work. Their acquired data contributed greatly to this dissertation.

Finally, I would like to thank my university supervisor Prof. Dr. Fritz Rathjen for the official supervision of my PhD project.

Personal Acknowledgments

Besonders danke ich meinen Eltern und meiner Großmutter dafür, dass sie mir durch ihre persönliche und auch finanzielle Unterstützung zuerst das Studium und dann diese Doktorarbeit ermöglicht haben.

Danke auch an meinen Bruder Max für die schönen Telefonate, Treffen und gemeinsamen Ausflüge.

Ich danke den vielen lieben PhD Studenten und TA's am MDC, allen voran Sebastian Günther (nebst Rina), den Jungs und Mädels der AG Lipp, Caro Bernert (nebst Basti), Katja Welsch und allen die ich hier nicht aufzählen kann für die vielen schönen Momente während und auch außerhalb der Arbeitszeit.

Der größte Dank geht an Karen für fünf wunderbare Jahre, für ihre Unterstützung während der Doktorarbeit und ihr Verständnis für so manch ausgefallenes Hobby meinerseits.

Contents

1. Introduction

1.1 Venom peptide toxins in research and therapy

Complex processes such as brain function and neuronal activity rely on ion channels and receptors as the essential framework for every neuronal circuit. Thus, extensive knowledge about the function, structure and precision of ion channels, receptors and modulators is crucial for understanding how the nervous system works under physiological and pathophysiological conditions. Recent reviews describe the increasing interest in peptide venom toxins from predatory organisms such as scorpions, snakes and marine cone snails for specific inhibition of ion channels and receptors in basic research and to develop new drug therapies[1-6]. The high degree of specificity with which venom peptide toxins bind to voltage-gated sodium (VGSC or Na_v), calcium (VGCC or Ca_v), and potassium (K_v) ion channels, and ligand-gated receptors such as nicotinic acetylcholine receptors (nAChRs), N-methyl-D-aspartate (NMDA) and G-protein coupled receptors (GPCRs), make them ideal tools for deciphering the connections between cell types, and for reversibly manipulating the activity of selective cell subtypes.

Purified or synthesized venom toxins have been used extensively during the last decades in research to investigate the structure and function of specific ion channels (ligand or voltage-gated) and cell-surface receptors[1,7-9]. Very well-known examples are tetrodotoxin (TTX) from tetraodon pufferfish[10] and saxitoxin (STX) from shellfish[11] for blocking Na_v channels. Furthermore, α-bungarotoxin and other α-neurotoxins from *Elapidae* and *Hydrophidae* snakes were used to provide the first identification of nAChRs[12-14]. Similarly, α- and β-neurotoxins from scorpions have been used to modify Na_v channels by delaying inactivation (α), or shifting the membrane potential dependence (β)[15,16]. Specific therapeutic and clinical areas in which peptide toxins have already demonstrated their potential, include the treatment of chronic pain in human by ω-conotoxin MVIIA (commerzialized as Prialt®)[17-19], as well as in the study of Alzheimer's disease (candoxin)[20], and myasthenic autoimmune response (α-Bgtx)[21,22]. Furthermore, five other peptide toxins are currently tested in clinical trials phase I, and three in preclinical phase, most of them for pain therapy, but also for treatment of epilepsy, myocardial infarction and for neuroprotection[23].

1.2   Conotoxins: Peptide toxins derived from cone snails

Conotoxins originate from the venom of fish-hunting cone snails, which mostly can be found in coral reefs of tropical marine waters. These peptide toxins are small (~10–50 amino acids), disulfide rich and compact molecules[24]. Every *Conus* species studied so far has a repertoire of 100–200 different venom peptide components, with basically no molecular overlap between venoms of different species. Thus, the 500–700 living *Conus* species have evolved 50,000 to 140,000 different conopeptides[1,23]. The development of this huge diversity is driven by evolutionary processes in adaption to various pharmacological sites in a given targeted animal, and to the diversity of animals within the cone snail's niche[23].

Conopeptide encoding mRNAs consist of a single open reading frame, which is translated into a prepropeptide. The peptide precursors of the same gene superfamily share a highly conserved N-terminal signal sequence. In contrast, the mature peptide sequence is hypermutable, with the exception of conserved Cys residues[23]. Thus, similar to antibodies, conotoxin precursors show a juxtaposition of highly conserved and hypervariable regions. After secretion into the cone snail duct, conotoxin precursors are cleaved by proteases, thereby generating active toxins which are often subjected to posttranslational modifications[25]. The mature peptides in each gene superfamily generally have a typical arrangement of cysteine residues, which form a characteristic, complex disulfide backbone that allows the folding into stabilized structures (**Fig.1**).

Typically, cone snails target a given circuit at several different points by using combinations of conopeptides that function together to elicit a physiological response (e.g. paralysis). These combinations of conotoxins maximize the success rate of prey hunting or defense and have been called *cabals*[26]. For example, the *motor cabal*, which inhibits muscle contraction, includes ω-conotoxins, which target presynaptic Ca_v channels and thereby inhibit neurotransmitter release, μ-conotoxins that suppress the muscle action potential by blocking Na_v channels, and α-conotoxins that bind to postsynaptic nAChRs to prevent depolarization at the motor end plate[23]. Several classes of conotoxins can be distinguished by their target channels or receptors, like nAChR (α-conotoxins), Na_v channels (μ-, μO- and δ-conotoxins), Ca_v channels (ω-conotoxins), the N-methyl-D-aspartate (NMDA) receptor (conantokins), noradrenaline transporters (κ-conotoxins), and neurotensin receptors (contulakins)[1,27]. Given their impressive number and their specificity for very diverse ion channels and receptors,

conotoxins are suitable tools to discriminate between closely related subtypes of channels and receptors, of which many cannot be targeted with conventional antagonists. The conotoxins which were used in this work are described in the following.

1.2.1 α-conotoxin GID

α-conotoxin GID is a natural peptide toxin, which was isolated from the venom of the marine conesnail *Conus geographus* and is composed of 19 amino acids[28] (**Fig.1**). Important features of its sequence include a four-residue extended N-terminal tail upstream of the first cysteine, two post-translationally modified residues, γ-carboxyglutamic acid (γ) and hydroxyproline (O), and it lacks an amidated C terminus typical of most α-conotoxins. The three-dimensional structure of GID shows the classic two-loop structural motif of α-conotoxins, but the N-terminal tail is disordered in solution[29]. GID selectively inhibits the α7, α3β2 and α4β2 subtypes of the neuronal nAChR with IC_{50} values of 4.5, 3.1 and 152 nm, respectively[28]. The activity on the α3β4, α4β4 and muscle nAChRs was reported to be at least 1000-fold less[28]. Deletion of the N-terminal four residues [Δ1–4]GID has been shown to significantly decrease activity on the α4β2 receptor, while causing no change in potency on α7 and α3β2 receptors[28].

1.2.2 ω-conotoxin MVIIA

ω-conotoxin MVIIA is a highly selective and potent blocker of the voltage-gated calcium channel $Ca_v2.2$ (N-type). MVIIA was isolated from the conesnail *Conus magus*, is composed of 25 amino acids, and contains six cystein residues that form three dilsufide bridges[30] (**Fig.1**). MVIIA is a pore-blocker, i.e. it blocks the channel conductivity by binding to the outer vestibule of the pore region at domain III (S5-S6) of $Ca_v2.2$, with Tyr13 being essential for this interaction[31]. The binding affinity is <10 nM for $Ca_v2.2$ (N-type) (EC_{50} ~ 1 nM), compared to >1 mM for the Ca_v1 (L-type)[30,32]. The molecular structure of MVIIA is composed of a short triple-stranded antiparallel beta-sheet, which shows high similarity with the also $Ca_v2.2$ specific ω-conotoxin GVIA[33]. In fish, which is the natural prey for conesnails, MVIIA induces paralysis by blocking $Ca_v2.2$ in motor neurons. Importantly, MVIIA was developed to an analgesic drug (Prialt®) which is used in pain therapy by intrathecal application via minipumps[17-19], making it the first conotoxin used in therapy.

1.2.3 ω-conotoxin MVIIC

ω-Conotoxin MVIIC was reported to block the voltage-gated calcium channels $Ca_v2.1$ (P/Q-type, low affinity) and $Ca_v2.2$ (N-type, high affinity)[34]. MVIIC was isolated from *Conus magus* and consists of 26 amino acids with three disulfide bridges (**Fig.1**). Like MVIIA, it acts by binding to the pore of the channels. The solution structure of MVIIC was determined by NMR and showed a secondary structure consisting of an anti-parallel, triple-stranded beta-sheet with four turns[35].

1.3   Agatoxins: natural spider toxins

The venom that is used by the funnel web spider *Agelenopsis aperta* for prey hunting, is a highly concentrated cocktail of acylpolyamines and peptide toxins, which can be distinguished in α-, μ-, and ω-agatoxins, similar to the nomenclature of conotoxins[36]. α-agatoxins are use dependent, open channel blockers of postsynaptic glutamate receptor channels. Their action is synergized by the μ-agatoxins, which increase neurotransmitter release by modification of neuronal Na_v channel gating, causing the channels to open at the normal resting potential. These two toxin classes produce fast paralysis in insect prey. Furthermore, several ω-agatoxins induce long-lasting paralysis by acting in concert to block presynaptic Ca_v channels in nerve terminals[36]. In research, ω-agatoxins have been broadly used for the functional classification of mammalian Ca_v channel subtypes[32,37,38]. The agatoxins used in this work are described in the following.

1.3.1 ω-Agatoxin IIIA

ω-Agatoxin IIIA has a broad spectrum of activity, blocking all known neuronal high threshold calcium channels, including L- (Ca_v1), N- ($Ca_v2.2$), P/Q- ($Ca_v2.1$), and R-type ($Ca_v2.3$) channels with a K_d of ~1 nM[36]. In contrast to AgaIVA, the block induced by AgaIIIA is only partial[37,39]. Despite this partial block, the toxin completely prevents binding and block of Ca_v channels by ω-conotoxins GVIA, MVIIA, and MVIIC[36]. AgaIIIA is composed of 76 amino acids with 10 Cys residues, thus forming five dilsufide bridges (**Fig.1**).

1.3.2 ω-Agatoxin IVA

ω-Agatoxin IVA is a highly potent and specific blocker of the voltage-gated calcium channel $Ca_v2.1$ (P/Q-type) with an $IC_{50} < 1\text{-}3$ nM[39]. For P-type channels, a K_d of 1-3 nM[39] and for Q-type channels, a $K_d\sim100\text{-}200$ nM was reported[40]. AgaIVA is composed of 48 amino acids with four internal disulfide bonds[39] (**Fig.1**). The structure of AgaIVA shows a small three-stranded, anti-parallel ß-sheet, four loops, a solvent inaccessible core and disordered carboxy- and amino-termini[38]. AgaIVA blocks $Ca_v2.1$ via modification of voltage-dependent gating by shifting the activation voltage of the channel to positive potentials that are normally not reached during physiological activity of the cell[41]. The binding site has been located to the extracellular loop between transmembrane segments 3 and 4 in domain IV of $Ca_v2.1$ in direct proximity to the S4 transmembrane voltage sensor[42].

Figure 1. Overview of natural peptide toxins used in this work.

Source, channel specificity, sequence, and characteristic disulfide backbones of natural toxins used for the generation of new recombinant t-toxins. nAChR: nicotinic acetylcholine receptor. VGCC: voltage-gated calcium channel. GID: α-conotoxin GID. MVIIA: ω-conotoxin MVIIA. MVIIC: ω-conotoxin MVIIC. AgaIVA: Agatoxin IVA. AgaIIIA: Agatoxin IIIA.

1.4   Lentiviral vectors for gene delivery

HIV-1 lentiviral vectors (LV) have been extensively used as gene delivery tools because of their ability to infect dividing and non-dividing cells (e.g. neurons) with stable integration of the gene of interest into the host genome, without inducing immunogenic responses, unlike adenoviral vectors (Ad). Furthermore, generation and purification of lentiviral particles is relatively easy and they are able to incorporate larger inserts (~8 kb), compared to adeno-associated virus (AAV, ~3-4 kb). For the generation of pseudo-lentiviral particles as vectors, the accessory genes of HIV-1, which encode crucial virulence factors and are essential for HIV pathogenicity have been eliminated[43]. Furthermore, cis-acting elements in the native HIV-1 genome (non-coding sequence elements required for vector RNA synthesis, packaging, reverse transcription, and integration) have been separated from the trans-elements (encoding structural, enzymatic, and accessory proteins), by subcloning to different plasmids[43,44] (**Fig.2**). Division of these components to four different plasmids in the third generation of LV vectors minimizes the likelihood of generating replication competent lentivirus (RCL's), as this would require at least three recombination events. As an additional measure of safety, replication defective, self-inactivating (SIN) vectors have been generated, which use a CMV promoter with a deletion in the promoter/enhancer region in the 3' LTR, that is transposed onto the 5' LTR following the transduction of a target cell and thus prevents expression of full-length vector RNA in infected cells[43,45]. Also the efficiency of LV production has been enhanced by insertion of WPRE (woodchuck hepatitis virus posttranscriptional regulatory element) at the 3'end of the insert (Appendix: **Fig.43**), which increases the transgene expression more than fivefold by stabilizing the mRNA[46]. In contrast to wildtype HIV-1, most pseudo-lentiviral particles today use the vesicular stomatitis virus G protein (VSV-G) as envelope instead of the parental HIV-1 envelope[44,47]. The VSV-G envelope introduces three novel features to lentivirus vector particles: (I) it broadens the vector tropism to diverse tissue and cell types of various species *in vitro* and *in vivo*, (II) it stabilizes the vector particles during centrifugation, thereby allowing vector concentration by ultracentrifugation and (III) it changes lentiviral vector entry to an endocytic pathway, which reduces the requirements for viral accessory proteins for full infectivity[45,48].
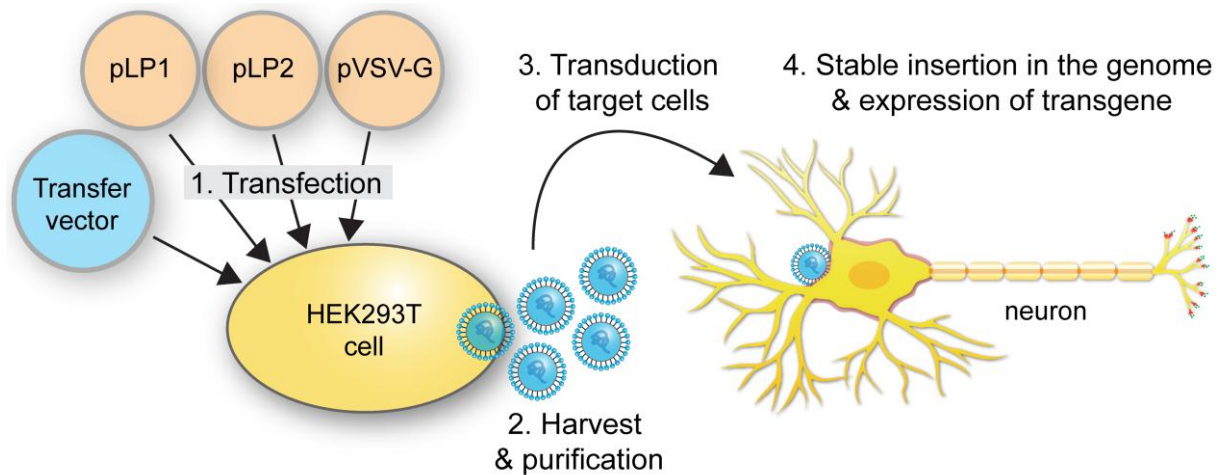
Figure 2. Schematic representation of lentivirus production.

Pseudo-lentiviral particles are generated by co-transfection of transfer vector (contains gene of interest), packaging plasmids pLP1 (*Gag* and *Pol*: encode the structural and enzymatic proteins required to form functional vector particles), pLP2 (*Rev*: encodes the Rev protein required for nucleocytoplasmic transport of full-length vector RNA) and pVSV-G (*VSV-G*: encodes for vesicular stomatitis virus G protein envelope) into HEK293T cells. Lentivirus is harvested ~48 h after transfection, purified and concentrated by ultracentrifugation, and stored at -80 °C. Target cells can be transduced by direct addition of LV suspension to the culture medium (*in vitro*), or by injection into the desired tissue area (*in vivo*). Upon transduction, the gene of interest is stably integrated into the host genome and subsequently expressed, depending on the chosen promoter and vector design.

In this work, I used three different lentiviral vectors allowing constitutive, inducible or Cre recombinase-dependent expression of the transgene. The expression in all three vectors, namely the constitutive lentiviral vector pFUGW[49], inducible pLVUT-tTR-KRAB[50] and the newly generated Cre-dependent vector pFU-cMVIIA-PE is driven by a human Ubiquitin C promoter. pLVUT-tTR-KRAB was used for the doxycycline (DOX) inducible expression of the t-toxin MVIIA-PE, which is followed in the construct by an IRES sequence and a tetR-KRAB fusion (**Fig.30**). tTR-KRAB, consists of the Krüppel-associated box (KRAB) domain that is found in many vertebrate transcriptional regulators, like zinc-finger proteins, and the tetracycline repressor (tetR) of *Escherichia coli*. In the absence of DOX, tTR-KRAB protein binds to *tetO* DNA sequences upstream and downstream of the transgene and suppresses the expression of t-toxin as well as tTR-KRAB by epigenetic silencing over a region of 2-3 kb through induction of heterochromatin formation[50]. However, in the presence of DOX, tTR-KRAB is released from *tetO*, thus allowing expression.

Furthermore, as it would be of great advantage to selectively express t-toxins only in a specific subset of cells, we aimed to apply the Cre/loxP recombination system. Therefore, we generated the Cre-dependent lentiviral vector pFU-cMVIIA-PE, which allows expression of MVIIA-PE only in Cre recombinase positive cells. The enzyme Cre recombinase was originally isolated from the P1 bacteriophage and belongs to the integrase family of site-specific recombinases. It catalyzes the recombination between two of its DNA recognition sites, called loxP[51,52]. These loxP sequences consist of a 34 bp consensus sequence, with a core spacer sequence of 8 bp and two 13 bp palindromic flanking sequences. Cre recombinase is able to bind to loxP, then a tetramer is formed, thus bringing two loxP sites together and subsequently the recombination occurs within the spacer area of the loxP sites[51,52]. Thus, the sequence in between the loxP sites gets excised. Since the first isolation and characterization of the Cre/loxP recombination system, this approach has been used to generate hundreds of different transgenic mouse lines, each one expressing Cre recombinase in a different subset of neurons[53]. This renders Cre-selective expression a powerful tool to study cell functions in defined cell types.

In our Cre-dependent lentiviral vector pFU-cMVIIA-PE, the expression of t-toxin is regulated by a loxP cassette flanking DsRed (Miething C., Duyster J., in preparation), which was subcloned in front of the t-toxin (**Fig.35**). In conditions without Cre-recombinase, only DsRed is expressed and generation of functional t-toxin is inhibited by an introduced frameshift in the DNA reading frame after DsRed, which generates several translational stop codons throughout the t-toxin sequence. Thus, the expression of functional t-toxin is possible only after successful excision of the *lox*P cassette by Cre-recombinase.

1.5   Ion channels used for selective inhibition by t-toxins

1.5.1   Nicotinic acetylcholine receptors

Nicotinic acetylcholine receptors (nAChRs) belong to the superfamily of ligand-gated ion channels that includes $GABA_A$-, glycine-, and $5\text{-}HT_3$ serotonin receptors. A wide variety of nAChR subtypes arise from combinations of different subunits, leading to a range of different functional and pharmacological properties. Neuronal nAChRs are assembled from five subunits, which are composed of four transmembrane domains each, and form a central, ion conducting pore[54,55] (**Fig.3**). 12 different types of nAChR subunits have been reported so far:

α2-α10 and β2-β4[54,56,57]. When expressed heterologously, α7, α8 and α9 can form homopentamers. In contrast, the α2-α6 and α 10 neuronal subunits form functional complexes only when they are co-expressed with β-subunits or with other α-subunits. α7 is the only homomeric subunit, which is widely distributed in the mammalian brain[56,58].

nAChRs are cation-selective, ligand-gated ion channels and show three main functional states in response to agonists: closed at rest, open pore, and closed desensitized[59]. Brief exposure to high concentrations of the neurotransmitter acetylcholine (ACh), causes an allosteric change in the subunit structure, which results in opening of the water-filled, cation-selective pore[60] (**Fig.3**). After a couple of milliseconds, the receptor closes to a non-conducting state. Antagonist ligands including neurotoxins stabilize the resting state of the channel, while agonist molecules trap the receptor in its open state[61]. For example, prolonged exposure to low concentrations of nicotine, as obtained from tobacco use, produces significant desensitization, which stabilizes the receptor in a closed state that is unresponsive to agonist[62].
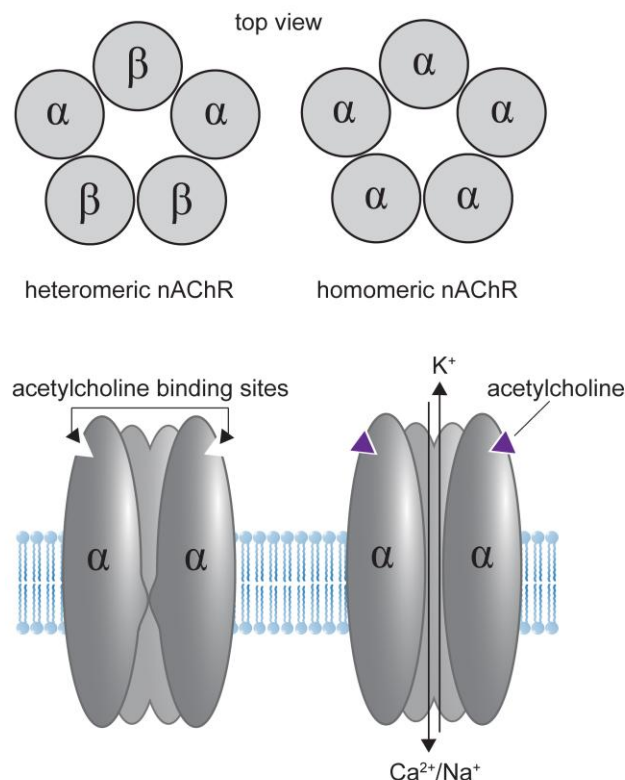
Figure 3. Composition and gating of neuronal nicotinic acetylcholine receptors (nAChRs).

nAChRs consist of five transmembrane subunits with the stechiometry 2α, 3β (heteromeric) or only α subunits (homomeric). Agonist binding (acetylcholine) occurs between an α subunit and the adjacent subunit, and induces conformational changes that allow opening of the cation-selective pore. (based on Paterson and Nordberg, 2000)

The diversity of nAChR subtypes and their somato-dendritic, axonal, presynaptic, or postsynaptic localization contribute to the various functions of these receptors in the central nervous system (CNS). Presynaptic nicotinic receptors enhance neurotransmitter release, and postsynaptic or nonsynaptic nAChRs mediate excitation as well as activity-dependent modulation of circuits and intracellular enzymatic processes. By modulating activity-dependent events, nAChRs participate in synaptic plasticity, which is important for attention, learning and memory, and development[59,63]. Decline, disruption, or alterations of nAChR mediated effects have been connected to various dysfunctions, such as schizophrenia, epilepsy, autism, Alzheimer's disease (AD), and addiction[59,64-66].

The $\alpha 7$ receptor is the most abundant nAChR in the brain besides the $\alpha 2 \beta 4$ receptor and has been shown to be localized at pre-, post-, and perisynaptic sites[56,67]. Dependent on their localization, $\alpha 7$ receptors modulate NT release, generate excitatory responses or induce downstream signaling pathways, respectively[56,67]. Interestingly, the $\alpha 7$ nAChR has the highest relative calcium permeability of all nAChRs, and its activation can induce presynaptic NT release even without contribution from voltage-gated calcium channels (VGCCs)[68,69]. $\alpha 7$ nAChRs can be specifically inhibited by α-bungarotoxin and methyllycaconitine (MLA)[69-71].

1.5.2 Voltage-gated calcium channels

Voltage-gated calcium channels (VGCC, Ca_v) play a key role in coupling changes in membrane potential to local calcium influx that initiates many different physiological effects, like neurotransmission, contraction, secretion, and gene expression[72]. Ten different members of the voltage-gated calcium channel family, each one with distinct roles in cellular signal transduction, have been characterized in mammals (**Table 1**). They are classified as members of a gene superfamily of transmembrane ion channel proteins that includes voltage-gated potassium (K_v) and sodium channels (Na_v)[73]. VGCCs are complex proteins composed of four distinct subunits that are encoded by multiple genes, the α_1 subunit and the auxiliary $\alpha_2\delta$, β and γ subunits[72] (**Fig.4**). The α_1 subunit is the largest subunit (190-250 kDa) and is essential for major ion channel functions, such as calcium permeation, voltage sensing and ion selectivity and gating. Furthermore, the α_1 subunit contains most of the known binding and interaction sites for channel regulation by toxins, drugs or second messengers[72,74]. Structurally, α_1 is organized in four homologous domains (I-IV), which consist of six transmembrane segments (S1-S6) each. The S4 segment serves as voltage sensor, while the

pore loop between transmembrane segments S5 and S6 in each domain determines ion conductance and selectivity[72,75]. An intracellular β subunit and a transmembrane, disulfide-linked $\alpha_2\delta$ subunit complex are components of most types of calcium channels. An additional γ subunit has also been found in skeletal muscle calcium channels. Although these auxiliary subunits modulate the trafficking and biophysical properties of the channel[76], the pharmacological and electrophysiological characteristics of calcium channels are primarily determined by the α_1 subunits[77]. The division of calcium channels into families is phylogenetically ancient, as homologues of each are found in the *C. elegans* genome, thus the genes for the different α_1 subunits have become widely dispersed on different chromosomes in mammalian genomes[72].
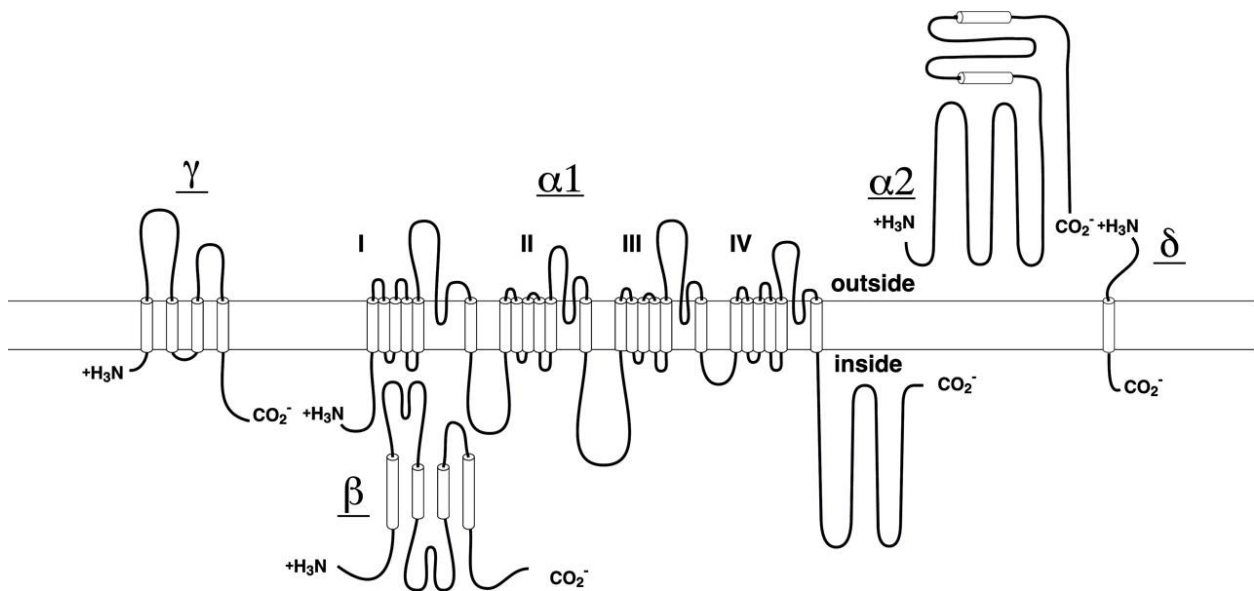
Figure 4. Illustration of voltage-gated calcium channel composition.

VGCCs consist of the pore-forming α_1 subunit and auxiliary $\alpha_2\delta$, β and γ subunits. The $\alpha1$ subunit is composed of four domains (I-IV). Each domain has six transmembrane sections of which segment 4 is responsible for voltage sensing (adapted from Catterall et al., 2005).

VGCCs can be divided into low-voltage-activated (LVA) and high-voltage activated (HVA) channels, based on their activation threshold (**Table 1**). LVA calcium channels ($Ca_v3.1$, $Ca_v3.2$, $Ca_v3.3$) open at a membrane potential above −70 mV, are characterized by small amplitude of single channel conductance with fast decay and are transient, hence their currents were also called T-type currents (T for transient). Calcium channels passing T-type currents are expressed in a wide variety of cell types, where they are involved in shaping the action potential and controlling patterns of repetitive firing. In contrast to LVA channels, HVA channels have an activation threshold above −20 mV. The typical currents of the first known HVA channels $Ca_v1.1$, $Ca_v1.2$, $Ca_v1.3$ were named L-type calcium currents (L for large and long-lasting), because of their large, single channel conductance and slow kinetics. They can be inactivated by nifedipine[76]. Later, experiments with neurons revealed novel calcium channels, namely $Ca_v2.2$, passing N-type currents (N for neuronal)[78] and $Ca_v2.1$, passing P/Q-type currents (P for Purkinje cells, where this currents were first characterized)[79]. The α_1 subunit of $Ca_v2.1$ was shown to exist in different splice variants, accounting for functionally distinct P-type or Q-type currents with varying combinations of both, dependent on the cell type[80]. Thus, in most cases $Ca_v2.1$ mediated currents are referred to as P/Q-type. The remaining currents of $Ca_v2.3$ after blocking all other HVA channels were named R-type currents (R for resistant) (**Table 1**).

$Ca_v.2.1$, $Ca_v.2.2$, and to a smaller proportion also $Ca_v.2.3$ calcium channels are essential for the neurotransmission at most fast synapses by mediating calcium entry into the presynapse upon depolarization of the cell membrane, caused by arriving action potentials. This Ca^{2+} influx into the presynapse enables the fusion of neurotransmitter (NT) filled vesicles with the synaptic membrane and subsequent NT release to the synaptic cleft[74] (**Fig.7**). As the NT release is proportional to the third or fourth power of Ca^{2+} influx, a 2-fold change in presynaptic Ca^{2+} influx results in an 8 to16-fold change in NT exocytosis[81]. Thus, regulation of presynaptic calcium channels is an efficient way to control synaptic transmission.

Table 1. Voltage-gated calcium channels: nomenclature, physiological function and pharmacology (based on Catterall et al., 2005)**.**

Channel	Current	Alpha 1 subunit	Voltage activation	Localization	Cellular functions	Specific antagonists
$Ca_v1.1$	L-type	α_{1S}	HVA	Skeletal muscle, transverse tubules	Excitation-contraction	Dihydropyridines, phenylalkylamines, benzothiazepines
$Ca_v1.2$		α_{1C}		Cardiac and smooth muscle myocytes, endocrine cells, neurons (somatodendritic)	Excitation-contraction coupling, hormone release, synaptic integration, transcriptional regulation	
$Ca_v1.3$		α_{1D}		Endocrine cells, neurons (somatodendritic), cardiac myocytes, cochlear hair cells	Hormone release, synaptic integration, transcriptional regulation, cardiac pace-making, hearing, NT release from sensory cells	
$Ca_v1.4$		α_{1F}		Retina cells, spinal cord, adrenal gland, mast cells	NT release from photo-receptors	
$Ca_v2.1$	P/Q-type	α_{1A}		Neurons (terminals and dendrites), neuroendocrine cells	NT release, dendritic Ca^{2+} transients, hormone release	ω-Agatoxin IVA
$Ca_v2.2$	N-type	α_{1B}		Neurons (terminals and dendrites), neuroendocrine cells		ω-conotoxin MVIIA
$Ca_v2.3$	R-type	α_{1E}		Neurons (somatodendritic and terminals)	Repetitive firing, dendritic Ca^{2+} transients	SNX-482
$Ca_v3.1$	T-type	α_{1G}	LVA	Neurons (somatodendritic), cardiac and smooth muscle myocytes	Pacemaking, repetitive firing	none
$Ca_v3.2$		α_{1H}		Neurons (somatodendritic), cardiac and smooth muscle myocytes		
$Ca_v3.3$		α_{1I}		Neurons (somatodendritic)		

1.6   The nigro-striatal pathway

In order to test the *in vivo* functionality of calcium channel specific t-toxins to silence synaptic transmission, a model system with a clear behavioral output was required. It has been shown in numerous studies of movement disorders, including Parkinson's disease that unilateral interruption of the nigrostriatal pathway leads to an imbalance in dopaminergic (DA) signaling to the striatum, and results in a rotational phenotype of the animal[82-85]. This rotational movement can be inversed or enhanced by activating the remaining dopamine systems with the dopamine receptor agonists apomorphine or amphetamine, respectively[82-85] (**Fig.5**). In this work, a variation of these experimental assays was used to test, whether t-toxin mediated inactivation of $Ca_v2.1$ and $Ca_v2.2$ channels could impair dopamine release from dopaminergic neurons onto striatal medium spiny neurons. Therefore, t-toxin lentivirus was injected unilaterally into the substantia nigra pars compacta (SNpc) of mice, and rotational behaviors were quantified 2-3 weeks later.

The nigro-striatal pathway is part of the basal ganglia, which are associated with a variety of functions, including motor control and learning. They consist of two primary input structures, two primary output structures, and two intrinsic nuclei.[86,87]. The input structures of the basal ganglia are the subthalamic nucleus (STN) and the striatum, which receives excitatory inputs from most areas of the cerebral cortex. The output structures are the substantia nigra pars reticulate (SNpr) and the globus pallidus internal segment (GPi). Both of them receive excitatory input from STN and inhibitory input from the striatum. The outputs from GPi and SNpr are inhibitory and project to motor areas in the brainstem and thalamus. The intrinsic nuclei are the globus pallidus pars externa (GPe) and substantia nigra pars compacta (SNpc). SNpc consists of dopaminergic neurons, receives input from the striatum and sends most of its output back to the striatum via the medium forebrain bundle (mfb) (**Fig.5a**)[86,87]. Basal ganglia disorders, like Parkinson's disease, which is caused by the death of DA neurons in SNpc, are characterized by an inability to correctly initiate and terminate voluntary movements, an inability to suppress involuntary movements, and an abnormal muscle tone[88].

The neurotoxin 6-hydroxydopamine (6-OHDA) has been used extensively for the unilateral lesion of DA neurons in the substantia nigra to induce circling behavior in rats, in order to dissect the nigro-striatal pathway and its role in motor coordination[82-85]. In response to the resulting striatal DA depletion, a receptor-mediated supersensitivity, caused by increasing affinity and number of striatal D2-receptors in denervated postsynaptic neurons develops[83]. This supersensitivity on the side of the lesioned hemisphere causes the reversal of the rotational direction, if DA agonists like apomorphine are administered (**Fig.5b**)[82,83].
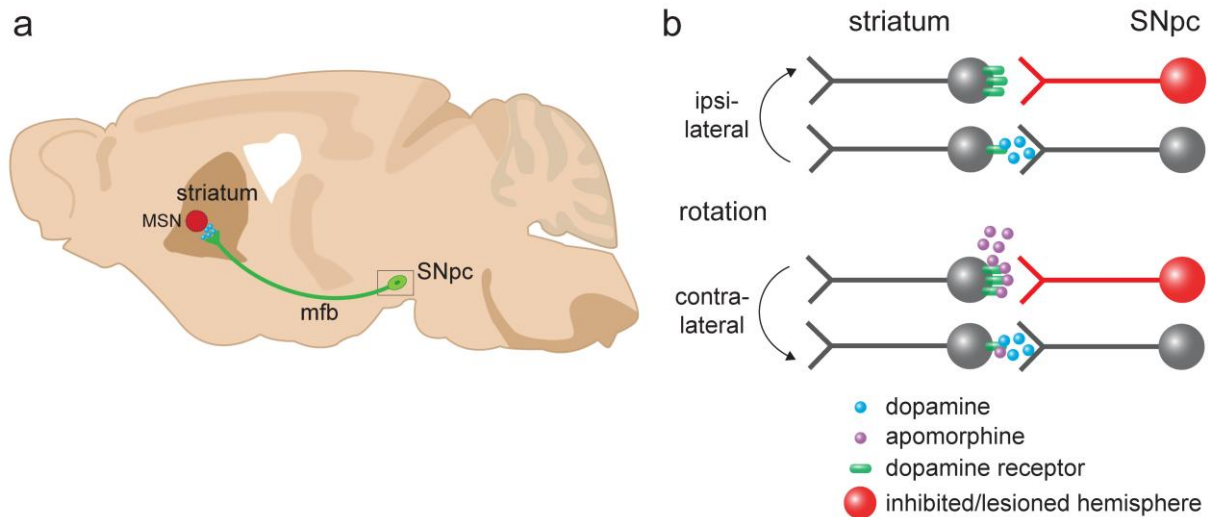
Figure 5. Simplified representation of the nigro-striatal pathway and induced rotational behavior.

(**a**) Sagittal view of the basic nigro-striatal pathway. Dopaminergic neurons of the substantia nigra pars compacta (SNpc) project to the striatum via the medial forebrain bundle (mfb), and release dopamine to medium spiny neurons (MSN). This input is relayed via several circuits to the neocortex, finally regulating important physical conditions, including motor coordination. (**b**) Lesioning or inhibition of dopaminergic neurons from only one hemisphere leads to an imbalance in dopaminergic signaling. Higher activity on the intact side, results in an ipsilateral rotational phenotype of the animal. If apomorphine, a dopamine receptor agonist, is administered, the imbalance is changed to the inhibited/lesioned side, due to increased receptor affinity and number of receptors, as physiological reaction to the missing innervation. This results in a change of the rotational behavior to contralateral circling.

1.7   Origin of membrane-tethered toxins

Many natural peptide toxins are potent modulators of ion channels and receptors and are able to discriminate between closely related subtypes. Previous work by the lab has demonstrated that peptide toxins retain their activity and specificity when they are recombinantly tethered to the plasma membrane via a glycosylphosphatidylinositol (GPI) anchor[89]. The structural homology of the endogenous prototoxin lynx1 with snake α-bungarotoxin gave rise to this tethered toxin (t-toxin) strategy of using the biological scaffold of lynx1 (secretory signal and GPI signal) to generate recombinant membrane-bound toxins[89] (**Fig.6**). Lynx1 is highly expressed in the mammalian CNS, physically interacts with nicotinic acetylcholine receptors (nAChR)[90,91], and belongs to the Ly6 superfamily of cholinergic modulators. These molecules represent a unique class of short proteins, with a characteristic 8-10 cysteine motif that determines their compact three-finger structure, and are either tethered to the cell surface via a glycosylphosphatidylinositol (GPI) anchor, like *lynx1*, or secreted as venom toxins (**Fig.6**).

The 1st generation of t-toxins (**Fig.6**) were shown recently to be active *in vitro* in *Xenopus leavis* oocytes and *in vivo* in zebrafish to block muscle nAChRs[89], in chick to inhibit nAChRs[92] and in Drosophila to modulate voltage-gated sodium channels (VGSCs)[93].

One advantage of the t-toxin approach over existing technologies lies in the enormous diversity of natural venom toxins which can be applied to this method. In addition, the cell-autonomous expression allows the study of cell networks and neuronal circuits by selective targeting of ion channel and receptor subtypes in specific cell populations, which is not possible with soluble compounds. Furthermore, long-lasting effects can be achieved with t-toxins, as they are not diluted by diffusion like soluble toxins and undergo a steady replenishment due to the expression within the target cell.
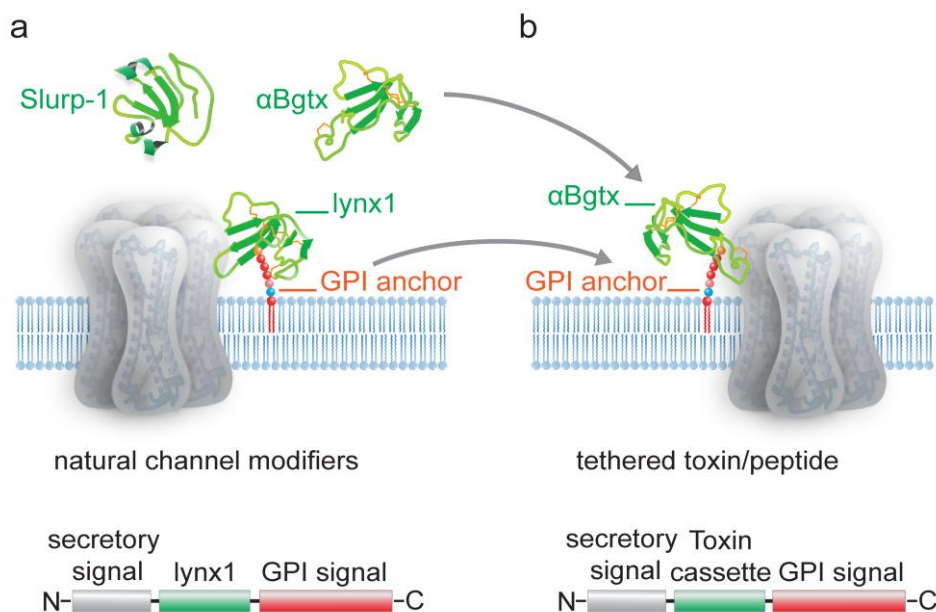
Figure 6. Scheme of Ly-6/uPAR channel modifiers and 1st generation tethered toxins (t-toxins).

(**a**) Examples of the Ly-6/uPAR superfamily include soluble Slurp-1, snake α-bungarotoxin (αBgtx) and the GPI-anchored cell-membrane bound lynx1. The schematic below the channel indicates the coding sequences associated with lynx1, namely an N-terminal secretory signal region, followed by the amino acid residues that correspond to the lynx1 peptide, and a C-terminal GPI anchor. (**b**) The structural homology of lynx1 with αBgtx gave rise to the t-toxin strategy of using the biological scaffold of lynx1 (secretory signal and GPI signal) to generate recombinant membrane-bound toxins such as the illustrated t-αBgtx. The schematic below the drawing of the channel indicates the coding regions that were conserved from lynx1 (secretory signal and GPI signal), and those that were altered to accommodate the αBgtx (the toxin sequence, flag tag, and linker region).

1.8   Aims of this work

The aim of this work is the optimization of the membrane-tethered toxin strategy[89,94], to enable the inhibition of voltage-gated calcium channels (Ca_V) and nicotinic acetylcholine receptors (nAChR), respectively, in order to interfere with neurotransmission *in vitro* and *in vivo*. We conceived this work to expand the t-toxin approach and to establish for the first time the utility of t-toxins to specifically inhibit calcium currents *in-vivo* in mice. As described in the following, this should be accomplished by the integration of new modules and peptide toxins to generate novel t-toxins, and by using lentiviral vectors and stereotaxic injections for gene delivery to targeted cells.

1.8.1   Aim 1: Construct optimization of t-toxins

As described above, the 1st generation of t-toxins (**Fig.6**) retained their blocking capability *in vitro* and *in vivo* in different model organisms[89,93,95]. However, the detection and visualization of these t-toxins was dependent on immunostaining against the flag epitope. Since many applications require direct monitoring of the expression and localization, this work aimed at the generation of fluorescent t-toxins by integration of the fluorescent markers enhanced green fluorescent protein (EGFP), the GFP-variant Venus, or mCherry (red fluorescence).

Furthermore, the GPI anchor was substituted in some constructs with the PDGF-receptor transmembrane domain in order to further increase the stability of membrane integration. The integration of the transmembrane domain was also necessary because the pore blocking activity of ω-conotoxins MVIIA/MVIIC, by binding to the ion channel pore, could possibly be disturbed by the fluorescent reporters. In contrast, the gating modifying agatoxins, which bind to domains more distant to the channel pore, allow the N-terminal attachment of fluorescent markers. Thus, transmembrane domain constructs possess intracellular localization of fluorescent markers, and in GPI anchored t-toxins the fluorescent markers are located extracellular (**Fig.8**).

1.8.2 Aim 2: Establishment of lentiviral delivery and stereotaxic injection of t-toxins

As we wanted to use a reliable and efficient system for t-toxin delivery to neurons *in vitro* and *in vivo*, the generation and application of lentiviral particles, harboring the t-toxins had to be established in this work. Thus, three different lentiviral vectors were tested to allow constitutive, doxycycline-inducible or Cre recombinase-dependent expression in order to broaden the range of possible applications of t-toxins. Another aim was to set up the stereotaxic injection equipment and procedure, which is required for lentivirus delivery to the brain of anesthesized, living mice.

1.8.3 Aim 3: Generation of new t-toxins and application *in vitro* and *in vivo*

The newly generated t-toxins should serve as genetic tools for silencing neurotransmission *in vitro* and *in vivo* by inhibiting $Ca_v2.1$ and $Ca_v2.2$ calcium channels, as these two channels are essential for the neurotransmission at most fast synapses by mediating calcium entry into the presynapse. Inhibition of these channels with t-toxins would allow the long-term modulation of neurotransmission in various neuronal circuits in a broad range of model organisms, thus allowing studies of $Ca_v2.1$ and $Ca_v2.2$ function and distribution, as well as of the contributions of certain subtypes of cells to neuronal circuits (**Fig.7**).

Therefore, we aimed at blocking $Ca_v2.1$ and $Ca_v2.2$ channels with new t-toxins by integration of the agatoxins AgaIIIA and AgaIVA to generate AgaIIIA-VG and AgaIVA-VG, respectively (**Fig.1**,**8**). Additionally, we used ω-conotoxins MVIIA and MVIIC to produce MVIIA-PE, MVIIA-PC and MVIIC-PE, respectively (**Fig.1**,**8**). For ensuring full functionality of the constructs, the expression was analyzed in HEK and HeLa cells and rat hippocampal neurons *in vitro,* and the blocking capabilities on one or both channels were tested in HEK293-$Ca_v2.2$ cells and rat hippocampal neurons *in vitro* and in lentivirus injected mice *in vivo*.

Another aim of this work was to selectively inhibit specific nAChRs by α-conotoxin GID based t-toxins. The expression of generated t-toxins GID-PE (green fluorescence) and GID-PC (red fluorescence) (**Fig.1**,**8**) was therefore analyzed in HEK and HeLa cells and cultured rat hippocampal neurons*,* and the blocking capabilities on different nAChRs were tested in *Xenopus laevis* oocytes.
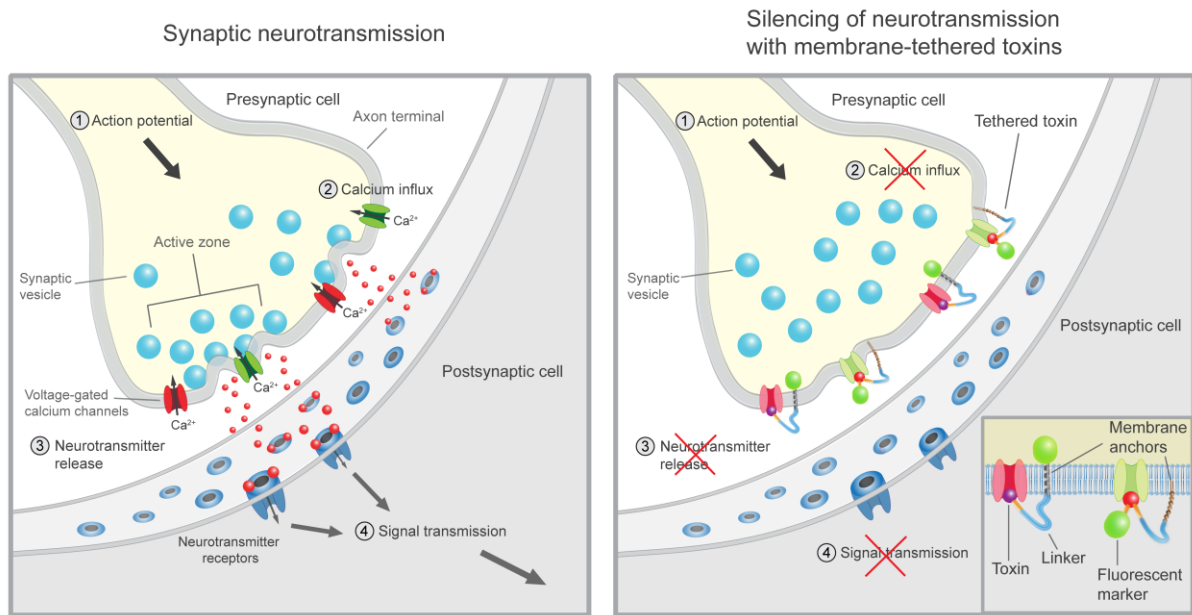
Figure 7. Illustration of synaptic neurotransmission and tethered toxin induced block of neurotransmission .

Depolarization of the cell membrane due to arriving action potentials leads to opening of $Ca_v2.1$ and/or $Ca_v2.2$ voltage-gated calcium channels. The resulting influx of calcium into the presynapse triggers the fusion of neurotransmitter (NT) filled vesicles and causes subsequent NT release into the synaptic cleft. Finally, the NT molecules bind to postsynaptic receptors, leading to excitatory or inhibitory signals in the postsynaptic cell, depending on the type of receptor (left column). One of the aims of this work was to develop calcium channel specific t-toxins to inhibit calcium influx via $Ca_v2.1$ and/or $Ca_v2.2$ calcium channels, in order to silence neurotransmission (right column).
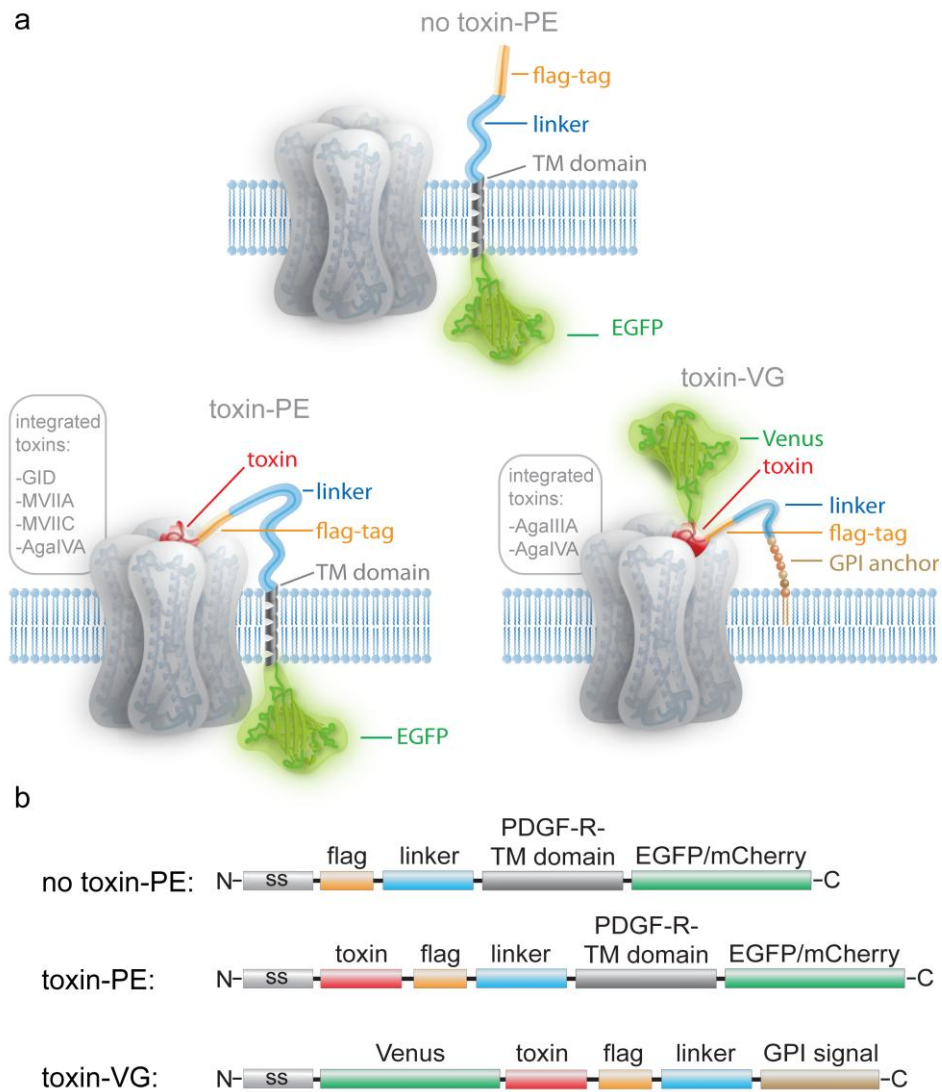
Figure 8. Illustration of 2nd generation membrane-tethered toxins generated in this work.

(**a**) Schematic representation of the negative control no toxin-**PE**, containing the **P**DGF receptor transmembrane (TM) domain and a C-terminally fused **E**GFP. Toxin-**PE** contains the **P**DGF receptor TM domain and **E**GFP plus a peptide toxin at the N-terminal end. Alternatively, EGFP can be substituted by m**C**herry (**PC**, red fluorescence). In contrast, toxin-**VG** carries an extracellular **V**enus as it is tethered to the membrane via a **G**PI anchor. (**b**) Modular composition of used t-toxins.

2. Material and Methods

2.1 Preface

2.1.1 Chemicals

Name	Composition
Acridin ointment	WDT eG, Garbsen, Germany
Agatoxin IVA	Peptide Institute Inc., Osaka, Japan
Agarose, ultra-pure	Invitrogen GmbH, Karlsruhe, Germany
Antibiotic-Antimycotic	Invitrogen GmbH (Gibco), Karlsruhe, Germany
Ammonium chloride	Carl Roth GmbH & Co. KG, Karlsruhe, Germany
Ampicillin sodium salt	Sigma-Aldrich Chemie GmbH, Schnelldorf, Germany
R-(-)-apomorphine hydrochloride hh	Sigma-Aldrich Chemie GmbH, Schnelldorf, Germany
B27-Supplement	Invitrogen GmbH (Gibco), Karlsruhe, Germany
BES	Sigma-Aldrich Chemie GmbH, Schnelldorf, Germany
Betaisodona	Mundipharma, Limburg/Lahn, Germany
Bovine serum albumin (BSA)	Sigma-Aldrich Chemie GmbH, Schnelldorf, Germany
Bromphenolblue	Carl Roth GmbH & Co. KG, Karlsruhe, Germany
Calcium chloride dihydrate	Merck KgaA, Darmstadt, Germany
Chloroform	Carl Roth GmbH & Co. KG, Karlsruhe, Germany
Collagenase Type I	Sigma-Aldrich Chemie GmbH, Schnelldorf, Germany
Cytosine-β-D-arabinofuranoside	Sigma-Aldrich Chemie GmbH, Schnelldorf, Germany
Dimethyl sulfoxide (DMSO)	Merck KgaA, Darmstadt, Germany
CNQX	Tocris Bioscience, Ellisville, MO, USA
D-AP5	Tocris Bioscience, Ellisville, MO, USA
dNTP-Mix	Sigma-Aldrich Chemie GmbH, Schnelldorf, Germany
Doxycycline hyclate	Sigma-Aldrich Chemie GmbH, Schnelldorf, Germany
EDTA disodium-dihydrate	Carl Roth GmbH & Co. KG, Karlsruhe, Germany
Ethanol	Carl Roth GmbH & Co. KG, Karlsruhe, Germany
Ethidium bromide	Carl Roth GmbH & Co. KG, Karlsruhe, Germany
FBS (fetal bovine serum)	Invitrogen GmbH (Gibco), Karlsruhe, Germany
D-(+)-glucose	Sigma-Aldrich Chemie GmbH, Schnelldorf, Germany
D-MEM	Invitrogen GmbH (Gibco), Karlsruhe, Germany
DNAse I	Sigma-Aldrich Chemie GmbH, Schnelldorf, Germany
Glacial acetic acid	Carl Roth GmbH & Co. KG, Karlsruhe, Germany
GlutaMAX^{TM}	Invitrogen GmbH (Gibco), Karlsruhe, Germany
Glycine	Carl Roth GmbH & Co. KG, Karlsruhe, Germany
Glycerol	Carl Roth GmbH & Co. KG, Karlsruhe, Germany
HBSS (10x)	Invitrogen GmbH (Gibco), Karlsruhe, Germany
HEPES	Carl Roth GmbH & Co. KG, Karlsruhe, Germany
Horse serum	Invitrogen GmbH (Gibco), Karlsruhe, Germany
Immu-Mount™	Thermo Scientific, Pittsburgh, PA, USA
IPTG	Sigma-Aldrich Chemie GmbH, Schnelldorf, Germany
Isopropanol	Carl Roth GmbH & Co. KG, Karlsruhe, Germany
Ketamin 10 %	WDT eG, Garbsen, Germany
Lipofectamine™ 2000	Invitrogen GmbH, Karlsruhe, Germany
ω-conotoxin MVIIA	Peptide Institute Inc., Osaka, Japan
ß-mercaptoethanol	Sigma-Aldrich Chemie GmbH, Schnelldorf, Germany
Methanol	Carl Roth GmbH & Co. KG, Karlsruhe, Germany
$MgCl_2$ (50 mM)	Invitrogen GmbH, Karlsruhe, Germany
Mineral oil	Carl Roth GmbH & Co. KG, Karlsruhe, Germany

Neurobasal medium	Invitrogen GmbH (Gibco), Karlsruhe, Germany
Nicotine-tartrate	Sigma-Aldrich Chemie GmbH, Schnelldorf, Germany
O.C.T.™ Tissue Tek	Sakura Finetek, Zoeterwoude, Netherlands
Oligonucleotides	BioTeZ Berlin Buch GmbH, Berlin, Germany
Opti-MEM®	Invitrogen GmbH (Gibco), Karlsruhe, Germany
Paraformaldehyde	Sigma-Aldrich Chemie GmbH, Schnelldorf, Germany
PBS (10x)	Invitrogen GmbH (Gibco), Karlsruhe, Germany
PCR Rxn buffer (10x)	Invitrogen GmbH, Karlsruhe, Germany
Penicillin/streptomycin	Invitrogen GmbH (Gibco), Karlsruhe, Germany
Peptone	Carl Roth GmbH & Co. KG, Karlsruhe, Germany
Poly-D/L-ornithine hydrobromide	Sigma-Aldrich Chemie GmbH, Schnelldorf, Germany
Poly-L-lysine 0.01 %	Sigma-Aldrich Chemie GmbH, Schnelldorf, Germany
Protease inhibitor tablets complete mini	Roche Pharma AG, Grenzach-Wyhlen, Germany
Regephitel®	Alcon Pharma GmbH, Freiburg, Germany
Rompun® (2% Xylazin)	Bayer Vital GmbH, Leverkusen, Germany
Sodium chloride	Carl Roth GmbH & Co. KG, Karlsruhe, Germany
Sodium hydrogen sulfate	Sigma-Aldrich Chemie GmbH, Schnelldorf, Germany
Sodium hydroxide	Sigma-Aldrich Chemie GmbH, Schnelldorf, Germany
Sucrose	Sigma-Aldrich Chemie GmbH, Schnelldorf, Germany
TEA	Sigma-Aldrich Chemie GmbH, Schnelldorf, Germany
Tricaine	Sigma-Aldrich Chemie GmbH, Schnelldorf, Germany
TRIS	Carl Roth GmbH & Co. KG, Karlsruhe, Germany
Triton X-100	Sigma-Aldrich Chemie GmbH, Schnelldorf, Germany
Trypsin-EDTA (0.25 %)	Invitrogen GmbH (Gibco), Karlsruhe, Germany
Trypsin inhibitor Type I-S (soybean)	Sigma-Aldrich Chemie GmbH, Schnelldorf, Germany
Tween 20	Serva Electrophoresis GmbH, Heidelberg, Germany
Xylene cyanol	Carl Roth GmbH & Co. KG, Karlsruhe, Germany
X-Gal	Carl Roth GmbH & Co. KG, Karlsruhe, Germany
Yeast extract	Carl Roth GmbH & Co. KG, Karlsruhe, Germany

Table 2. Chemicals used in this work

2.1.2 Composition of prepared buffers and solutions

All buffers and solutions were prepared using Type I water (MQ) with a resistivity of 18 Mohm-cm produced with a Barnstead E-pure water purification system.

Name	Composition
0.2 M $Na_2H_2PO_4$	15.5% 1 M Na2HPO4, 4.5 % 1 M NaH2PO4 in MQ, pH 7.4
1 kb DNA ladder	1 kb plus DNA ladder (Invitrogen), 10 mM Tris-HCl, 50 mM NaCl, 1x DNA loading buffer
2x BBS	50 mM BES, 280 mM NaCl, 1.5 mM Na_2HPO_4, pH 6.95 (with NaOH)
4% PFA	4% paraformaldehyde in 1 x PBS with 0.2 M $Na_2H_2PO_4$ pH 7.4
6x loading dye	0.2 % Xylene cyanol, 0.2 % Bromphenolblue, 30 % Glycerol
50x TAE	242 g/l Tris base, 5.71 % (v/v) Glacial acetic acid, 0.05 M EDTA, pH 8.0
Apomorphine solution	7.5 mg Apomorphine hydrochloride, 0.2 % ascorbic acid, saline

Blocking solution for immunostaining without permeabilization	1 x PBS with 10 % goat serum
Blocking solution for immunostaining with permeabilization	1 x PBS with 10 % goat serum and 0.3 % Triton X-100
Cryosection buffer	0.1 M phosphate buffer with 25% glycerol and 25 % ethylene glycol, pH 7.4
Hippocampus culture dissection buffer	1x HBSS with 25 mM Glucose and 15 mM HEPES
Hippocampus culture digestion buffer	1 mg trypsin in 10ml 1xPBS with 20 mM glucose, 15 mM HEPES and 1 mM EDTA
Hippocampus culture digestion inhibition buffer	15 mg trypsin inhibitor type I-S in 12 ml Neurobasal medium
LB agar	LB-medium + 15 % (w/v) agarose
Lysis buffer (Western Blot)	150 mM NaCl, 50 mM HEPES, 10 % Gylcerol, 1 %Triton X-100
PBS (10x)	80 g/l NaCl, 2 g/l KH2PO4, 2 g/l KCl, 21.6 g/l Na2HPO4•7H2O
Saline	0.9 % NaCl in MQ
TBS (10x)	0.5 M Tris/HCl pH 7.9, 1.5 M NaCl, 0.2 g/l KCl
TBS-T	TBS + 0.05 % Tween-20
TE buffer	10 mM Tris pH 8.0, 1 mM EDTA

Table 3. Composition of buffers and solutions

2.1.3 Solutions for electrophysiology

Name	Measured cells	Composition
Calcium-free Ringer buffer	Xenopus oocytes	82,5 mM NaCl, 2 mM KCl, 1 mM $MgCl_2$ and 10 mM HEPES at pH 7.4
OR-2 buffer	Xenopus oocytes	82.5 mM NaCl, 2,5 mM KCl, 1 mM $MgCl_2$, 1 mM $CaCl_2$, 1 mM $NaHPO_4$ and 5mM HEPES at pH 7.8
Bath solution for $Ca_v2.2$ recordings	HEK293-Ca_v2.2	140 mM NaCl, 10 mM $BaCl_2$, 1 mM $MgCl_2$, 10 mM Hepes, 15 mM Glucose (7.4 pH, 330 mosm/kg osmolarity)
Pipette solution $Ca_v2.2$ recordings	HEK293-Ca_v2.2	115 mM CsCl, 20 mM TEACl, 10 mM EGTA, 2 mM $MgCl_2$, 10 mM Hepes, 4 mM Mg-ATP, 0.5 mM Na-GTP (7.4 pH, 280 mosm/kg osmolarity)
Bath solution for paired pulse recordings of eIPSC's	Rat hippocampal neurons	105 mM NaCl, 3 mM KCl, 10 mM HEPES, 5mM glucose, 2mM $CaCl_2$, 1mM $MgCl_2$, 10 µM DNQX and 50 µM DL-APV
Pipette solution for paired pulse recordings of eIPSC's	Rat hippocampal neurons	3 mM NaCl, 90 mM KCl, 5 mM EGTA, 5 mM HEPES, 5 mM glucose, 0.5 mM $CaCl_2$ and 4 mM $MgCl_2$
Bath solution for paired pulse recordings of eEPSC's	Rat hippocampal neurons	105 mM NaCl, 3 mM KCl, 10 mM HEPES, 5mM glucose, 2mM $CaCl_2$ and 1mM $MgCl_2$, 10 µM bicuculline, 1 µM strychnine and 100 µM APV
Pipette solution for paired pulse recordings of eEPSC's	Rat hippocampal neurons	3 mM NaCl, 90 mM KCl, 5 mM EGTA, 5 mM HEPES, 5 mM glucose, 0.5 mM $CaCl_2$, 4 mM $MgCl_2$ and 2 mM QX314

Table 4. Used solutions for electrophysiology

2.1.4 Bacteria strains

Name	Genotype
E.coli TOP10	F-*mcr*A Δ(*mrr-hsd*RMS-*mcr*BC) φ80*lac*ZΔM15 Δ*lac*X74 *rec*A1 *ara*D139 Δ(*ara*leu) 7697 *gal*U *gal*K *rps*L (StrR) *end*A1 *nup*G
E.coli DH5α	F-φ80*lac*Z ΔM15 Δ(*lac*ZYA-*arg*F) U169 *rec*A1 *end*A1 *hsd*R17(rk⁻, mk⁺) *pho*A *sup*E44*thi*-1 *gyr*A96 *rel*A1 *ton*A
E.coli Hb101	F- *sup*E44, *hsd*S20(r$_B^-$, m$_B^-$), *rec*A13, *ara*-14, *pro*A2, *lac*Y1, *gal*K2, *rps*L20, *xyl*-5, *mtl*-1, *leu*B6, *thi*-1

Table 5. Bacteria strains used in this work

2.1.5 Cell lines

Name	Source	Affiliation/Address
HEK 293T	System Biosciences (SBI)	Mountain View, CA, USA
HEK 293_Ca$_v$2.2	M. Missler	Westfälische Wilhelms-Universität Münster
HeLa	D. Besser	Max-Delbrück Center, Berlin-Buch

Table 6. Cell lines used in this work

2.1.6 Culture media

Name	Composition
LB medium	10 % Tryptone, 5 % Yeast extract, 10 % NaCl, adjusted to pH 7.0
Mammalian cell culture medium	10 % FBS in D-MEM with GlutaMAX™
Rat hippocampus culture start medium	Neurobasal medium with 1x B27-supplement, 1x Antibiotic/Antimycotic, GlutaMAX (0.5mM), glutamate (0.01 mM), 1% FBS and ß- mercapto-ethanol (0.025 mM)
Rat hippocampus culture medium	Neurobasal medium with 1x B27-supplement, 1x Antibiotic/Antimycotic, GlutaMAX (0.5mM) and ß- mercaptoethanol (0.025 mM)
Mouse cortex culture start medium	Neurobasal medium with 1x B27-supplement, 1x Antibiotic/Antimycotic, GlutaMAX (0.5mM), glutamate (0.01 mM) and 1% FBS
Mouse cortex culture medium	Neurobasal medium with 1x B27-supplement, 1x Antibiotic/Antimycotic, GlutaMAX (0.5mM) and cytosine ß-D-arabinofuranoside (5 μM)

Table 7. Culture media used in this work

2.1.7 Plasmids

Name	Source	Affiliation/Address
pCS2+	Addgene Inc.	Cambridge, MA, USA
pFUGW	Addgene Inc.	Cambridge, MA, USA
pLVUT-tTR-KRAB	obtained from P. Aebischer	École Polytechnique Fédéral de Lausanne, Switzerland
Lentiviral packaging plasmids pLP1, pLP2, pLP-VSV-G	ViraPower™ Lentiviral expression system; Invitrogen GmbH (Gibco)	Karlsruhe, Germany
pMSCV-LSL-GFP	obtained from J. Duyster	Technical University, Munich, Germany
pRSET-B-mCherry	obtained from R. Tsien	University of California, San Diego, USA

Table 8. Plasmids used in this work

2.1.8 Primers

Name	Sequence 5'- 3'	Usage
AgeI-koz-ss-F	CATACCGGTGCCACCATGTCTGCACTTCTG	Toxin cassette subcloning
BamHI-PDGF-R	GGATCCTACGTGGTTTCTTCTGCC	PDGF-R-TM subcloning
mCherry-BamHI-F	GTAGGATCCGTATGGTGAGCAAGGGCGAG	mCherry subcloning
mCherry-EcoRI-R	ATCGAATTCTTACTTGTACAGCTCGTCCATG	mCherry subcloning
mCherry-XbaI-R	AGTTCTAGATTACTTGTACAGCTCGTCCATGCCG	mCherry subcloning
EGFP-EcoRI-R	CTGAATTCTTACTTGTACAGCTCGTCCATG	Toxin cassette subcloning
loxP2-AgeI-F	CTAACCGGTATAACTTCGTATAGCATAC	loxP-DsRed2-loxP subcloning
loxP2-AgeI-R	CTAACCGGTATATAACTTCGTATAATGTATG	loxP-DsRed2-loxP subcloning
Seq_F	CTTCTGATCCTAGCTCTTGTTG	sequencing
Seq_R	GTTCTGCTGGTAGTGGTCG	sequencing
Ub_F2	GTCCGCTAAATTCTGGC	sequencing
WPRE_R2	GCCATACGGGAAGCAATAG	sequencing
XhoI-PDGF-F	CTCGAGTTGCTGTGGGCCAGGACACG	PDGF-R-TM subcloning

Table 9. Oligonucleotides used in this work

2.1.9 Oligonucleotides for toxin sequence generation

Toxin name	Sequence 5'- 3'
AgaIIIA_F	atcatgcatagatatcggtggagactgtgacggagagaaggatgactgtcagtgctgtaggagaaacggttattgctcatgttactctttattcggctatctgaagagcggatgcaagtgtgtcgtaggcacgtcagctgagttccagggaatatgtagacgtaaagccaggcagtgctataattccgatcctgacaagtgcgagtcacataacaagcctaagagacgga
AgaIIIA_R	tccgtctcttaggcttgttatgtgactcgcacttgtcaggatcggaattatagcactgcctggctttacgtctacatattccctggaactcagctgacgtgcctacgacacacttgcatccgctcttcagatagccgaataaagagtaacatgagcaataaccgtttctcctacagcactgacagtcatccttctctccgtcacagtctccaccgatatctatgcatgat
AgaIVA_F	aagaagaagtgcatcgccaaggactacggcaggtgcaagtggggcggcaccccctgctgtaggggcaggggctgcatctgtagcatcatgggcaccaactgcgagtgcaagcccaggctgatcatggagggcctgggcctggcc
AgaIVA_R	ggccaggcccaggccctccatgatcagcctgggcttgcactcgcagttggtgcccatgatgctacagatgcagcccctgcccctacagcaggggtgccgcccccacttgcacctgccgtagtccttggcgatgcacttcttctt
GID_F	atacgcgacgaatgttgctctaatccagcttgcagggtcaacaatcctcacgtatgta
GID_R	tacatacgtgaggattgttgaccctgcaagctggattagagcaacattcgtcgcgtat
MVIIA_F	tgcaaaggcaagggcgcgaagtgctcccgcctcatgtatgactgttgcaccggatcgtgtaggtccggtaagtgc
MVIIA_R	gcacttaccggacctacacgatccggtgcaacagtcatacatgaggcgggagcacttcgcgcccttgcctttgca

2.1.10 Antibodies and markers

Name	Usage	Supplier
Anti-Flag M2, monoclonal, mouse	IS	Sigma-Aldrich Chemie GmbH, Schnelldorf, Germany
Anti-NeuN, monoclonal, mouse	IS	Millipore GmbH (Chemicon), Schwalbach, Germany
Anti-Tyrosine hydroxylase (TH), monoclonal, mouse	IHC	Sigma-Aldrich Chemie GmbH, Schnelldorf, Germany
Anti-GFP, polyclonal, rabbit	IHC	Invitrogen GmbH (Molecular probes), Karlsruhe, Germany
Alexa Fluor® 488 goat anti-rabbit IgG	IHC	Invitrogen GmbH (Molecular probes), Karlsruhe, Germany
Alexa Fluor® 594 goat anti-mouse IgG	IHC	Invitrogen GmbH (Molecular probes), Karlsruhe, Germany
Cy3 goat anti-mouse IgG	IS, IHC	Jackson ImmunoResearch Europe Ltd., Suffolk, UK
4´,6-diamidino-2-phenylindole, dilactate (DAPI)	IS, IHC	Invitrogen GmbH (Molecular probes), Karlsruhe, Germany
Anti-GFP, monoclonal, mouse 11E5	WB	Invitrogen GmbH (Molecular probes), Karlsruhe, Germany
Goat anti-mouse-HRP	WB	Jackson ImmunoResearch Europe Ltd., Suffolk, UK
1 kb plus DNA ladder	Agarose-gels	Invitrogen GmbH (Molecular probes), Karlsruhe, Germany
PageRuler™ prestained protein ladder	SDS-PAGE	Fermentas GmbH, St.Leon-Rot, Germany
RiboRuler™ high range RNA ladder	Agarose-gels	Fermentas GmbH, St.Leon-Rot, Germany

Table 10. Antibodies and markers

(IS: immunostaining, IHC: immunohistochemistry, WB: Western Blot)

2.1.11 Enzymes

Name	Source
Restriction enzymes	New England Biolabs GmbH, Frankfurt, Germany
Dnase (TypeI)	Sigma-Aldrich Chemie GmbH, Schnelldorf, Germany
T4 DNA Ligase	New England Biolabs GmbH, Frankfurt, Germany
Shrimp alkaline phosphatase	USB Europe GmBH, Staufen, Germany
Trypsin from bovine pancreas	Sigma-Aldrich Chemie GmbH, Schnelldorf, Germany

Table 11. Enzymes

2.1.12 Kits

Name	Supplier
Amersham™ ECL plus WB detection kit	GE Healthcare, Munich, Germany
EndoFree® plasmid maxi kit	Qiagen GmbH, Hilden, Germany
mMessage mMachine® SP6 kit	Applied Biosystems (Ambion), Austin, TX, USA
NuPAGE® 4-12% Bis-Tris gels	Invitrogen GmbH (Gibco), Karlsruhe, Germany
Plasma membrane protein extraction kit	BioVision Research, Mountain View, CA, USA
QIAfilter™ plasmid maxi kit	Qiagen GmbH, Hilden, Germany
QIAquick® gel extraction kit	Qiagen GmbH, Hilden, Germany
QIAprep® spin miniprep kit	Qiagen GmbH, Hilden, Germany
TOPO TA cloning® kit	Invitrogen GmbH (Gibco), Karlsruhe, Germany

Table 12. Overview of kits used in this work

2.1.13 Equipment and software

Molecular-/Microbiology:

X-cell *SureLock*™ mini cell system	Invitrogen GmbH (Gibco), Karlsruhe, Germany
FlexCycler	Analytik Jena AG, Jena, Germany
PerfectBlue mini-/midigel system	Peqlab Biotechnologie GmbH, Erlangen, Germany
Gel Jet Imager	Intas Science Imaging Instruments GmbH, Göttingen, Germany
BioPhotometer	Eppendorf AG, Hamburg, Germany
Microcentrifuge 5415D	Eppendorf AG, Hamburg, Germany
Immobilon polyvinylidene fluoride membranes (PVDF)	Millipore GmbH, Schwalbach, Germany
CL-X Posure™ film	Thermo Fisher Scientific Inc., Karlsruhe, Germany

Microscopy:

Fluorescence microscope 1:	
Zeiss Axiovert 200 objectives: EC Plan-NEOFLUAR (10x, 20x, 40x, 63x, 100x) illuminating system: Zeiss HBO100	Carl Zeiss AG, Oberkochen, Germany
Micsoscope camera: Cascade 650	Photometrics, Tucson, AZ, USA
Imaging software: MetaMorph 6.3r6	Molecular Devices, Downingtown, PA, USA
Fluorescence microscope 2:	
Keyence Biozero BZ8100E	Keyence, Neu-Isenburg, Germany
Confocal microscope:	
Leica TCS SP5	Leica Microsystems GmbH, Wetzlar, Germany

Imaging software: Leica application suite (LAS)	Leica Microsystems GmbH, Wetzlar, Germany
Stereomicroscope MZ9.5	Leica Microsystems GmbH, Wetzlar, Germany
KL2500 LCD microscope illumination	Schott Inc., Southbridge, MA, USA

Cell culture:

Incubator CB 150	Binder GmbH, Tuttlingen, Germany
Beckman Optima L-90K ultracentrifuge with SW32 Ti rotor	Beckman Coulter GmbH, Krefeld, Germany
Heraeus Multifuge 1S-R	Thermo Fisher Scientific Inc., Karlsruhe, Germany
BD FACSCalibur™ • 488nm argon laser, 635 nm diode laser • FL1 – Green emission (filter: 530/30) • FL2 – Red/Orange emission (filter: 585/42) • FL3 – Red emission (filter: 650 LP) • FL4 – Far Red emission (filter: APC – 661 nm) • software: CellQuest Pro	BD Biosciences, San Jose, CA, USA
Bandelin Sonoplus homogenizer	Bandelin Electronic GmbH & Co. KG, Berlin, Germany
Neubauer counting chamber	Paul Marienfeld GmbH & Co. KG, Lauda-Königshofen, Germany
Tissue culture plates 12 well Tissue culture plates 24 well	Becton Dickinson, Franklin Lakes, NJ, USA
Tissue culture flasks 75 cm^2/150 cm^2	TPP AG, Trasadingen, Switzerland
Cellstar serological pipettes 5/10/25ml	Greiner Bio-One International AG, Frickenhausen, Germany
MultiGuard™ Barrier Tips 2/20/200/1000μl	Sorenson BioScience Inc., Salt Lake City, UT, USA
Stericup vacuum filtration units, 150ml	Millipore GmbH, Schwalbach, Germany
Ultraclear centrifuge tubes 25x89 mm/16x102 mm	Beckman Coulter GmbH, Krefeld, Germany
Superfrost glass slides	Menzel GmbH & Co. KG, Braunschweig, Germany
Glass coverslips, 13mm	Karl Hecht KG, Sandheim, Germany

Electrophysiology:

GeneClamp 500B amplifier	Oocyte recordings	Axon Instruments Inc., Foster City, CA, USA
Bath Perfusion System valve controller (ALA-VM8)	Oocyte recordings	Ala Scientific Instruments, Farmingdale, NY, USA
PLI-100 pico injector	Oocyte recordings	Harvard Apparatus, Holliston, MA, USA
pCLAMP9 software	Oocyte recordings	Axon Instruments Inc., Foster City, CA, USA
EPC-9, EPC-10 patch-clamp amplifier	HEK cell & neuron recordings	Heka Electronic, Lambrecht, Germany
Micromanipulator SM-5, mini25	HEK cell & neuron recordings	Luigs & Neumann Feinmechanik + Elektrotechnik GmbH, Ratingen, Germany
Axioskop 2 FS plus microscope	HEK cell & neuron recordings	Carl Zeiss AG, Oberkochen, Germany
Analog Stimulus Isolator 2200	HEK cell & neuron recordings	A-M Systems Inc., Sequim, WA, USA
WinTida , Patchmaster, Fitmaster	HEK cell & neuron recordings	Heka Electronic, Lambrecht, Germany
Flaming/Brown micropipette puller P-97	HEK cell & neuron recordings	Sutter Instrument company, Novato, CA, USA
Patch pipettes (Borosilicate glass)	HEK cell & neuron recordings	World Precision Instruments, Sarasota, FL, USA

Stereotaxic injections:

Benchmark digital stereotaxic instrument with fine drive and Cunningham mouse and neonatal rat adaptor	Leica Microsystems GmbH (myNeuroLab), Wetzlar, Germany
MO-10 oil hydraulic micromanipulator	Narashige Scientific Laboratory, Tokyo, Japan
Micromotor drill	Leica Microsystems GmbH (myNeuroLab), Wetzlar, Germany
PCR micropipets 1-5 µl	Drummond scientific company, Broomall, PA, USA
Microelectrode puller FP-830	Narashige Scientific Laboratory, Tokyo, Japan
Sterican® needles	Braun Melsungen AG, Melsungen, Germany
Marlin® polyglycolic acid sutures	Catgut GmbH, Markneukirchen, Germany
Reglo digital tubing pump	Ismatec Laboratoriumstechnik GmbH, Wertheim-Mondfeld, Germany
Sliding microtome SM2000R	Leica Microsystems GmbH, Wetzlar, Germany

2.1.14 Statistical analyses

Numerical data in this work was analyzed with Microsoft Excel 2007, and quantified results are presented as means ± s.e.m. Two-sided t-test with unequal variance was applied with $P < 0.05$ considered statistically significant ($* \leq 0.05$, $** \leq 0.005$).

2.1.15 Animals

C57/Bl6 mice were housed with *ad libitum* access to food and water in air conditioned rooms at 22-23 °C with a standard 12 h light/dark cycle. Pregnant Wistar-Han rats were acquired from Charles-River (Sulzfeld, Germany) at embryonic day 19 (E19). For primary hippocampal cultures, rats were anesthetized with chloroform and immediately sacrificed by cervical dislocation. All procedures were in accordance with ethical guidelines laid down by the local governing body and approved by Landesamt für Gesundheit und Soziales, Berlin.

2.2   Molecular biology

2.2.1   Vector construction

All vectors were made using standard cloning procedures. Due to limitations in accessible restriction enzyme cutting sites in the lentiviral vector pFUGW, the subcloning procedures to generate t-toxins were carried out in pCS2+ plasmid. To generate pCS2-PE (pCS2-PDGF-R-TM-EGFP), the PDGF-receptor transmembrane domain was amplified by PCR from pDisplay™ (Invitrogen, Germany) with primers carrying overhanging ends and inserted into pCS2-EGFP at the 5' end of EGFP using XhoI and BamHI sites, respectively. Subsequently, the *lynx1* secretory pathway signal sequence (secretion signal), a flag epitope and a linker region [Gly-Asn] x 8 were cut from an already existing construct and inserted at the 5' end of the PDGF-R-TM domain between SphI and XhoI sites. Toxin sequences were generated earlier after back-translation of known aminoacid codes by annealing of overlapping oligonucleotides and subsequent TOPO-TA cloning. Lentiviral constructs carrying tethered toxins (pFU-t-toxin-PE) were generated by insertion of amplified toxin sequences between the *lynx1* secretion signal and the flag sequence in pCS2-PE (pCS2-PDGF-R-TM-EGFP) at PstI and ClaI cutting positions.

pCS2-AgaIVA-VG (pCS2-Agatoxin IVA-ppVenus-GPI signal) was generated by insertion of the amplified toxin sequence at BglII and ClaI sites between *lynx1* secretion signal with ppVenus at the 5' end and the flag sequence with a linker region and the lynx1 GPI signal at the 3' end. pCS2-PC (pCS2-PDGF-R-TM-mCherry) and pCS2-t-toxin-PC were generated by replacing EGFP from pCS2-PE and pCS2-t-toxin-PE with mCherry, amplified from pRSET-B-mCherry (primers: mCherry-BamHI-F, mCherry-XbaI-R).

The complete t-toxin sequences were finally subcloned into lentiviral vector pFUGW between AgeI and EcoRI cutting sites after PCR amplification with overhanging primers (AgeI-koz-ss-F, EGFP-EcoRI-R) to introduce the desired restriction enzyme sites.

To generate the doxycycline-inducible lentiviral construct iMVIIa-PE (pFU-MVIIA-flag-linker-PDGF-R-TM-EGFP-IRES-tetR-KRAB), a second EcoRI cutting site between the KRAB domain and WPRE of pLVUT-tTR-KRAB had to be deleted by cutting at the flanking BstBI and EcoRV sites and religating. Subsequently, the complete t-toxin cassette from pFU-MVIIA-PE was inserted at the 5'end of the IRES domain between AgeI and EcoRI sites.

The Cre-recombinase dependent lentiviral construct cMVIIA-PE was generated by insertion of the loxP-DsRed2-loxP cassette from pMSCV-LSL-GFP into the AgeI site of pFU-MVIIA-PE between the ubiquitin C promoter and the t-toxin cassette after addition of AgeI cutting sites on both ends by PCR amplification (primers: loxP2-AgeI-F, loxP2-AgeI-R).

Sequences and vector maps of the generated constructs were created with Vector NTI 10.3 (Invitrogen) and are attached in the appendix (**p.100**).

2.2.2 Primer design

In general, the melting temperatures of a set of PCR primers should be similar (~60-75 °C), the GC content should be 40-60 % and no secondary structures like hairpins and cross-pairing of the primers should be able to develop. The primer sequences were checked with Vector NTI 10.3 (Invitrogen, Germany) and the online software program Netprimer (www.premierbiosoft.com/netprimer) for suitability. Extended primers carrying overhanging ends were used in order to insert restriction enzyme sites in PCR-amplified DNA fragments to be able to clone the fragment in frame into expression vectors. The primers used in this work were ordered from Biotez Berlin-Buch GmbH (Berlin, Germany) and sequences are shown in **Table 9**.

2.2.3 Amplification of DNA fragments by PCR

PCR (polymerase chain reaction) was carried out for analytical purposes in order to detect sequences in extracted plasmid DNA (analytical PCR), or from bacterial colonies after transformation (analytical colony PCR), and to generate DNA fragments for subcloning of sequences (preparative PCR). The reaction mix was prepared on ice, adding the polymerase last and was composed as shown in **Table 13**. For colony PCR, the DNA template was substituted by a part of a bacterial colony, picked with a sterile plastic pipette and transferred to the PCR tube. All PCR reactions were carried out in a FlexCycler (Analytik Jena, Germany). The PCR thermocycler program was adjusted to the respective primers and fragment lengths, but the standard program is shown in **Table 14**. Finally, PCR products were analyzed on 1-1.5 % agarose gels.

Table 13. Standard PCR mix for one reaction

Amount	Substance
5 µl	10 x PCR buffer
3 µl	$MgCl_2$ (50 mM)
2 µl	dNTP mix (80 mM)
1 µl	DNA template (50 ng)
1 µl	Primer forward (50 µM)
1 µl	Primer reverse (50 µM)
0.1 µl	Taq-Polymerase
37 µl	MQ
50 µl	

Table 14. Standard PCR program

Temperature	Time	Cycles	Function
94 °C	3 min	1x	denaturation step, Taq activation
94 °C	30 s		denaturation step
x °C*	30 s	25 x	annealing step
72 °C	x min**		extension step
72 °C	5-10 min	1x	final extension step
15 °C	storage	1x	

* depending on the primer melting temperatures (50-65 °C)

** depending on the fragment length (e.g. ~1 min for 1 kb)

2.2.4 Agarose gel electrophoresis

DNA samples were run on a 1-1.5 % agarose gel in the PerfectBlue™ system (Peqlab, Germany). Mid-size gels with 130 ml volume or small-size gels with 80 ml volume were prepared by heating the appropriate amount of agarose in 1x TAE buffer. 0.001 % ethidiumbromide was added to the precooled agarose solution and the gel was poured into the gel slides and allowed to cool down to polymerize. Samples were mixed with 6x DNA loading dye and ~200-500 ng of DNA (analytic gels) or 1-4 µg of DNA (preparative gels) were added per gel pocket. The 1 kb plus DNA ladder (Invitrogen, Germany) was used as DNA size marker. Electrophoresis was carried out at 80-100 volts for 80 min and gels were subsequently analysed under UV light in the Gel Jet Imager (Intas, Germany).

2.2.5 Gel purification of DNA

The QIAquick® gel extraction kit (Qiagen, Germany) was used to isolate and purify enzyme digested or PCR-amplified plasmid DNA after agarose gel electrophoresis. The bands of interest were cut out of a 1% agarose gel under UV light and liquefied in 400 µl QC buffer at 55 °C for 10 min. The extraction was performed according to the manual and the DNA was eluted in 30 µl of MQ.

2.2.6 TOPO TA cloning

The TOPO TA cloning® kit (Invitrogen, Germany) was used to directly subclone PCR fragments without prior enzymatic digestion into the TOPO plasmid pCR2.1. The system utilizes the enzyme DNA topoisomerase I, which functions both as a restriction enzyme and as a ligase. Its biological role is to cleave and rejoin DNA during replication of vaccinia virus by specifically recognizing the pentameric sequence 5´-(C/T)CCTT-3´ and forming a covalent bond with the phosphate group attached to the 3´ thymidine. The enzyme then ligates the ends of the cleaved strand and releases itself from the DNA. The TOPO vector pCR2.1 is provided linearized with topoisomerase I covalently bound to each 3´ phosphate, which enables the vectors to ligate DNA sequences with single adenosine overhangs at both ends. These overhangs are generated automatically during PCR by the nontemplate-dependent terminal transferase activity of Taq polymerase that adds a single deoxyadenosine (A) to the 3´ ends of PCR products. The TOPO cloning was performed according to the manual and colonies were grown on ampicillin (100 µg/ml) containing agar plates, which had been pre-treated with 40 µl of 40 mg/ml X-gal and 40 µl of 100 mM IPTG. For selection of positive colonies

blue/white screening was used. The mechanism is based on disruption of the lacZ gene (β-galactosidase) in pCR2.1 by integration of PCR fragments and therefore colonies appear white. Whereas cells containing empty pCR2.1 still remain able to express β-galactosidase, which converts X-gal to galactose and 5,5'-dibromo-4,4'-dichloro-indigo, an insoluble blue molecule and thus colonies appear blue. 5-8 white colonies were inoculated in 5 ml LB medium with 100 µg/ml ampicillin and grown o/n at 37 °C. After performing plasmid extraction with the QIAprep® spin miniprep kit (Qiagen, Germany), plasmids were further analyzed by analytical PCR and restriction digest and then used for subcloning procedures.

2.2.7   Restriction digest and subcloning

DNA was enzymatically digested using specific endonucleases (NEB, Germany)) with 10 U of the restriction enzyme and 1x final dilution of the required restriction buffer added to 0.5-4 µg of plasmid DNA. The final volume was adjusted to 50 µl with MQ water and the samples were incubated for 1.5–2 h for test digestions or o/n for digestions to subclone sequences at the temperature required for the respective restriction enzyme. Vector dephosphorylation with shrimp alkaline phosphatase (1 U added at the end of digestion for 1 h) was used to decrease the amount of religated vector backbones lacking the insert of interest after transformation. All ligations were carried out as sticky end ligations with 3-6 fold molar ratios of inserts to vectors. Ligations were performed in a total volume of 10 µl containing 2 µl of T4 DNA ligase (NEB, Germany) and 1x ligation buffer at 16 °C o/n or at RT for >4 h.

2.2.8   Preparation of CaCl$_2$ competent *E. Coli* cells

For preparation of CaCl$_2$ competent *E.coli*, 100 ml LB medium was inoculated with 1 ml overnight culture of *E.coli* cells (e.g. Hb101, DH5α) and incubated with shaking at 37 °C until an OD$_{600}$ = 0.35. The following steps were carried out at 4°C. The cells were harvested in 50 ml tubes by centrifugation (2700 g; 10 min; 4 °C) and the pellet was resuspended in 40 ml 0.1 M MgCl$_2$. Subsequently, the cells were pelleted again by centrifugation (2.700 g; 10 min; 4 °C) and resuspended in 20 ml of 50 mM CaCl$_2$. After incubation on ice for 30 min and centrifugation (2700 g; 10 min; 4 °C), the pellet was resuspended in 2 ml of 50 mM CaCl$_2$ + 15 % (v/v) glycerol. A final incubation step on ice for 1 h was followed by aliquoting 200 µl of the cell solution per 1.5 ml tube and immediately freezing the tubes in liquid nitrogen. The competent cells were stored at -80 °C.

2.2.9 Transformation

Heat-shock transformation was applied to self-made chemically competent *E.coli*. The cells were thawed on ice, 100µl were mixed with 10 µl of the ligation preparation and incubated on ice for 10-20 min. The tubes were then transferred to 42 °C for 90 s, followed by immediate incubation on ice for 2 min. Afterwards, 500 µl LB medium was added and the cells were incubated at 37 °C for 1-2 h with shaking at 200 rpm to allow cell proliferation and expression of the antibiotic resistance marker. Finally, cells were spread on agar plates containing the appropriate antibiotic (ampicillin 100 µg/ml or kanamycin 50 µg/ml) and incubated in a 37 °C incubator (Heraeus, Germany) o/n.

2.2.10 Glycerol stock preparation

For long-term storage of bacteria, glycerol stocks were prepared by mixing 0.7 ml bacteria overnight culture with 0.7 ml of 40 % glycerol. The tubes were shortly vortexed, immediately frozen in liquid nitrogen and stored at -80 °C. For plasmid preparation, a heat-sterilized inoculating loop was lowered into the frozen glycerol stock and then shortly placed into 5 ml LB medium with appropriate antibiotics. The cells were cultured at 37 °C o/n and then subjected to plasmid extraction.

2.2.11 Plasmid DNA extraction

Plasmid DNA extraction was carried out using the QIAprep® spin miniprep kit with 1.2 ml bacterial culture or the QIAfilter™ plasmid maxi kit with 400 ml culture (Qiagen, Germany). All steps were performed according to the manual. DNA concentration was measured with the BioPhotometer (Eppendorf, Germany) and for maxipreps adjusted to 1 µg/µl with TE buffer resulting in a total volume of 0.7-1.2 ml. For lentiviral plasmids 130 µl aliquots were prepared for single-use. All DNA was stored at -20 °C.

2.2.12 Sequencing

DNA sequencing was carried out by Invitek Gesellschaft für Biotechnik & Biodesign mbH, Berlin. For double-stranded plasmid-DNA typically 10 µl of DNA (0.1 µg/µl) and 10 µl of sequencing primers (10µM) was sent to Invitek. Sequencing results were obtained as text file (.seq) and chromatogram files (.ab1), which were analyzed with Vector NTI 10.3 (Invitrogen) and Chromas 1.45 (Griffith University, Australia).

2.2.13 *In vitro* transcription

50 µg of plasmid DNA in pCS2+ was linearized in a total volume of 300 µl with 100 U of the appropriate restriction enzyme at 37 °C for 4 h. Afterwards, 300 µl lysis buffer was added to the mix and incubated at 37 °C for 30 min. Phenol/chloroform extraction was followed by precipitation and incubation at -20 °C for 2 h. Subsequently, the pellet was washed with 70 % ethanol and dried. 3 µg of plasmid DNA was used as starting material for *in vitro* transcription. The following steps were carried out using the mMessage mMachine® SP6 kit (Applied Biosystems (Ambion), USA) according to the manual. After resuspension in 50 µl nuclease-free water, RNA quality was assessed by agarose gel electrophoresis and expected sizes compared to the RiboRuler™ high range RNA ladder (Fermentas, Germany). The RNA quantity was measured spectrophotometrically in the BioPhotometer (Eppendorf, Germany). Purified RNA was used in oocyte injections for two-electrode voltage clamp (**2.4.1**).

2.3 Cell culture

2.3.1 Cell culture of HEK293T and HeLa cells

HEK293T cells and HeLa cells were cultured in cell culture flasks (75 cm^2, 150 cm^2) with Dulbecco's modified Eagle medium (DMEM + GlutaMAX™), supplemented with 10 % FBS (Invitrogen, Germany) at 37 °C and 5 % CO_2 in a Binder CB150 incubator. Cells were passaged every 3-4 days after reaching 80-90 % confluence by washing with 5 ml 1 x PBS and trypsinizing with 1-3 ml 0.25 % Trypsin-EDTA for 2 min. Digestion was stopped by adding 7 ml DMEM + GlutaMAX™ with 10 % FBS, and 0.5-1 ml of cells was seeded in a new culture flask with 10 ml/30 ml medium (75 cm^2/150 cm^2). For immunostaining, the cell number after trypsinization was determined by counting eight squares (0.1 mm^3 volume each) in a Neubauer hematocytometer, calculating the mean and multiplying it with dilution factor and with 10^4 to obtain the number of cells per ml. Subsequently, 5 x 10^4 cells per well were seeded on poly-l-lysine (0.0005 % in 1 x PBS) coated glass coverslips (13 mm) in a 24 well plate. The cells were transduced with lentivirus immediately after seeding or transfected 24 h after seeding. Three days later, cells were washed with 1 x PBS and fixed with 4 % PFA for 10 min at 4 °C, before they were used for immunostaining.

2.3.2 Preparation of freezing stocks of HEK293T and HeLa cells

For long term storage, freezing stocks of HEK293T and HeLa cells were prepared. Low-passage cells were cultured in 150 cm^2 cell culture flasks to 80-90 % confluence, then trypsinized and pelleted by centrifugation at 1000 rpm for 2 min. The cell pellet of one culture flask was resuspended in 3 ml ice-cold cell culture freezing medium, consisting of DMEM + GlutaMAX™ and 10 % FBS with 10 % DMSO. The cells were aliquoted in 2 ml cryotubes (1 ml each) and subjected to a controlled freezing process with -1 °C/min in a Cryo 1 °C freezing container (Nalgene, Thermo Fisher Scientific, Denmark) from RT to -70 °C. The next day, cells were transferred to a liquid nitrogen tank and were placed in the gas phase above the nitrogen (-178 to -150 °C) for long-term storage.

2.3.3 Thawing of HEK293T and HeLa cell freezing stocks

Freezing stocks of HEK293T and HeLa cells were rapidly thawed in a 37 °C water bath, then 9 ml prewarmed DMEM + GlutaMAX™ with 10 % FBS were added and cells were pelleted at 1000 rpm for 2 min. In order to remove the DMSO from the freezing medium, the supernatant was discarded completely. Finally, the cells were resuspended in 30 ml culture medium in a 150 cm^2 cell culture flask and cultured at 37 °C and 5 % CO_2, with a second medium exchange the next day. HEK293T cells were passaged at least twice after thawing before they were used for virus preparation.

2.3.4 Lentivirus production

Recombinant lentiviral vectors were prepared using transient transfection in HEK293T cells. 4.5×10^6 HEK293TN cells were seeded on 24 x 10 cm dishes, which had been pre-coated for 30 min with poly-l-lysine (0.0005 % in 1 x PBS). The next day, the lentiviral transfer vector plus the packaging vectors pLP1, pLP2 and the envelope vector pLP-VSV-G (Invitrogen, Germany) were cotransfected with calcium-phosphate transfection into the HEK293TN cells. The transfection mix was prepared with solutions prewarmed to 37 °C as follows: 7 μg lentiviral vector, 4 μg pLP1, 2 μg pLP2 and 2 μg pLP-VSV-G were added to 435 μl MQ and while vortexing, 500 μl 2x BBS and 50 μl 2.5 M $CaCl_2$ were added. Finally, after one minute incubation time at RT, 1 ml of transfection mix was added dropwise to each dish and distributed by shaking gently. After 16 hours, the medium was replaced by 9 ml OptiMEM®️ (Invitrogen (Gibco), Germany) per dish without FBS. The virus containing medium was harvested 24-30 h after medium change, cleared by centrifugation at 3000 rpm for 10 min at 4 °C and filtered through 0.45 μm Stericup®️ vacuum filtration units (Millipore, Germany).

2.3.5 Lentivirus concentration

Ultracentrifugation of harvested lentivirus was applied in order to increase final titers ~100-400 fold. The filtered supernatant was transferred to 35 ml ultraclear centrifuge tubes (Beckman Coulter, Germany), which had been placed in ultracentrifugation buckets. The centrifugation was carried out in a Beckman Optima L-90K ultracentrifuge using a SW32 Ti rotor at 50,000 g for 3 h with a purification layer of 1-3 ml 20 % sucrose (w/v) in 1 x PBS added to the bottom of the tubes. Subsequently, the virus was resuspended in 50-500 µl 1 x PBS by slowly shaking on ice for 1 h. In order to eliminate possibly remaining virus aggregates, the solution was centrifuged at 10,000 rmp for 10-20 s and the supernatant was transferred to a fresh tube. The virus solution was aliquoted in amounts of 5-50 µl in cryo-tubes with conical inserts and screw-caps, and stored at -70 °C. For *in vivo* applications, the virus solution was further purified by a consecutive second ultracentrifugation step of the pooled resuspended virus samples in 17 ml centrifugation buckets for 18 h at 20,000 g with the virus placed on top of a 5 ml 20 % sucrose cushion layer and afterwards resuspended and stored as before.

2.3.6 Lentivirus titration

The titer of concentrated lentiviral stocks was determined by transducing HEK293T cells with limiting virus dilutions. 2 µl virus resuspension were added to 198 µl of 1 x PBS to generate a 1:100 dilution, of which 100 µl was used to establish a dilution row (resulting dilutions were 1/200, 1/400, 1/800, 1/1600, 1/3200, 1/7200 and 1/14400). Then, 50 µl of each viral dilution was added to 1×10^5 HEK293T cells per well of a 24-well plate immediately after seeding the cells. Cells were incubated at 37 °C with 5 % CO_2 for 72 h before the medium was removed and cells were washed with PBS (0.5 ml), and trypsinized. After transferring the cells to 1.5 ml tubes, they were quickly pelleted by centrifugation (1000 rpm, 2 min), resuspended in 500 µl 1 x PBS and transferred to FACS tubes. Finally, the GFP positive cells were quantified by FACS analysis and the transducing units per ml, representing the number of infectious lentiviral particles, were calculated according to the following formula:

$$\textbf{TU/µl} = (\textbf{P} \times \textbf{N} / \textbf{100} \times \textbf{V}) \times \textbf{1/DF}$$

P: % GFP$^+$ cells, N: number of cells at time of transduction (1×10^5), V: volume of dilution added to each well (50 µl) and DF: dilution factor. Only dilutions yielding 1-20 % of GFP-positive cells in a linear range were considered for titer calculations, as below 1 % FACS

analysis may not be accurate and above 20 % the chance for multiple infections increases. On average, titers of non-concentrated lentivirus productions were in the range of 5 x 10^6 transducing units (TU)/ml and concentrated virus titers were 5 x 10^8 – 2 x 10^9 TU/ml.

2.3.7 FACS analysis

HEK293T cells were analyzed on a FACSCalibur™ system equipped with a 488 nm Argon laser and a 635 nm diode laser according to the instructions of the manufacturer. Briefly, HEK293T cells were trypsinized, washed once with medium and subsequently with 1 x PBS. If virus producing cells were used, a 10 min fixation period with 4 % PFA for 10 min was added. After adjusting the settings with a control sample, EGFP fluorescence was detected (FL1 filter: 530/30) in transfected or transduced cells and the percentage of EGFP positive cells as well as the mean fluorescence intensity (MFI) were measured.

For long-term analysis of doxycycline (DOX) inducible tethered toxin expression, HEK293T cells in a six well plate were transduced with iMVIIA-PE with a multiplicity of infection (MOI) of 10, so that > 80 % of cells were infected. Four days after the infection, cells were passaged to two separate six well plates, one with and one without addition of DOX (1 µg/ml). FACS analysis of cells from three independent wells was carried out for 21 days every 2-3 days, starting at day 7 after infection. The DOX treatment was reversed at day 5 and 13, by removing/adding DOX to the cultures, in order to analyze the reversibility and repeatability of DOX induced t-toxin expression.

2.3.8 Protein extraction of transfected HEK293T cells

Cell extracts from calcium-phosphate transfected HEK293T cells were prepared using a plasma membrane protein extraction kit (BioVision, USA) according to the instructions of the manufacturer. Briefly, 5-10 x 10^6 cells per sample were trypsinized, centrifuged and washed in cold 1 x PBS. After resuspending the cells in 500 µl homogenize buffer mix, they were homogenized with a Bandelin Sonoplus (Berlin, Germany) ultrasound system (3 x 1 min at max power). The solution was centrifuged for 10 min at 700 g at 4 °C and the supernatant was collected. A consecutive second centrifugation step for 30 min at 10,000 g at 4 °C was carried out to obtain cytosolic fraction in the supernatant and cellular membrane fraction in the pellet. Finally, the membrane fraction was resuspended in 500 µl homogenize buffer mix and both fractions were analyzed in SDS-PAGE and Western Blot.

2.3.9 SDS-PAGE and Western blotting

Protein samples were analyzed by discontinuous SDS-PAGE (sodium dodecyl sulfate-polyacrylamide gelelectrophoresis) by separation in a polyacrylamide gel according to their molecular weight using the Xcell SureLock™ mini-cell system (Invitrogen, Germany). NuPAGE® LDS sample buffer (4 x) and reducing agent (10 x) was added to all samples. After heating the samples to 70 °C for 10 min, the proteins were separated (10 μg per lane) according to their molecular weight on 4–12 % gradient polyacrylamide gels at 150 V for 90 min. The electrophoresis was performed with 1 x NuPAGE® MES SDS running buffer and 500 μl of NuPAGE® antioxidant added to the upper chamber. Afterwards, the gel was removed from the chamber and used for Western blotting. Western blotting is the process of transferring proteins from a polyacrylamide gel to a membrane where they are fixed and can be detected by specific antibodies. Before use, Immobilon polyvinylidene fluoride (PVDF) membranes (Millipore, Germany) were soaked in methanol for 1 min and washed in water for 5 min. The membrane was then incubated for 10 min in 1 x NuPAGE® transfer buffer together with the gel as well as blotting and filter papers. The blotting sandwich was built according to the manual. The transfer was carried out in semi-wet conditions with 1x NuPAGE® transfer buffer for 90 min at 30 V in the Xcell SureLock™ mini-cell system (Invitrogen, Germany). Afterwards, the membrane was shortly washed in 1 x TBS-T. Before immunostaining, the membrane was blocked in 5 % milk powder in TBS-T for 1-2 h at RT. Subsequently, the membrane was incubated in 1/400 anti-GFP (mouse, monoclonal) in blocking solution at 4 °C o/n. This step was followed by 4 x 10 min washing steps with TBS-T to ensure complete removal of unbound antibody. Then, the membrane was incubated with a goat anti-mouse-HRP (horse radish peroxidase) secondary antibody (1/10,000 in blocking solution) for 1.5 h. Horseradish peroxidase catalyzes the oxidation of hydrogen peroxide to 3-aminophthalate via several intermediates, which leads to emission of low intensity light that can be enhanced by certain chemicals up to 1000-fold, thereby simplifying detection and increasing the sensitivity of the reaction (enhanced chemiluminescence (ECL)). Following four washing steps (10 min each), the signal of bound antibody was detected using the ECL plus western blotting detection system (GE Healthcare, Germany), which generates a chemifluorescent signal at 440 nm that can be detected on a fluorescence imager as well as on film. 1 ml of solution A was mixed with 25 μl solution B and incubated with the membrane for 30 s. The membrane was then wrapped in transparent film, placed into a cassette and exposed to a CL-X Posure™ film (Thermo Scientific, Germany) for 1-30 min to detect the chemiluminescence. The films were developed in a film processor apparatus (Fuji, Japan).

2.3.10 Primary neuronal cultures

2.3.10.1 Rat hippocampus culture

Dissociated neuronal hippocampal cultures were prepared from embryonic day 19 rat embryos. Pregnant Wistar-Han rats (Charles River, Germany) were anesthetized with chloroform, killed by cervical dislocation, and the abdomen was sprayed with 70 % ethanol. Embryos were removed from the uterus and dissected in ice-cold dissection buffer. After scalp and skull had been removed, the brains were transferred to a fresh dish with dissection buffer on ice. The cortices were isolated by cutting dorsal to ventral between midbrain and cortex and after removing the meninges with two forceps, the hippocampi were cut out. Following incubation of the sliced hippocampi in digestion buffer containing trypsin for 8 min at 37 °C, the reaction was stopped by replacing the digestion buffer with digestion inhibition solution for 3 min. Subsequently, the tissue pellet was resuspended in 2 ml culture medium, and the cells were triturated by pipetting up and down 10-15 times with 1 ml and 200 μl pipettes. The tube was then left standing for three minutes in order to allow non-dissociated tissue fragments to sink to the bottom of the tube, and the upper 1.5 ml of the cell suspension were transferred to a new tube. The number of dissociated neurons was determined by counting eight squares (0.1 mm^3 volume each) in a Neubauer hematocytometer, calculating the mean and multiplying it with dilution factor and 10^4 to obtain cell number per ml. Finally, the cells were seeded in 1 ml of hippocampus culture start medium with a density of 2.5 x 10^5 cells per well on 13 mm glass coverslips, which had been pre-coated overnight with poly-D-/L-ornithine in MQ (50 μg/well) that was removed and after drying replaced by DMEM + 10 % FBS. Both the positively charged ornithine and serum proteins provide a basis for neurons to bind to the glass surface. The culture plate was incubated at 37 °C and 5 % CO_2 and one third of the medium (300 μl) was replaced with hippocampus culture medium twice a week, starting at DIV 5.

2.3.10.2 Mouse cortex culture

Cortex culture of E16 mouse embryos was prepared similarly to rat hippocampus culture. First, an E16 pregnant mouse was killed by cervical dislocation, the abdomen was sprayed with 70 % ethanol and opened. Then, the embryos were removed from the uterus and placed in a 10 cm dish containing ice-cold dissection solution. After decapitation, the heads were transferred to a fresh dish with dissection buffer, the brains were isolated and the meninges removed. Subsequently, the cortices were separated, cut into smaller pieces in order to

increase the reaction surface for trypsin and then transferred to a new tube with 10 ml dissection buffer. There, the supernatant was aspirated, replaced by digestion solution containing trypsin, and incubated at 37 °C for 8 min with gentle agitation. After stopping the reaction by adding digestion inhibition solution for 3 min to the tissue, the cells were mechanically dissociated in 2 ml cortex culture start medium by slowly pipetting up and down 10-15 times with a 1 ml pipette, followed by a 200 µl pipette. The tube was left standing for three minutes in order to allow non-dissociated tissue fragments to sink to the bottom of the tube and the upper 1.5 ml of the cell suspension was transferred to a new tube. The cell number was determined as described above and finally 2.5×10^5 cells per well were seeded in 1 ml of mouse cortex culture start medium in a 24 well plate on poly-D-/L-ornithine (50 µg/well) coated glass coverslips. One third of the medium was replaced by mouse cortex culture medium without glutamate in order to reduce glutamate toxicity in the culture but containing 5 µM AraC (cytosine ß-D-arabinofuranoside) to inhibit gliacell proliferation twice a week starting at DIV 4.

2.3.11 Immunostaining of cultured cells

For immunostaining of cultured HEK293T and HeLa cells or neurons, cells were grown on coated glass coverslips and fixed with 4 % PFA for 10 min at 4 °C. This was followed by three washing steps in 1 ml 1 x PBS for 3 min each and incubation for 1 h in 1 ml blocking solution, which consisted of 1 x PBS with 10 % goat serum. In order to solubilize membrane proteins to allow intracellular access of the antibodies, the blocking solution for intracellular immunostainings (e.g. NeuN) also contained 0.3 % Triton X-100 and the first antibody solution contained 0.1 % Triton X-100. Subsequently, the coverslips were incubated upside-down in a wet chamber in 50 µl of primary antibody solution (1/300 monoclonal anti-flag M2; (Sigma-Aldrich, Germany) or 1/100 monoclonal anti-NeuN (Millipore (Chemicon), Germany) with 1 % goat serum) for 2-5 h at RT or o/n at 4 °C. The wet chamber consisted of a 10 cm cell culture dish, in which a prewetted filter paper with a layer of parafilm on top had been placed to prevent exsiccation of antibody solutions. After washing two times in 1 ml 1 x PBS for 10 min, the coverslips were incubated in 50 µl secondary antibody solution for 1-2 h (1/1000 Alexa Fluor 594 goat anti-mouse IgG or 1/1000 Alexa Fluor 488 goat anti-mouse IgG (Invitrogen, Germany)) + 1/1000 DAPI (Invitrogen, Germany). Finally, after 3 washing steps à 10 min with 1 ml of 1 x PBS, the coverslips were mounted to objective slides in a drop of ImmuMount™.

2.4 Electrophysiology

2.4.1 Electrophysiological recordings of nAChRs in *X. laevis* oocytes

The oocyte expression vector pCS2+ containing one of the nAChR mouse subunits $\alpha 3$, $\alpha 7$ and $\beta 4$ was used to synthesize the corresponding cRNAs *in vitro* as described[91]. Oocytes were surgically removed from adult *Xenopus laevis* females, which were anesthetized with Tricaine (Sigma-Aldrich, Germany) and incubated in calcium-free Ringer buffer (82,5 mM NaCl, 2 mM KCl, 1 mM $MgCl_2$ and 10 mM HEPES at pH 7.4) containing 2 mg/ml collagenase Type I (Sigma-Aldrich, Germany) for 2 h at RT with constant shaking. Oocytes were washed in OR-2 buffer (82.5 mM NaCl, 2,5 mM KCl, 1 mM $MgCl_2$, 1 mM $CaCl_2$, 1 mM $NaHPO_4$ and 5mM HEPES at pH 7.8) and allowed to recover in OR-2/L-15 1:1 medium supplemented with 1 % penicillin/streptomycin (Invitrogen, Germany) at 18 °C overnight. Each oocyte was injected with 20 nl of a cRNA mix, containing either 2 ng of $\alpha 7$, $\alpha 3/\beta 4$ or $\alpha 4/\beta 2$ nAChR subunit mix alone, or in combination with 4 ng t-toxin cRNA using a PLI-100 pico injector (Harvard Apparatus, USA). Macroscopic currents were recorded between 2 and 5 days after injection with a GeneClamp 500B amplifier (Axon Instruments, USA) using a two-electrode voltage clamp with active ground configuration. Borosilicate glass electrodes (0.5-2 MΩ) were filled with 3 M KCl. The extracellular recording solution contained (in mM): 82.5 NaCl, 2 KCl, 1 $CaCl_2$, 1 $MgCl_2$ and 10 HEPES at pH 7.4. Nicotine-tartrate (Sigma-Aldrich, Germany) was prepared in extracellular solution at concentrations of 10 nM to 100 mM. Solutions were gravity fed with a flow rate of ~5 ml/min using a Bath Perfusion System valve controller (ALA-VM8, Ala Scientific Instruments, USA). Currents were analyzed using pCLAMP 9 software (Axon instruments, USA) with 10 Hz sampling rate. Membrane potential was clamped to -70 mV and only oocytes with leak currents <100 nA were used for measurements. Data was analyzed using the clampex and clampfit software (Axon Instruments, USA).

2.4.2 Recordings of evoked calcium currents in HEK293-Ca$_v$2.2 cells

HEK293-Ca$_v$2.2 cells, which stably express the calcium channel subunits α_{1B}, $\beta 3$ and $\alpha 2\delta$ of Ca$_v$2.2 (also known as N-type calcium channel)[96] were cultured at 37 °C with 5 % CO_2 in Dulbecco's modified Eagle's medium (DMEM + GlutaMAX™) supplemented with 10 % FBS (Invitrogen, Germany). The cells were grown to 80 % confluence, split with 0.25 % trypsin-EDTA and plated onto 13 mm glass coverslips, which had been pre-coated with poly-

l-lysine (0.0005 % in 1 x PBS) for 30 min. 3-4 days after t-toxin lentivirus infection, N-type mediated calcium currents were analyzed by whole-cell patch-clamp recordings. The coverslips were transferred to a custom made recording chamber with external bath solution containing (in mM): 140 NaCl, 10 $BaCl_2$, 1 $MgCl_2$, 10 HEPES, 15 Glucose (7.4 pH, 330 mosm/kg osmolarity). Patch pipettes (borosilicate glass) were pulled using a micropipette puller P-97 8 (Sutter Instruments, USA) and showed resistances of 3-4 Mohms. The internal pipette solution contained (in mM): 115 CsCl, 20 TEACl, 10 EGTA, 2 $MgCl_2$, 10 Hepes, 4 Mg-ATP, 0.5 Na-GTP (7.4 pH, 280 mosm/kg osmolarity). Whole-cell patch-clamp recordings were performed using an EPC9 patch-clamp amplifier (List Electronics, Germany). Voltage-gated calcium currents were recorded in response to voltage steps from -90 mV holding potential to test potentials between -80 and +50 mV (200 ms), and were quantified as peak currents in response to voltage steps from -90 mV to 0 mV. Ca^{2+}-currents were corrected by using the P/4 protocol. Serial resistance (R_s) was estimated from current transients induced by 10 mV depolarizing voltage commands from a holding potential of -90 mV. R_s was compensated by 70 % and cells with an R_s >20 Mohm or cells with >20 % changes of R_s during the experiment were excluded. Whole-cell membrane capacitance (C_M) was estimated by integration of the capacitive current transient and division by the respective stimulation voltage. Current densities (pA/pF) were expressed as the quotient of maximal current amplitude and C_M. Data acquisition and analysis were performed with software WinTida (Heka Electronic, Lambrecht, Germany).

2.4.3 Paired-pulse recordings in rat hippocampal culture

The action of t-toxin on synaptic activity was analyzed by quantification of evoked inhibitory postsynaptic currents (eIPSCs) and excitatory postsynaptic currents (eEPSCs) in rat hippocampal neuron cultures. The bath solution contained (mM): 105 NaCl, 3 KCl, 10 HEPES, 5 glucose, 2 $CaCl_2$ and 1 $MgCl_2$. The recording pipette solution contained (mM): 3 NaCl, 90 KCl, 5 EGTA, 5 HEPES, 5 glucose, 0.5 $CaCl_2$ and 4 $MgCl_2$. eIPSCs were isolated by blocking glutamatergic input (DNQX, 10 µM; DL-APV, 50 µM). For eEPSCs recordings QX314 (2mM) was added to the pipette solution and bicuculline (10µM), strychnine (1µM) and APV (100µM) were added to the bath solution. Evoked postsynaptic currents (eIPSCs and eEPSCs) were induced with a stimulation pipette in close proximity to presynaptic neurons (10 µA, 0.5 ms). To confirm recorded eIPSC and eEPSC currents, bicuculline or CNQX was routinely applied to block remaining GABAergic or glutamatergic currents,

respectively. The stimulation rate ensured recovery of presynaptic terminals from previous stimulation (intersweep interval: 30 s). Data acquisition and analysis were performed with software WinTida, Patchmaster and Fitmaster (HEKA Electronics, Darmstadt, Germany).

2.5 *In vivo* analyses

2.5.1 Stereotaxic injections

C57/Bl6 mice aged 7-11 weeks were anesthesized with intraperitoneal injection of a ketamine/xylazine mix (130 mg/kg and 10 mg/kg, respectively), and 10-15 min after the injection placed in a Benchmark stereotaxic frame with a Cunningham mouse adaptor (Leica Microsystems GmbH (myNeuroLab), Germany). The eyes were covered with Regephitel® ointment in order to prevent desiccation, and betaisodona solution was applied to the scalp for disinfection. After removing the scalp hair, the skull was exposed by placing an incision from the medial caudal part of the scalp to medial rostral and scraping off the periosteum with a scalpel. As a reference mark for the brain coordinates, which are used for exact spatial placement of the injection cannula, bregma, the anatomical point on the skull at which the coronal suture is intersected perpendicularly by the sagittal suture, was determined. Next, the second reference mark, termed lambda, which represents the point on the skull where the two parietal bones and the occipital bone are connected, was identified. In order to adjust the dorsal/ventral (D/V) positioning of the head, bregma and lambda were set to the same D/V coordinate. After also adjusting the head for the same D/V coordinates of the medial/lateral (M/L) axis on both hemispheres, the injection coordinates were determined and small holes in the skull were generated at these points using a micromotor drill with a 0.35 mm diameter bit. The dura mater was carefully opened with a sterile needle. For the injection of virus, glass PCR micropipets (Drummond, USA) were used, which had been pulled before with a microelectrode puller (Narashige, Japan) to create a narrow, fine tip of ~10-12 mm length. The so created cannula were filled from the backside with 2 µl of lentivirus, followed by 2.5 µl of mineral oil in a laminar flow hood by applying gentle suction with a 10 ml syringe at the tip. A metal plunger was inserted into the upper part of the prepared injection cannula and both were installed in the stereotaxic apparatus. The skull level adjacent to the drilled hole was set as D/V coordinate zero and the cannula was then moved to the injection coordinates and slowly lowered into the brain to the desired D/V coordinate. Subsequently, 1 µl of virus was injected using a MO-10 oil hydraulic micromanipulator (Narashige, Japan) with a flow rate of ~0.1 µl/min into the substantia nigra pars compacta (SNpc) at the following

coordinates (in mm): anterior-posterior (from Bregma): -2.6 and -3.1; lateral +1.1 and +1.3 and dorso-ventral (from the skull) -4.6 and -4.35. During the whole injection, the cannula was slowly moved dorsally (0.3 mm in total) in order to increase the injectable volume and area. Afterwards, the cannula was left in place for 10 min, allowing the virus solution to disperse in the tissue, before it was retracted slowly. The mouse was taken out of the adapter and the incision in the scalp was sewed with absorbable Marlin® polyglycolic acid sutures (Catgut, Germany). Finally, acridine ointment was placed on the suture to prevent infection and the mice were allowed to wake up from anesthesia under a warming lamp. After this, mice were kept single-caged for 7 days under S2 conditions, before cages, bedding and flasks were disinfected and the mice were transferred to new cages and kept under S1 conditions henceforth. All procedures were in accordance with ethical guidelines laid down by the local governing body and approved by Landesamt für Gesundheit und Soziales, Berlin.

2.5.2 Behavioural analysis

For rotational behavior analysis, stereotactically injected mice were transferred to a 50 x 25 cm arena under soft illumination during the day-light period 12-16 days after surgery. A fixed camera connected to a video tracking system (Biobserve Viewer) was used to count 360° circles of freely moving mice for 15 minutes, starting 5 minutes after i.p. injection of saline or apomorphine solution (0.5 mg/kg). Net-turns were determined by subtracting contraversive from ipsiversive turns.

2.5.3 Perfusion of mice

Intracardiac perfusion of mice was carried out under deep anesthesia 10 min after i.p. injection of ketamine/xylazine mix (260 mg/kg and 20 mg/kg, respectively). The absence of paw reflex was confirmed and the thoracic cage was opened by cutting along an oval shape starting from the sternum. A 27 gauge injection needle was placed into the left ventricle of the heart, followed by a small incision in the right ventricle. Mice were then perfused with 5 ml ice-cold 1 x PBS, followed by 10 ml 4 % PFA using a Reglo Digital tubing pump (Ismatec, Germany) with a flow rate of 1.3 ml/min. The brains were removed, post-fixed for 4 h in 4 % PFA and transferred to 20 % sucrose in 1 x PBS o/n.

2.5.4 Cryosections of perfused mouse brains

Sagittal or coronal brain sections were prepared using a SM2000R sliding microtome (Leica Microsystems GmbH, Germany). Perfused and sucrose incubated brains were fixed at the microtome stage on a layer of O.C.T.™ Tissue Tek (Sakura Finetek, Netherlands) by freezing through surrounding dry ice. 40 µm thick brain sections were generated by manually moving the microtome blade. The sections were transferred to cryosection buffer (0.1 M phosphate buffer with 25% glycerol and 25 % ethylene glycol, pH 7.4) and stored at -20 °C until further analysis.

2.5.5 Immunostaining of brain sections

For immunostaining of brain sections, the cryosection buffer was removed and the sections were washed two times in 1 x PBS. In order to reduce unspecific antibody binding, the sections were incubated in serum from the same species in which the secondary antibody was raised. Furthermore, Triton X-100, a nonionic detergent was used to solubilize membrane proteins in order to allow intracellular access to the antibodies. Therefore the blocking solution contained 10 % goat serum and 0.3 % Triton X-100 in 1 x PBS and was applied for 1h. For staining of dopaminergic neurons, sections were placed in 1/1000 anti-tyrosine hydroxylase (TH) antibody solution (monoclonal, mouse; Sigma-Aldrich, Germany) containing 1 % goat serum and 0.1 % Triton X-100 o/n. Afterwards, sections were washed two times in 1 x PBS for 10 min, and incubated with 1/1000 Cy3-conjugated goat anti-mouse secondary antibody (Jackson ImmunoResearch, UK) and 1/2000 DAPI for 2 h. Subsequently, slices were washed two times for 15 min in 1 x PBS and mounted on object slides with ImmuMount™ (Thermo Scientific, USA). Co-staining of EGFP and TH in brain sections was achieved by simultaneous incubation o/n in 1/1000 anti-GFP (polyclonal, rabbit; Invitrogen, Germany) and 1/1000 anti-TH (monoclonal, mouse; Sigma-Aldrich, Germany) in 1 x PBS with 0.1 % Triton X-100. This was followed by two 10 min washing steps in 1 x PBS and incubation for 2 h in 1/1000 Alexa Fluor[®] 488 goat anti-rabbit IgG with 1/1000 Cy3 goat anti-mouse IgG and 1/2000 DAPI in 1 x PBS with 0.1 % Triton X-100. Afterwards, slices were washed two times for 15 min in 1 x PBS and mounted on object slides with ImmuMount™ (Thermo Scientific, USA). Images were acquired using a Leica SP5 confocal microscope with Leica application suite (LAS) software and processed with Adobe Photoshop CS3.

2.5.6 Quantification of immunostained brain sections

Images of brain sections were acquired with a Keyence Biozero BZ8100E fluorescence microscope with 4 x objective and subsequent haze-reduction using the system software. The images were analyzed using ImageJ software with the colocalization plug-in, after creating binary images with fixed thresholds. Areas of GFP expression, TH staining and overlaying areas of TH and GFP staining were measured and the percentage of TH stained areas with GFP expression was calculated in Microsoft Excel 2007.

3.   Results

3.1   Targeting nicotinic acetylcholine receptors with t-toxins

3.1.1   Toxin selection

α-conotoxin GID was selected for this study because of the reported selectively for the most abundant neuronal nAChR subtypes, namely α7 and α4β2 with IC_{50} values of 4.5 and 152 nm, respectively[28]. The activity at the α3β4, α4β4 and muscle nAChRs was reported to be at least 1000-fold less[28]. Therefore, t-GID was generated in order to create a new genetic method for blocking the most abundant nAChRs, allowing the investigation of nAChR function and their contribution in different neuronal circuits.

3.1.2   Composition of GID t-toxin variants

In order to assess the influence of the linker length between α-conotoxin GID and the PDGR-receptor transmembrane domain (TM domain) on the toxin activity, four different constructs were generated (**Fig.9**). The longer linkers carried Gly-Asn repeats in order to provide rotational freedom and therefore high flexibility for facilitated toxin binding to the channel. Linker lengths were in the range of 10-69 amino acids (**Table 15**).
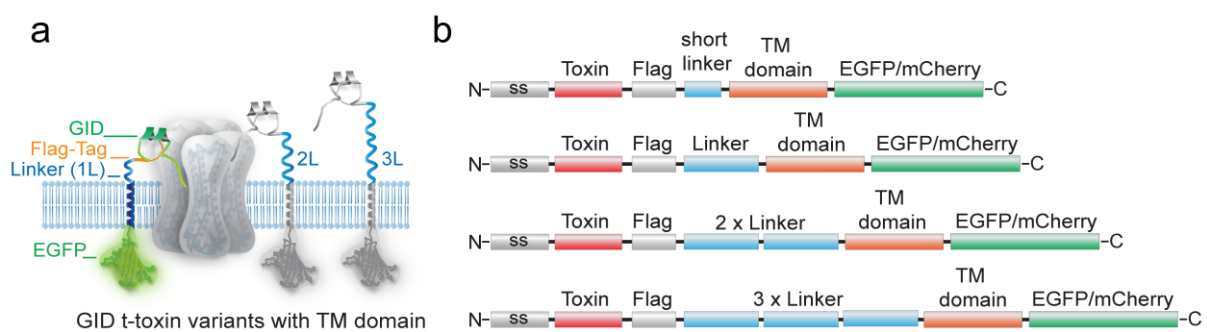
Figure 9. Variants of t-GID generated in this work.

(**a**) Illustration of t-GID constructs with different linker lengths binding to a nAChR. (**b**) Schematic representation of modular composition of t-GID variants containing the lynx1 secretion signal (ss), a flag epitope for immunostaining, different linker sizes, the PDGF-receptor transmembrane domain (TM domain) and the fluorescent marker EGFP(green) or mCherry (red).

Toxin name	Linker name	Length [aa]	sequence
GIDs-PE/PC	Short linker	10	D-[A]^2-[G]^2-ALCNA
GID1L-PE/PC	Long linker	23	[A]^3-[GN]^7-GDGNGG
GID2L-PE/PC	2 x Long linker	46	([A]^3-[GN]^7-GDGNGG)^2
GID3L-PE/PC	3 x Long linker	69	([A]^3-[GN]^7-GDGNGG)^3

Table 15. Lengths and sequences of used linkers in the t-GID constructs.

3.1.3 Expression analyses of t-GID

3.1.3.1 Immunocytochemical analyses

Before functional assays were carried out, the expression and localization of t-GID was analyzed in transfected and transduced mammalian cell culture (**Fig.10**) and rat hippocampus culture (**Fig.11**). HeLa cells were seeded on glass coverslips in 24 well cell-culture plates and transfected with t-GID variants using Lipofectamine™ 2000 (Invitrogen, Germany), or t-GID lentivirus. Immunostaining of the fixed, but not permeabilized, cells shows bright fluorescence at the plasma membrane, which colocalizes with the t-GID-fused EGFP/mCherry fluorescent markers in merged images.
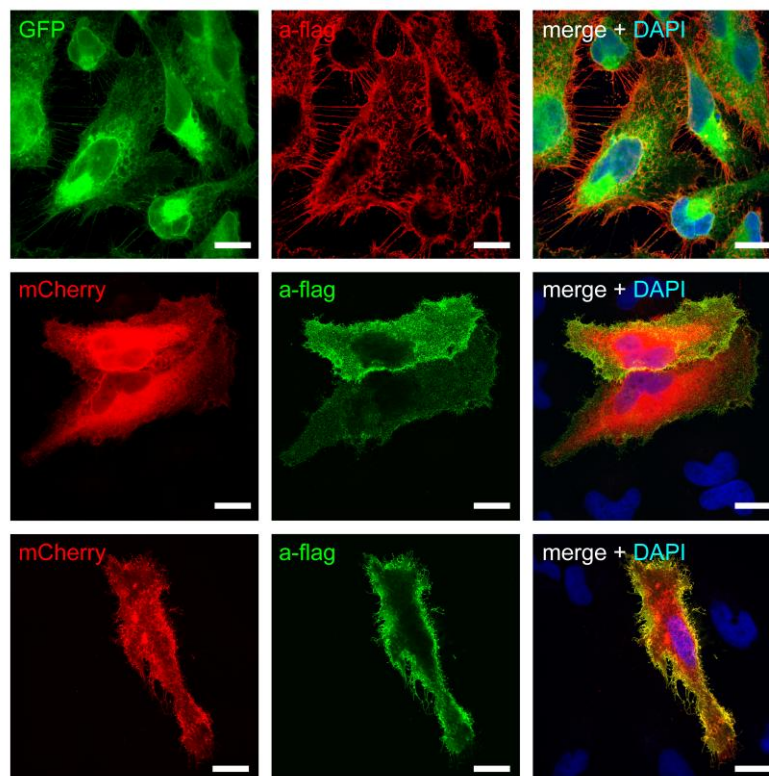
Figure 10. t-GID expression and detection at the plasma membrane in HeLa cells.

HeLa cells, transduced with GIDs-PE (upper lane), GIDs-PC (middle lane) or GIDl-PC (lower lane), show robust EGFP/mCherry fluorescence and bright anti-flag immunostaining in non-permeabilized cells, indicative of membrane localization. Blue represents nuclear DAPI staining. Scale bars, 10 µm.
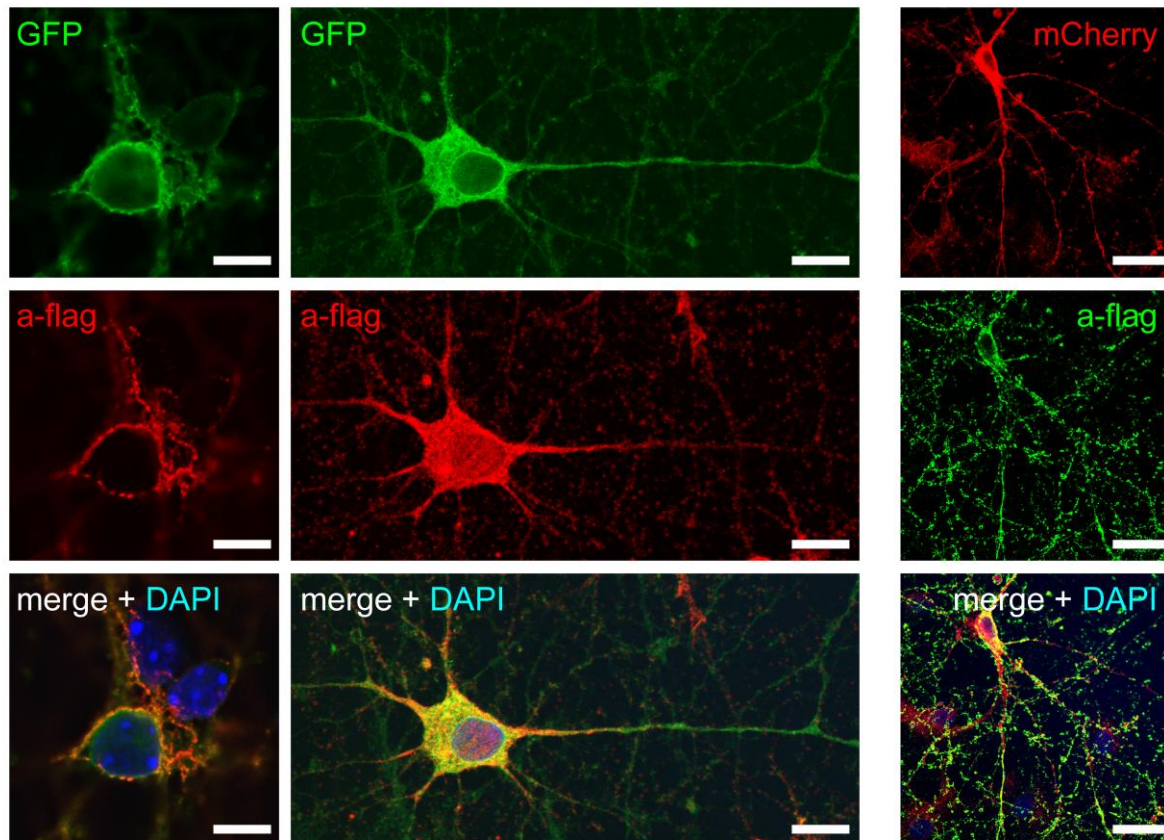
Figure 11. t-GID immunostaining in transduced rat hippocampus culture.

Rat hippocampal neurons were infected with GIDs-PE (left and middle column) and GIDs-PC (right column) and immunostained against the flag epitope (a-flag) in non-permeabilized cells. Cells show strong t-toxin expression and anti-flag staining, indicative of membrane integration in somatodendritic as well as axonal regions. Nuclear DAPI staining is represented in blue. Scale bars, 10 μm (left and middle column) and 25 μm (right column).

3.1.3.2   Western Blot analysis

Expected molecular weights of expressed t-GID fusion-proteins were verified by SDS-PAGE and subsequent Western Blot analysis. Protein extracts were prepared from stably transduced HeLa cells, which were generated by infection with t-GID lentivirus with a MOI 5 (multiplicity of infection: virus particles/cell). The protein extracts (10 μg) were subjected to SDS gel electrophoresis, transferred to a PVDF membrane and visualized by anti-GFP immunodetection. The results confirmed the expected molecular weights of 38 kDa (GIDs-PE) and 39 kDa (GID1L-PE) and showed a higher proportion of staining in membrane fractions than in cytosolic fractions, indicating predominant membrane localization of expressed t-GID (**Fig.12**).
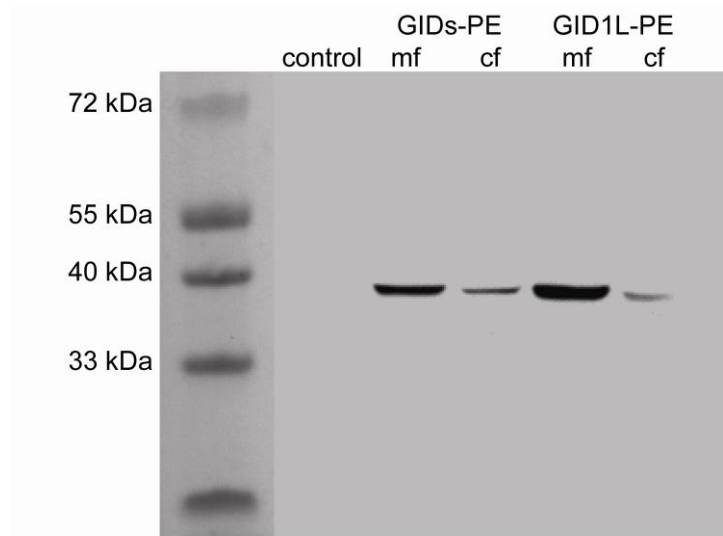
Figure 12. Western Blot analysis of t-GID variants.

Anti-GFP staining of protein extracts from t-GID stably transduced HeLa cells detects molecular weights of ~38 kDa, as expected by in-silico analysis. The higher proportion of staining in the membrane fraction (mf) compared to cytosolic fraction (cf) indicates a predominant membrane localization of the expressed t-GID.

3.1.4 Functional analysis in *Xenopus* oocytes

The functionality of the different t-GID constructs was analyzed by whole-cell patch-clamp recordings in *Xenopus laevis* oocytes. For this purpose, oocytes were co-injected with cRNA of both nAChR subunits and t-toxins. Currents were induced by nicotine application. As shown in **Figure 13**, the blocking capability of t-GID on α7 nAChR mediated currents was highly dependent on the length of the linker sequence between toxin and TM domain (see also **Fig.9**). For the short (10 aa, GIDs-PE) and 1x long (23 aa, GID1L-PE) linker variants, the currents were almost completely blocked, resulting in reduction of peak current amplitudes by 99.3 ± 0.3 % and 98.7 ± 0.9 %, respectively. Whereas longer linkers (GID2L-PE and GID3L-PE, 46 aa and 69 aa) had less or no significant effect on the current (77.0 ± 7.5 % and 34.2 ± 22.1 % of block, respectively).
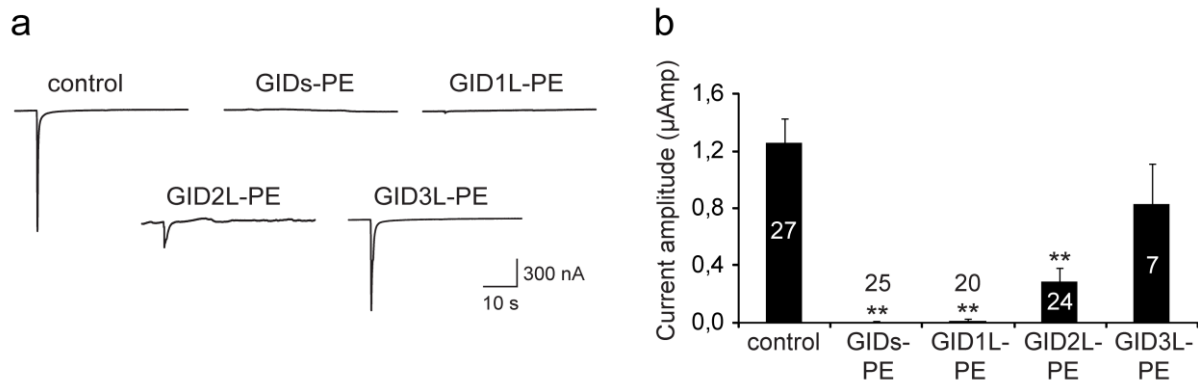
Figure 13. Blocking activity of t-GID variants on α7 nAChR currents in *Xenopus* oocytes.

Electrophysiological whole-cell patch-clamp recordings of *Xenopus* oocytes co-injected with cRNA of t-GID and α7 nAChR subunits show block of nicotine-induced currents dependent on the linker length. (**a**) Representative traces and (**b**) quantification of peak current amplitudes show complete block of nicotine-induced α7 nAChR currents for short (10 aa, GIDs-PE) and long (23 aa, GID1L-PE) linker variants, while longer linkers (GID2L-PE and GID3L-PE, 46 aa and 69 aa) lead to decreased blocking capability. Data represent mean values ± s.e.m. Number of recorded cells displayed in/above columns.

Next, the blocking capability of t-GID variants on α3β4 nAChR mediated currents was analyzed. Despite the reported low affinity of GID on α3β4 nAChR[28], t-GID expression resulted in 61.0 ± 6.3 % and 55.5 ± 6.7 % block of currents for the short (GIDs-PE) and 1x long (GID1L-PE) linker variants, respectively (**Fig.14**). The influence of linker lengths was also detectable for α3β4 nAChR, similarly to the measurements on α7 nAChR. Thus, constructs with longer linkers (GID2L-PE and GID3L-PE) showed no blocking activity on α3β4 mediated currents (**Fig.14**).

.
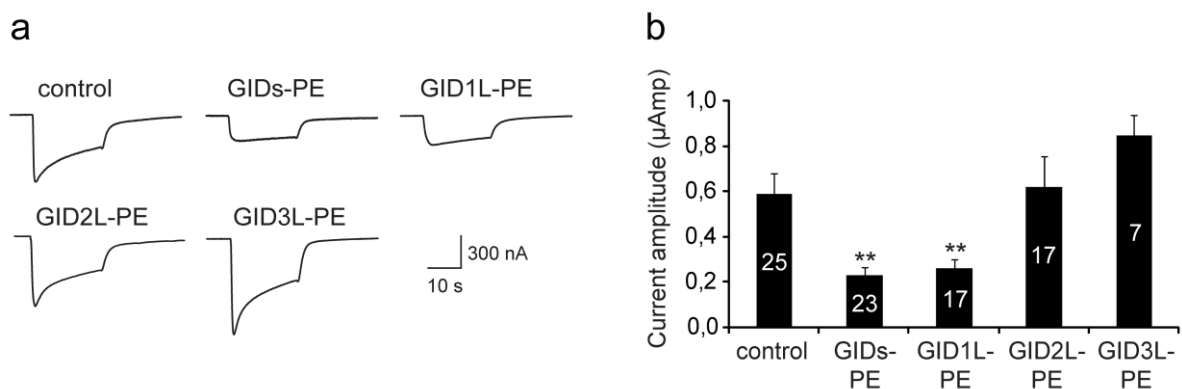
Figure 14. Blocking activity of t-GID variants on α3β4 nAChR currents in *Xenopus* oocytes.

Electrophysiological whole-cell patch-clamp recordings of *Xenopus* oocytes co-injected with cRNA of t-GID and α3β4 nAChR subunits show partial block of nicotine-induced currents dependent on the linker length. (**a**) Representative traces and (**b**) quantification of peak current amplitudes display partial block of nicotine-induced α3β4 nAChR currents for short (10 aa, GIDs-PE) and long (23 aa, GID1L-PE) linker variants, while longer linkers (GID2L-PE and GID3L-PE, 46 aa and 69 aa) show no blocking effect. Data represent mean values ± s.e.m. Number of recorded cells displayed in/–above columns.

Besides α7 and α3β4 nAChRs, α-conotoxin GID has previously been reported to be able to bind to α4β2 nAChRs (IC_{50}: 152 nM)[28]. Therefore, the blocking activity of t-GID variants was also assessed in oocytes co-injected with α4β2 nAChR cRNA. However, none of the t-GID constructs showed block of the nicotine-induced current, irrespective of the linker length (**Fig.15**).
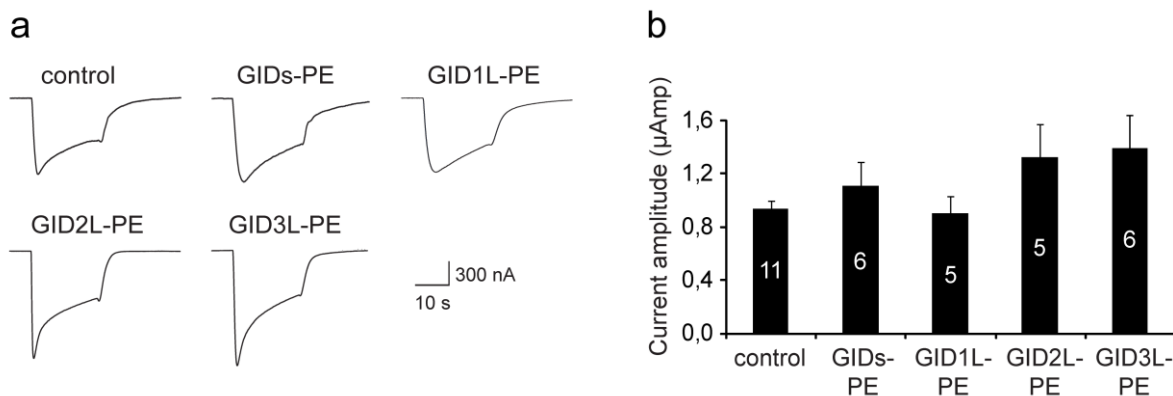
Figure 15. Blocking activity of t-GID variants on α4β2 nAChR currents in *Xenopus* oocytes.
Electrophysiological whole-cell patch-clamp recordings of *Xenopus* oocytes co-injected with cRNA of t-GID and α4β2 nAChR subunits show no block of nicotine-induced currents, independent of the linker length. (**a**) Representative traces and (**b**) quantification of peak current amplitudes show no block of nicotine-induced α4β2 nAChR currents for all t-GID variants. Data represent mean values ± s.e.m. Number of recorded cells displayed in/above columns.

Taken together, these results show a very high blocking activity of GIDs-PE and GID1L-PE on α7 nAChR (>98 %) and to a smaller extend also on α3β4 nAChR (>55 %), whereas longer linkers as in GID2L-PE and GID3L-PE impaired, or even completely abolished the toxin activity. Contrary to previous reports[28], none of the t-GID variants was able to reduce α4β2 nAChR mediated currents. However, this new selectivity obtained with t-GID opens the possibility for future studies to use GIDs-PE for blocking α7 nAChR and partially also α3β4 nAChR without affecting α4β2 nAChRs, in order to dissect these channels and investigate their contribution in different neuronal circuits.

3.2   Silencing neurotransmission with t-toxins by targeting calcium channels

3.2.1 Toxin selection

To achieve specific and potent inhibition of $Ca_v2.1$ and $Ca_v2.2$ mediated calcium currents, the best characterized venom peptides with high blocking specificities for these channels, namely conotoxins MVIIA[30,32] and MVIIC[34], as well as spider agatoxins AgaIIIA and AgaIVA[37,39,40] were selected. These toxins were integrated in transmembrane domain containing (PE: PDGF-receptor transmembrane domain-EGFP; PC: PDFR-TM-mCherry) or GPI anchored (VG: Venus-GPI) constructs (**Fig.1**,**8**). Resulting constructs were designated MVIIA-PE (green fluorescence), MVIIA-PC (red fluorescence), MVIIC-PE, AgaIVA-PE, AgaIVa-VG and AgaIIIA-VG.

3.2.2 Expression analyses of calcium channel t-toxins in mammalian cells

HeLa cells and HEK 293T cells were transduced with t-toxins (no toxin-PE, MVIIA-PE/PC, AgaIVA-VG) with a MOI 5 and cultured for several days to weeks. For immunocytochemical analysis, cells were seeded on coated glass coverslips and stained without permeabilization, using an antibody directed against the flag epitope. Images acquired with a confocal microscope revealed bright EGFP or mCherry fluorescence and overlapping anti-flag staining at the membrane, indicative of a membrane localization of t-toxins (**Fig.16a**). In order to confirm the expected molecular weights of expressed t-toxins, Western Blot analysis of protein extracts from transduced HEK293T cells was performed. Immunodetection with anti-flag antibody showed signals in the expected size range between ~35-40 kDa (**Fig.16b**). AgaIVA-VG samples showed a double band (38 kDa and 36 kDa), consisting of unprocessed peptide with cleaved hydrophobic signal sequence for GPI attachment (36 kDa), and the mature form with GPI-anchor attached (38 kDa) (**Fig.16b**).
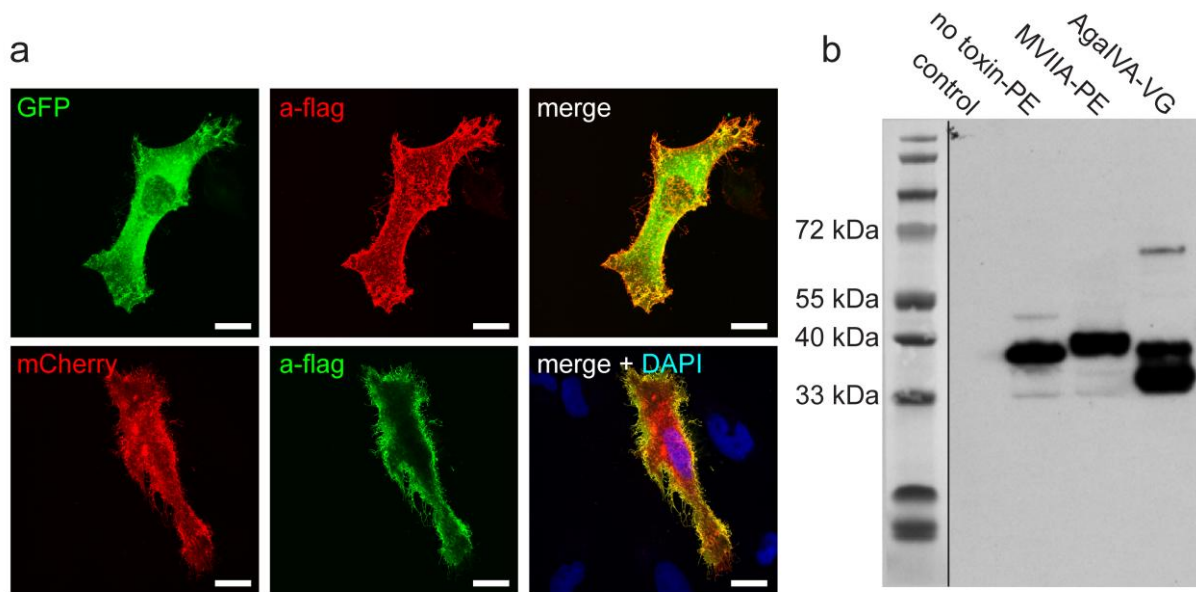
Figure 16. Immunostainings of t-toxins and Western Blot analysis

(**a**) HeLa cells transduced with MVIIA-PE (upper panel) or MVIIA-PC (lower panel) show direct fluorescence and are positive for flag immunostaining without prior cell permeabilization, indicative of membrane localization of t-toxins. Scale bars, 10 µm. (**b**) Western Blot analysis directed against the flag-tag of protein extracts from transduced HEK293T cells indicate expected molecular weights of expressed t-toxins (no toxin-PE: 36,5 kDa, MVIIA-PE: 39,2 kDa, AgaIVA-VG: 38 kDa and 36 kDa (double band shows unprocessed peptide with cleaved hydrophobic signal sequence for GPI attachment, and the mature form with GPI anchor attached).

3.2.3   Expression analyses of calcium channel t-toxins in neurons

Transduction of cultured rat hippocampal neurons with calcium channel t-toxins and subsequent immunostainings directed against the flag-epitope 3-5 days after infection, showed bright EGFP direct fluorescence and strong, overlapping anti-flag signal at the cell membrane (**Fig.17**). In addition, transduction with the red fluorescent variant MVIIA-PC resulted in bright red fluorescence and expected anti-flag immunostaining (**Fig.18**). Importantly, efficient double-infection of neurons with both t-toxins MVIIA-PC (red) and AgaIVA-VG (green), was also achieved in rat hippocampus culture, in which most of the neurons expressed both t-toxins (**Fig.18**).
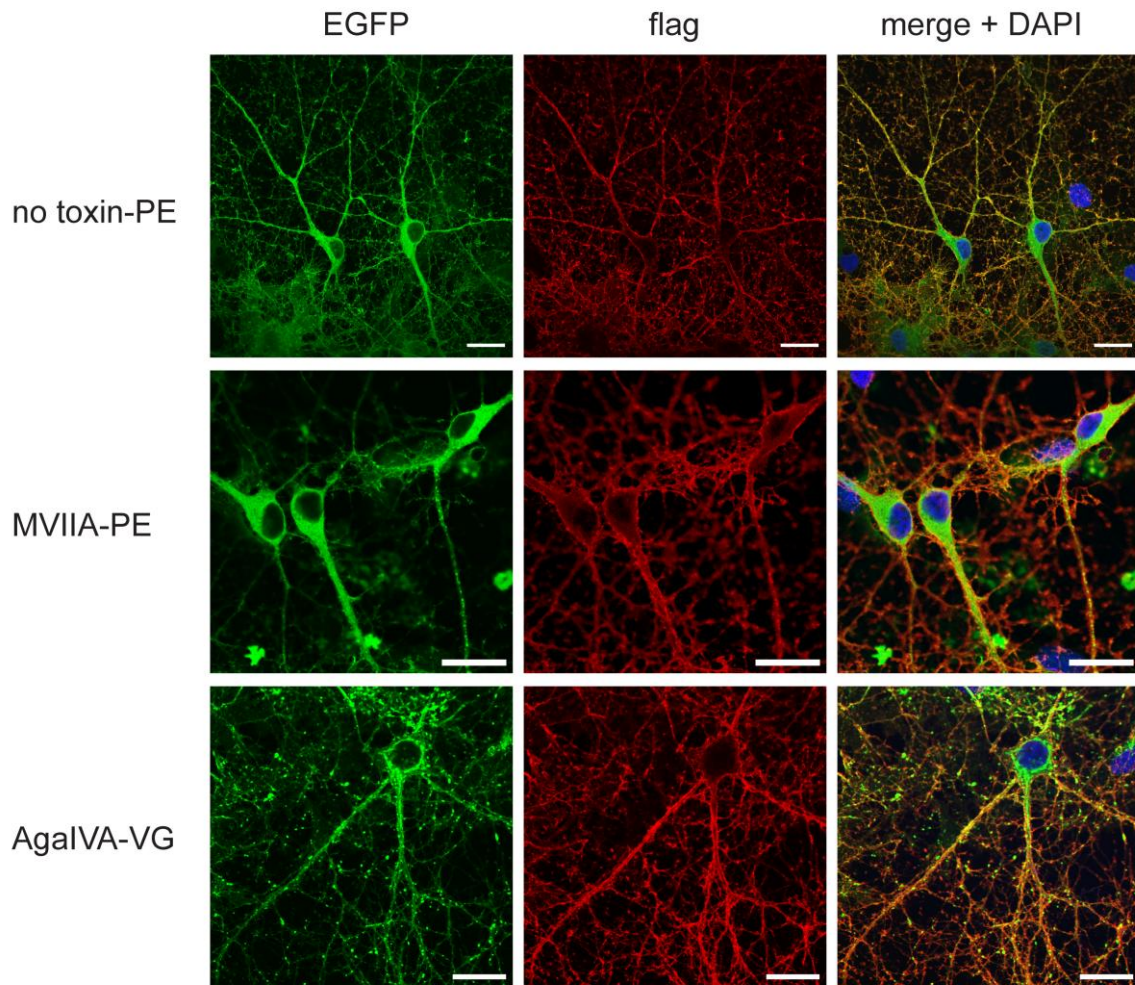
Figure 17. Expression analyses of green fluorescent t-toxins in rat hippocampal neurons.

Direct fluorescence of EGFP (green), flag-epitope immunofluorescence (red) and merged images in transduced neurons of rat hippocampus culture. Cells were not permeabilized, thus anti-flag staining indicates membrane localization of t-toxins. Cells show strong t-toxin expression and presence in somatodendritic as well as axonal region. DAPI staining (blue) indicates cell nuclei. Scale bars, 20 µm.
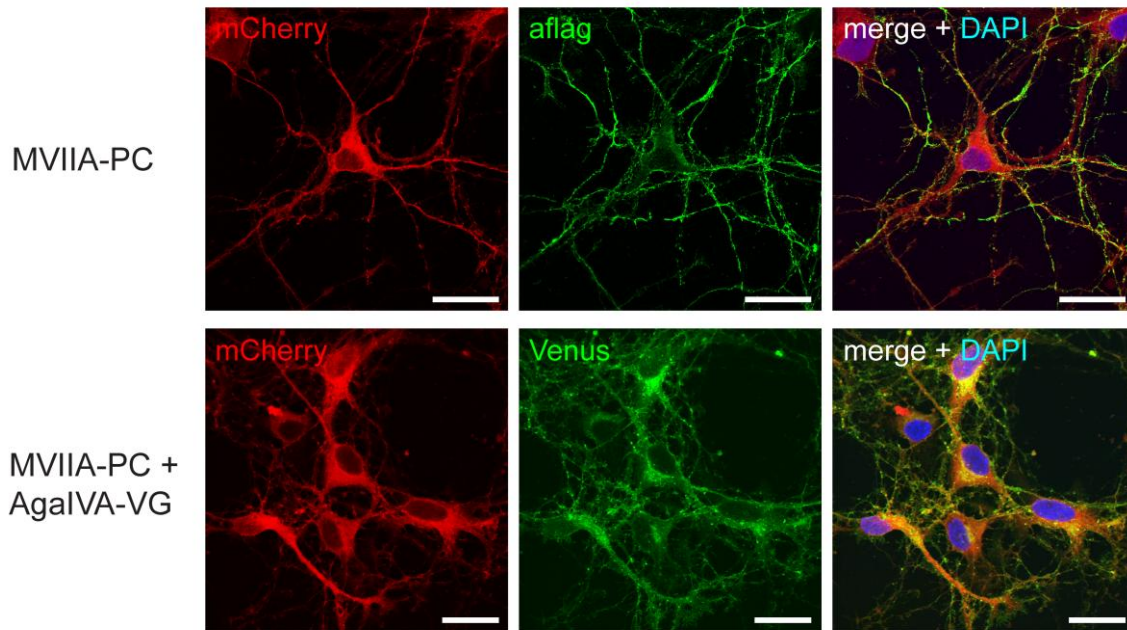
Figure 18. Expression analyses of red fluorescent t-toxins in rat hippocampal neurons.

Direct fluorescence of mCherry (red), flag-epitope immunofluorescence (green) and merged image in MVIIA-PC transduced neuron (upper panel). In co-infection of MVIIA-PC and AgaIVA-VG, both mCherry (red) and Venus (green) fluorescence is detectable, and colocalizes in merged image (lower panel), indicating efficient expression of both t-toxins. DAPI staining (blue) detects cell nuclei. Scale bars, 25 µm.

3.2.4   Functional *in vitro* analyses

3.2.4.1   Electrophysiological recordings in HEK293-Ca$_v$2.2 cells

The functional activity of calcium channel t-toxins was first assessed in patch-clamp recordings in HEK293 cells stably expressing the channel subunits α_{1B}, $\beta 3$ and $\alpha 2\delta$ that form Ca$_v$2.2[96]. Expression of t-toxins resulted in a nearly complete block of voltage-gated calcium currents in cells infected with MVIIA-PE (95 ± 1 % decrease in current density), as expected given the high affinity of soluble MVIIA for Ca$_v$2.2 channels[30] (**Fig.19**). Furthermore, calcium currents were unaffected by lentiviral expression of AgaVIA-VG, indicating no cross-reactivity of this t-toxin with Ca$_v$2.2 channels, as anticipated by the specificity of AgaIVA for Ca$_v$2.1[97] (**Fig.19**). Despite the reported affinity of AgaIIIA for Ca$_v$1 and Ca$_v$2.2[98], and of MVIIC for both Ca$_v$2.1 and Ca$_v$2.2[97], AgaIIIA-VG and MVIIC-PE expression in HEK293-Ca$_v$2.2 cells showed no blocking activity.
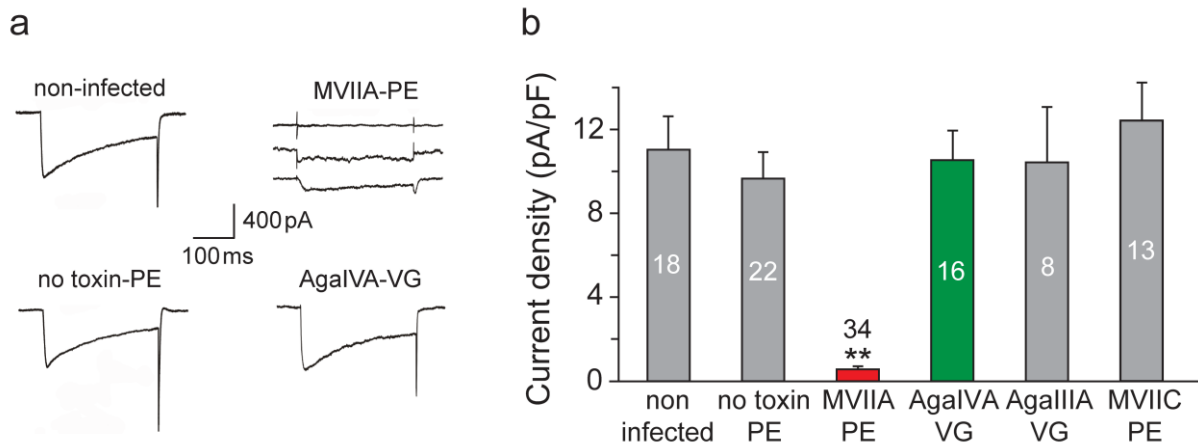
Figure 19. Electrophysiological analyses of t-toxin activity in a HEK293-Ca$_v$2.2 stable cell line.

HEK293-Ca$_v$2.2 cells expressing the Ca$_v$2.2 calcium channel were transduced with the indicated lentivirus (**a**) Representative traces of voltage-gated calcium currents show no changes between non-infected cells and cells infected with the control lentivirus (no toxin-PE) or AgaIVA-VG lentivirus, whereas infection with MVIIA-PE results in an almost complete block of the current. (**b**) Current density quantification shows highly significant block of currents only in MVIIA-PE infected cells (95 +/- 1% decrease), reflecting the inhibition of Ca$_v$2.2 calcium channels. P = 2 x 10^{-7}. No effect of AgaIVA-VG was observed, as expected by its specificity for Ca$_v$2.1. Despite the reported affinity of AgaIIIA and MVIIC for both Ca$_v$2.1 and Ca$_v$2.2, AgaIIIA-VG and MVIIC-PE showed no blocking activity.

In order to demonstrate the cell-autonomy of t-toxins and exclude the possibility that they are released from the membrane, co-cultures of non-infected and MVIIA-PE infected HEK293-Ca$_v$2.2 cells were generated and grown together for >72 h. Electrophysiological analyses of the mixed cultures indicated that calcium currents are only inhibited in the cells that express MVIIA-PE (91 +/- 1 % decrease in current density, P = 0.000001), and not in neighboring non-infected cells (7 +/- 9 % decrease in current density, P = 0.70) (**Fig.20**).
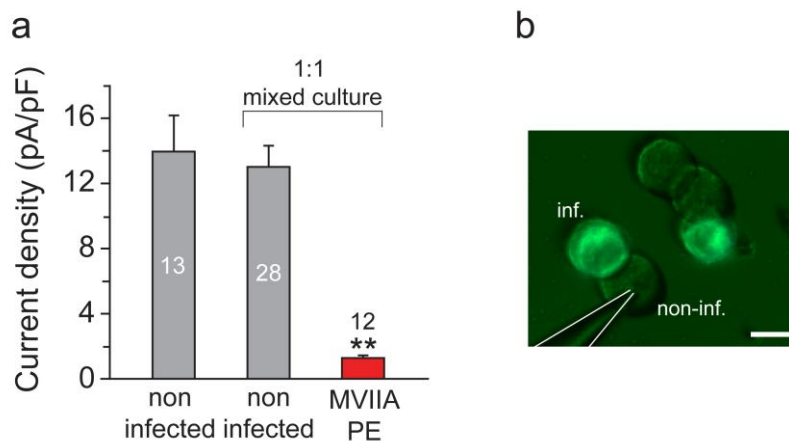
Figure 20. Analysis of t-toxin cell-autonomous mode of action.

(**a**) Voltage-gated calcium recordings in mixed cultures of non-infected and MVIIA-PE infected HEK293-Ca$_v$2.2 cells show block of currents only in t-toxin expressing cells, but not in adjacent, non-infected cells. (**b**) Mixed cultures of HEK293-Ca$_v$2.2 cells used for recordings, showing MVIIA-PE infected (green) and non-infected cells. Scale bar, 10 μm.

3.2.4.2   Electrophysiological recordings in rat hippocampal neurons

The activity of t-toxins in mammalian neurons was tested in hippocampal cultures, a model system, in which the properties of VGCC types and their contribution to neurotransmission have been extensively studied[99-101]. In order to quantify the probability of synaptic NT release, as a measure of the inhibition of $Ca_v2.1$ and $Ca_v2.2$ calcium currents, presynaptic neurons were stimulated consecutively with two short pulses and the amplitudes of the first (ePSC1) and second postsynaptic responses (ePSC2) were recorded in coupled postsynaptic neurons (**Fig.21**). The resulting paired-pulse ratio (PPR), which represents the ratio of the second postsynaptic response ($ePSC_2$) over the first postsynaptic response ($ePSC_1$) is used as a measure of presynaptic NT release[102] (**Fig.21**, **Par.4.3**). PPR values <1.0 indicate paired-pulse depression (PPD), whereas values >1.0 reflect paired-pulse facilitation (PPF). If PPD or PPF occurs at a given synapse depends on the type of synapse[81].
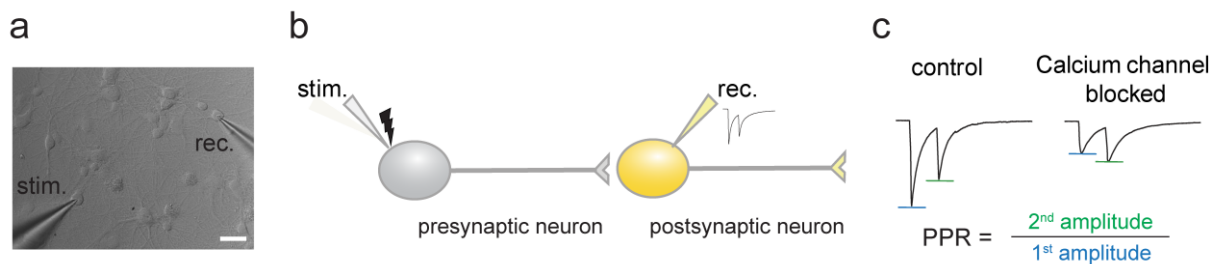
Figure 21. Schematic representation of paired-pulse recordings in rat hippocampus culture.
(**a**) Phase-contrast image of a stimulated presynaptic and a recorded postsynaptic neuron in whole-cell patch-clamp configuration. Scale bar, 30 µm. (**b**) Illustration of stimulation and recording condition. (**c**) Example traces of voltage-gated calcium currents, induced by paired-pulse stimulation, show pair pulse depression (PPD) in control conditions and pair pulse facilitation (PPF) if calcium channels are blocked. The paired-pulse ratio (PPR) represents the ratio of 2nd amplitude to 1st amplitude and thus is a measure of presynaptic neurotransmitter release.

In our hippocampal neuronal cultures with the chosen recording conditions, we found PPD to be the common form of response to paired-pulse stimulation in control (non-infected) neurons. This effect can be seen in representative traces of paired-pulse responses (**Fig.22**), and quantifications of first amplitudes (**Fig.23a**) and PPRs (**Fig.23b**). Furthermore, no changes between non-infected neurons and neurons infected with the no-toxin-PE control could be observed. Both control conditions (non-infected and no toxin-PE infected) show large first postsynaptic responses and smaller second responses with low PPR ratios ($eIPSC_2/eIPSC_1 < 0.6$) (**Fig.22,23**).

In contrast, neuronal cultures transduced with MVIIA-PE or AgaIVA-VG lentivirus showed significantly reduced first postsynaptic currents (**Fig.22**,**23a**) and higher PPR ($eIPSC_2/eIPSC_1$ > 0.8) (**Fig.23b**) with a tendency to paired-pulse facilitation, indicative of altered release probability. The soluble toxins MVIIA and AgaIVA were used to confirm the t-toxin activity, as they have been reported to block $Ca_v2.2$ and $Ca_v2.1$ channels, respectively, in cultured hippocampal neurons[99,101]. As shown in **Figure 23**, currents in naive neurons, in which these calcium channels have been blocked by exposure to the soluble MVIIA and AgaIVA toxins (hatched columns), closely resemble currents in the corresponding t-toxin-expressing neurons (solid colored columns), demonstrating that the t-toxins retain their ion channel specificity. In addition, no further inhibition of calcium currents was observed by application of soluble toxins to neurons expressing MVIIA-PE and AgaVIA-VG (hatched columns; **Fig.23**), indicating that the t-toxins can completely inhibit all targeted VGCCs present in a neuron.

In order to assess if simultaneous inactivation of $Ca_v2.1$ and $Ca_v2.2$ channels could be achieved with t-toxins, neurons were transduced with both MVIIA-PC and AgaIVA-VG in a 1:1 ratio. When a virus suspension with the same MOI as in single infections was used, i.e. MOI=2.5 virus paticles/cell, postsynaptic currents were reduced by 91 ± 2 % (**Fig.23a**) and very small paired-pulse responses with high PPR (1.36 ± 0.14) were obtained (**Fig.23b**). However, when the MOI was increased to 7.5 virus particles/cell, inhibitory postsynaptic currents could no longer be detected, indicating complete silencing of GABAergic neurotransmission in the chosen recording conditions (**Fig.22**,**23**).
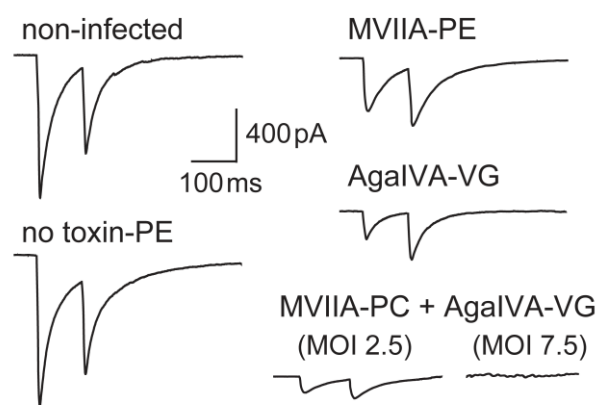
Figure 22. Example traces showing t-toxin induced block of calcium channels.

Traces of paired-pulse recordings in transduced rat hippocampal neurons indicate the marked decrease of eIPSC amplitudes and the shift of the paired-pulse ratio in single and double infections of t-toxins. In contrast, no changes between non-infected neurons and neurons infected with the no-toxin-PE control were observed.
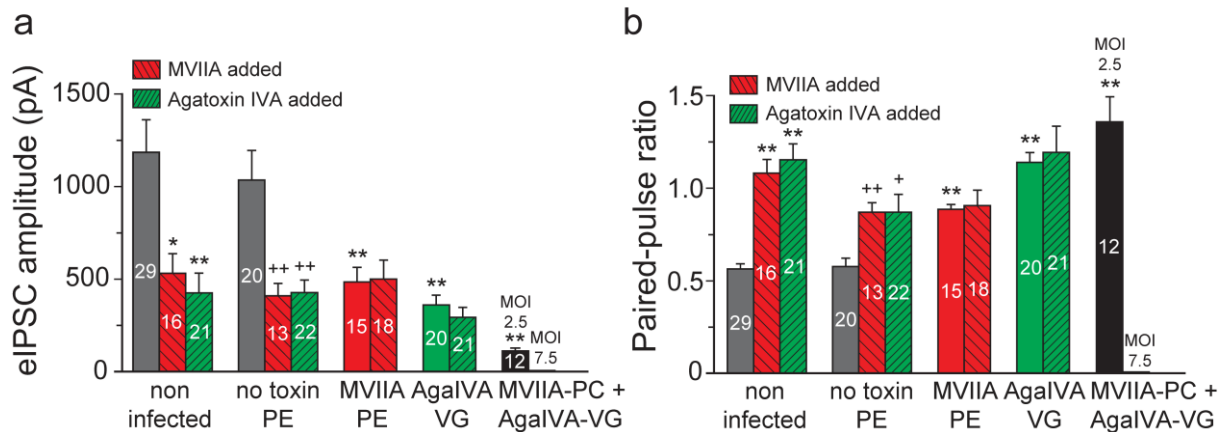
Figure 23. T-toxins inhibit GABAergic neurotransmission in rat hippocampal neurons.

Paired-pulse recordings show increased (**a**) eIPSC first amplitudes and (**b**) paired-pulse ratios in neurons transduced with MVIIA-PE (solid red columns), and AgaIVA-VG (solid green columns). Addition of soluble toxins by bath application (soluble MVIIA: red hatched columns, AgaIVA: green hatched columns) caused significant inhibition of currents in control and no toxin-PE neuronal cultures, whereas currents of cells infected with t-toxins were unchanged by addition of soluble toxins. Co-infection of MVIIA-PC and AgaIVA-VG with equal virus load as single infections (MOI = 2.5) produced further decrease of amplitude and increase in PPR, while a MOI of 7.5 resulted in complete silencing of neurotransmission, i.e. responses to the stimulation were absent, indicative of blocking GABAergic transmission. $*^{/+}P \leq 0.05$; $**^{/++}P \leq 0.005$; $*$ compared to non-infected control; $+$ compared to corresponding t-toxin infection. Number of recorded cells is shown in/above columns.

Next, the ability of t-toxins to also interfere with glutamatergic neurotransmission was measured by paired-pulse recordings of evoked excitatory postsynaptic currents (eEPSCs). It could be shown that glutamatergic synaptic transmission is impaired in neurons transduced with both t-toxins at MOI 5 ($eEPSC_1$ reduction of 80 ± 4 % and PPR increase of 102 ± 7 %; (**Fig.24**), in a manner comparable to GABAergic transmission (eIPSCs).

These results demonstrate that the combined use of MVIIA-PE/PC and AgaIVA-VG t-toxins selective for $Ca_v2.1$ and $Ca_v2.2$ channels is an effective strategy for interfering with GABAergic, as well as glutamatergic neurotransmitter release at presynaptic terminals. Furthermore, when the expression of both t-toxins in the target cells is ensured, i.e. by using adequate levels of virus load, complete silencing of neurotransmission can be achieved.
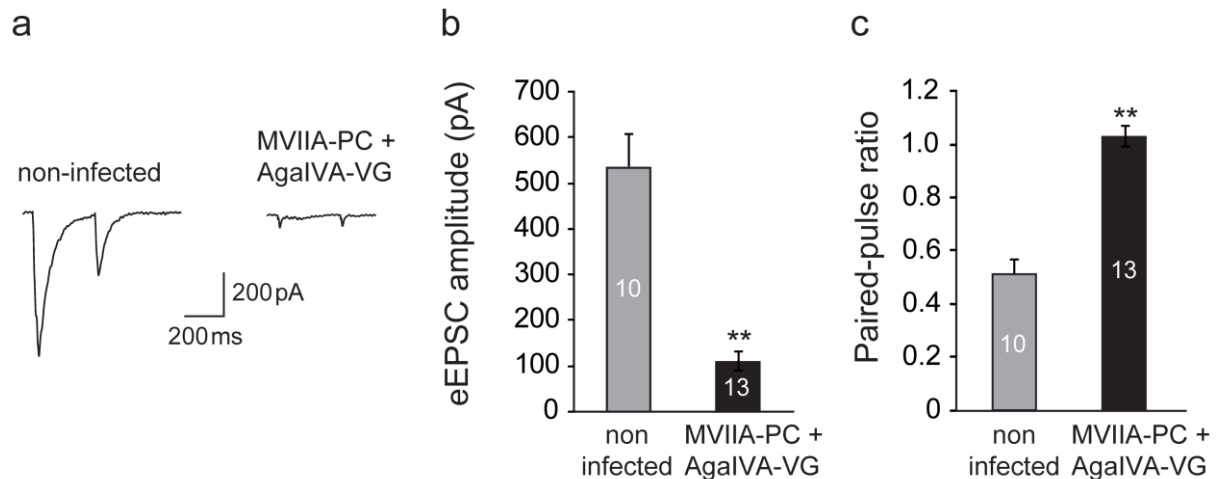
Figure 24. T-toxins inhibit glutamatergic transmission in rat hippocampal neurons.
Paired-pulse recordings of rat hippocampal neurons showed (**a,b**) decrease of eEPSC amplitudes and (**c**) increase in PPR in MVIIA-PC and AgaIVA-VG co-infected neurons (MOI 5), indicative of interference with glutamatergic transmission similarly to inhibition of GABAergic transmission (Fig.23). P=0.0003 (**b**), and P=0.000003 (**c**). Number of recorded cells are shown in the columns.

To analyze the possibility of blocking both $Ca_v2.1$ and $Ca_v2.2$ with a single toxin, we used ω-conotoxin MVIIC, which has been reported to inhibit both $Ca_v2.1$ and $Ca_v2.2$[97]. The generated t-toxin MVIIC-PE was tested by eIPSC paired-pulse recordings in transduced rat hippocampal neurons. However, no significant differences in first amplitude or PPR could be observed (**Fig.25**). Similarly, Agatoxin IIIA, a toxin with affinities for L- (Ca_v1), N- ($Ca_v2.2$), P/Q- ($Ca_v2.1$), and R-type ($Ca_v2.3$) channels[36,98], was used to generate the construct AgaIIIA-VG. Infected cells showed no significant changes of first amplitudes, but increased PPR of 0.75 ± 0.04 (P=0.045). Because of the failure of reaching clear and satisfying block of calcium channels with MVIIC-PE or AgaIIIA-VG in HEK293-$Ca_v2.2$ cells (see **Fig.19**) and in rat hippocampus culture (**Fig.25**), the work with these two constructs was not further pursued. In contrast, when AgaIVA was subcloned into the transmembrane construct version to generate AgaIVA-PE, transduced neurons showed decreased first amplitudes (71 ± 3 % decrease) and increased PPR (1.08 ± 0.07), comparable to AgaIVA-VG. However, anti-flag immunodetection of AgaIVA-PE was much weaker than for AgaIVA-VG (data not shown). Therefore, AgaIVA-VG was chosen for further analysis.
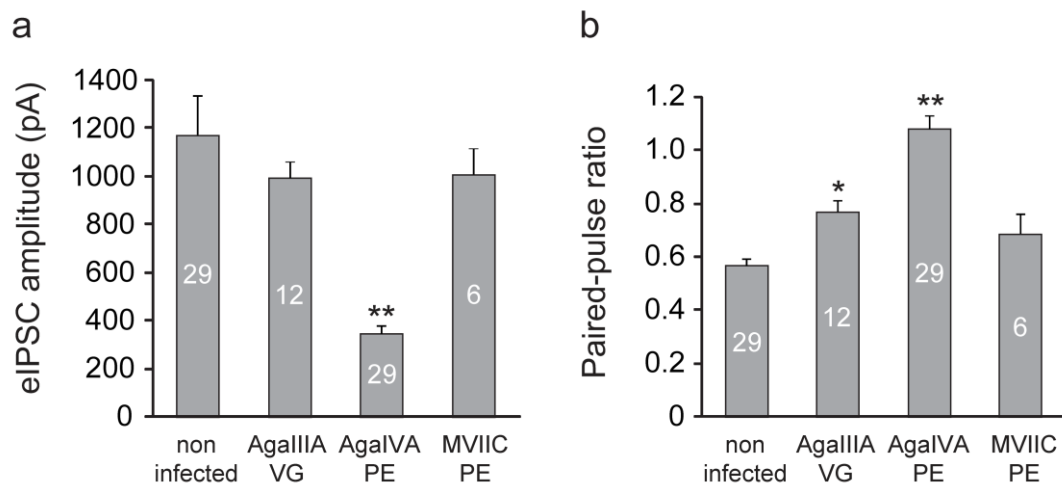
Figure 25. Functional studies of additional t-toxins.

AgaIIIA-VG, AgaIVA-PE and MVIIC-PE were analyzed by eIPSC paired-pulse recordings in transduced rat hippocampal neurons. (**a**) Quantitative analysis of eIPSC first amplitudes showed significant changes only for AgaIVA-PE (P=0.001), whereas (**b**) the paired-pulse ratios of both AgaIIIA-VG and AgaIVA-PE infected cells were significantly increased (P=0.045; P=0.00004).

3.2.5 Influence of t-toxins on neuronal survival and cellular properties

In order to detect possible negative side-effects of t-toxin expression, like neurotoxicity or altered electrical properties of the cells, several experiments were carried out. First, neurons of rat hippocampus culture were infected with t-toxin lentivirus with a high MOI of 10 and cultured for six days. Afterwards, cells were fixed and subjected to immunostaining of the neuronal marker NeuN, which allowed to count the cell number for each transduction and to compare neuronal survival rates. As shown in **Figure 26**, the number of surviving neurons was not significantly changed in any of the transductions, indicating no neurotoxicity of t-toxin expression in the tested conditions.
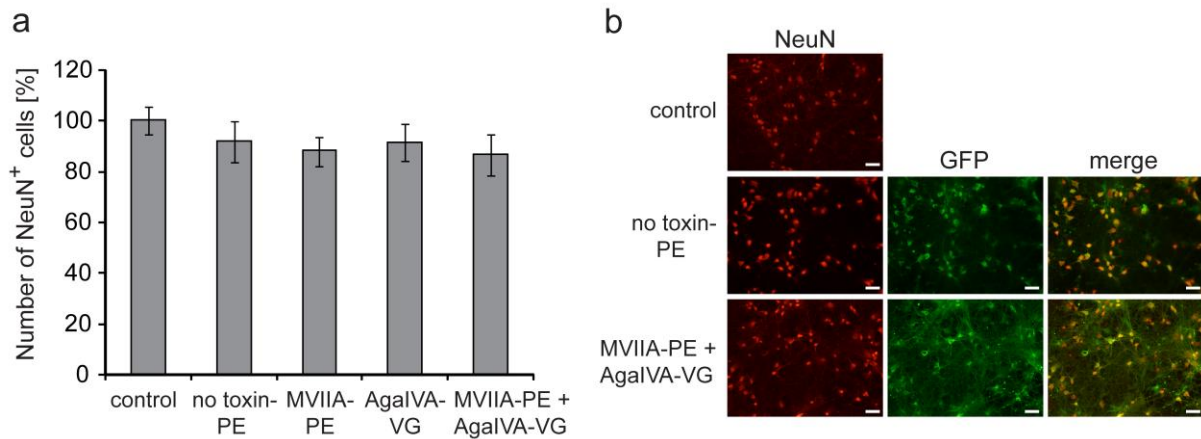
Figure 26. T-toxin expression does not impair neuron survival.

(**a**) Neurotoxicity was not detected in t-toxin transduced hippocampal neurons by staining with neuronal marker (NeuN) six days after infection, and quantification of surviving neurons with respect to control conditions (non-infected) (MOI=10; data of three independent experiments). (**b**) Fluorescence images showing NeuN stained neurons (red), GFP/Venus expression (green) and merge. Scale bars, 50 μm.

Secondly, electrophysiological recordings were performed to determine whether the electrical properties of neurons were changed after infection and t-toxin expression. Quantification of measured whole cell capacitances and membrane resistances showed no significant changes of neurons with t-toxin expression (**Fig.27**). In addition, amplitudes of sodium currents, induced by depolarizing pulses from -70 to +20 mV in voltage clamp recordings, did not display differences between control (non-infected) and MVIIA-PE + AgaIVA-VG infected cells (**Fig.28**). Furthermore, evoked spiking pattern and frequency of action potentials in current clamp recordings was not changed in t-toxin transduced neurons compared to non-infected or no toxin-PE infected cells (**Fig.29**). Although changes in ion channel expression in response to t-toxin expression cannot be completely ruled out, these data indicate that specific blockade of $Ca_v2.1$ and $Ca_v2.2$ calcium channels does not result in major adaptations of other channels that regulate the basic electrical properties required for cell function.

a

b
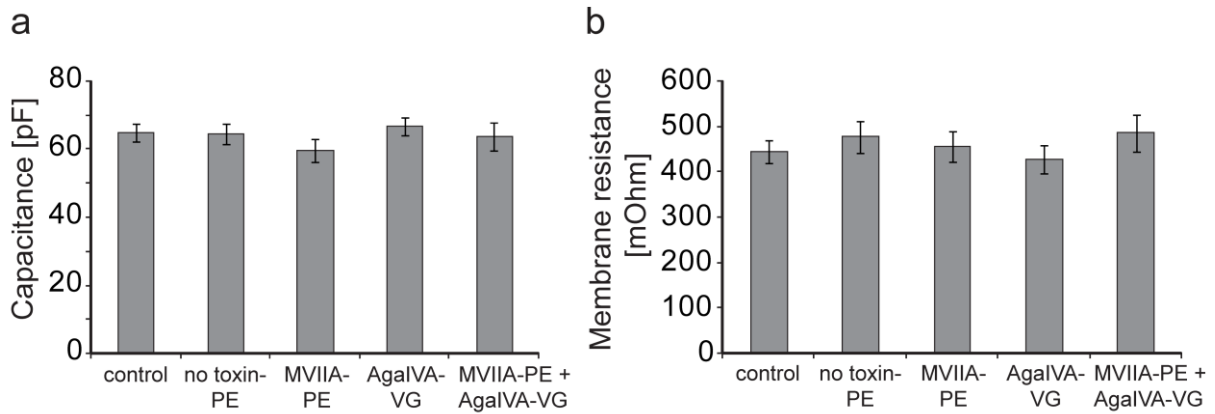
Figure 27. Passive membrane properties of t-toxin infected neurons remain unchanged.

(**a**) The capacitance, as well as (**b**) the membrane resistance of hippocampal neurons infected with the control lentivirus (no toxin-PE) or with the t-toxin lentiviruses MVIIA-PE and AgaIVA-VG, show no significant difference to non-infected control cells, indicating that t-toxin expression does not impair neuronal membrane properties.

a

b
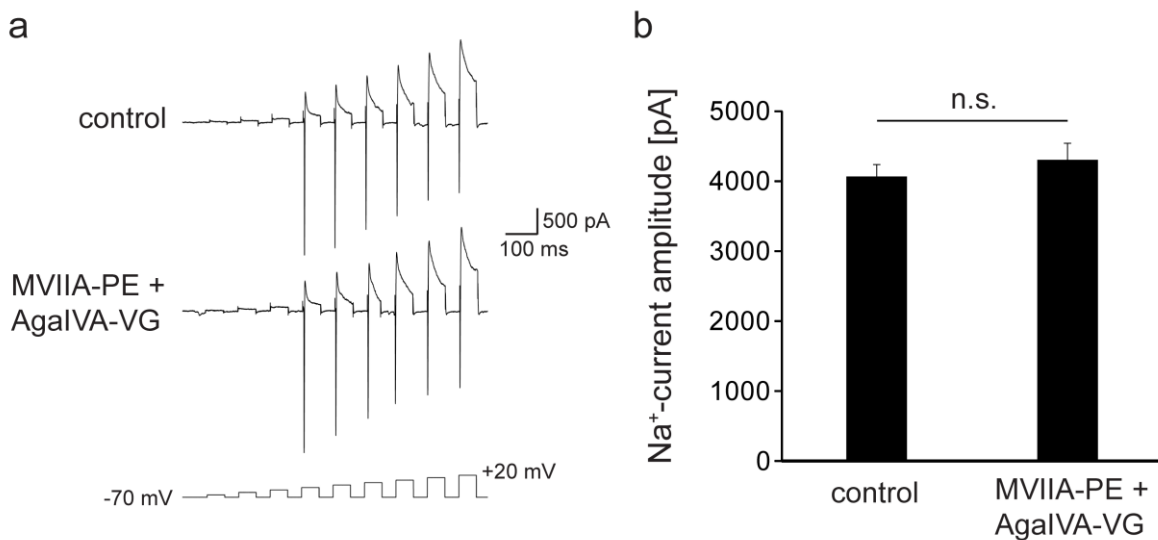
Figure 28. Sodium currents are not altered by t-toxin expression.

(**a**) Voltage-gated sodium currents induced by depolarizing pulses from -70 to +20 mV show no differences between control (non-infected) and MVIIA-PE + AgaIVA-VG infected rat hippocampal neurons. (**b**) Sodium current maximal amplitudes were unaltered between control (non-infected) and MVIIA-PE + AgaIVA-VG infected cells. p=0.48, n=10 cells each.
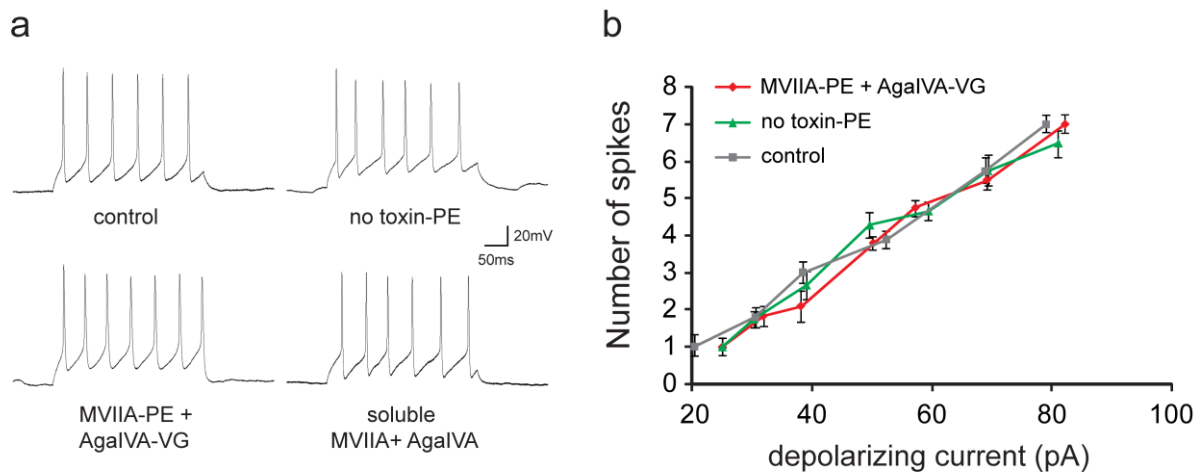
Figure 29. T-toxin expression does not interfere with action potential generation.
(**a**) Representative example traces of spiking behavior in control (non-infected), no toxin-PE, MVIIA-PE + AgaIVA-VG infected rat hippocampal neurons, or in the presence of soluble MVIIA + AgaIVA, indicating unaltered action potential firing properties in current clamp recordings. (**b**) Quantification of spiking behavior by application of depolarizing current to infected hippocampal neurons shows no significant differences between control cells and no toxin-PE or MVIIA-PE + AgaIVA-VG expressing cells (n=7 for each).

3.2.6 Analyses of inducible t-toxin constructs

In order to broaden the range of possible applications of the t-toxin approach, and achieve reversible manipulation of neuronal activity, an inducible lentiviral construct, incorporating a t-toxin cassette, was generated. Therefore, the tTR-KRAB doxycycline-inducible lentiviral vector[50] was used to express tethered MVIIA-PE (designated iMVIIA-PE) upon doxycycline (DOX) treatment (**Fig.30**). HEK293T cells transduced with iMVIIA were treated with DOX (1 µg/ml) and monitored for 21 days by FACS analysis with the DOX treatment being reversed after 5 and 13 days (**Fig.31**). These analyses indicated robust and very tight control of the expression, depending on the presence of DOX, with 4-6 days until fluorescence peak level were reached (**Fig.31**). After removing DOX from the culture by medium exchange, the fluorescence of cells dropped to control levels within 5-6 days, revealing a complete protein turnover of remaining MVIIA-PE within this time frame.
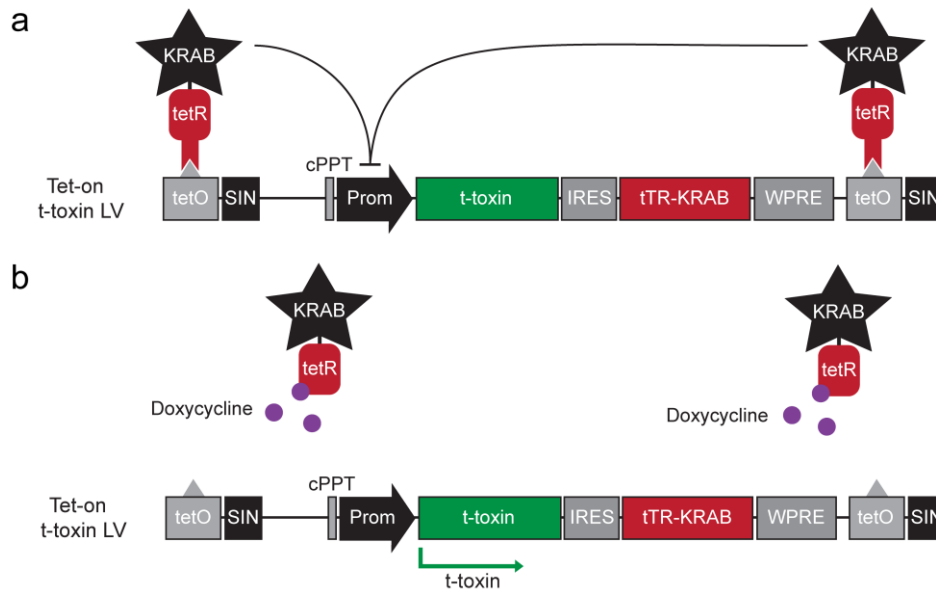
**Figure 30. Schematic representation of Tet-on t-toxin lentiviral vector iMVIIA-PE.**

iMVIIA-PE contains the t-toxin MVIIA-PE followed by an IRES sequence and a tetR-KRAB fusion construct in pLVUT-tTR-KRAB [50]. (**a**) In the absence of doxycycline (DOX), tTR-KRAB protein binds to *tetO* and suppresses the expression of t-toxin as well as tTR-KRAB by epigenetic silencing over a region of 2-3 kb through induction of heterochromatin formation. (**b**) In the presence of DOX, tTR-KRAB is not able to bind to *tetO*, thus enabling expression.
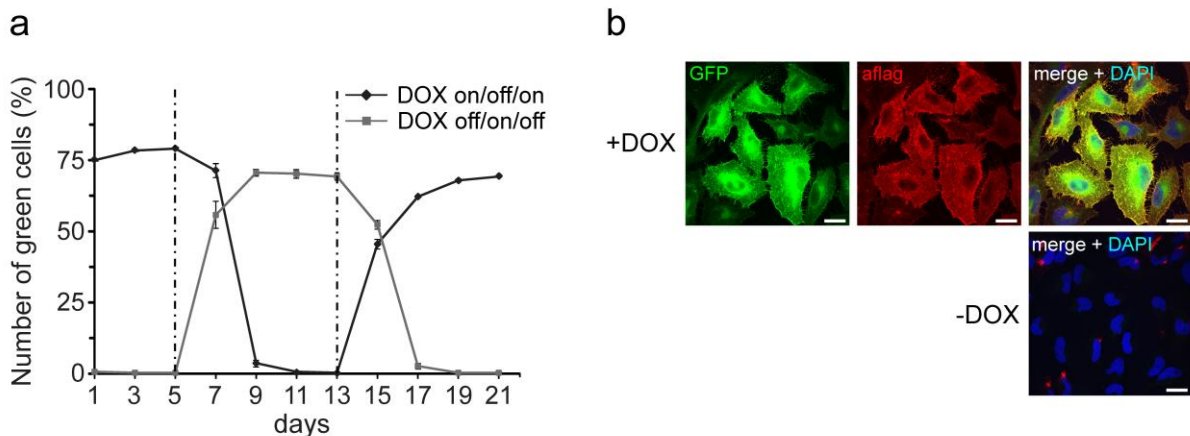
Figure 31. Expression analyses of iMVIIA-PE in mammalian cell culture.

(**a**) FACS analysis of two independently transduced HEK293T cell cultures shows reversible expression of iMVIIA-PE in conditions ± DOX (1 µg/ml) over 21 days in culture. FACS analysis was started one week after transduction and DOX treatment was reversed after 5 and 13 days. (**b**) HeLa cells transduced with iMVIIA-PE display strong EGFP fluorescence, indicative of t-toxin expression and flag signal at the plasma membrane in immunostaining of non-permeabilized cells after 5 days of DOX administration (upper panel). Whereas no staining or EGFP fluorescence could be detected in simultaneously infected cells, but left untreated of DOX (lower panel). Scale bars, 10 µm.

Similarly to mammalian cell culture, rat hippocampal neurons infected with iMVIIA-PE showed expression of t-toxin only upon DOX treatment and no fluorescence could be detected in conditions without DOX (**Fig.32**). Furthermore, the functionality of expressed MVIIA-PE was assessed by paired-pulse recordings in hippocampal neurons. It could be shown that inhibition of postsynaptic currents occurs in the presence of DOX, but not when DOX was absent from the culture medium (**Fig.33**). To evaluate the efficacy of Tet-on t-toxins *in vivo,* stereotactic injections of iMVIIA-PE in the substantia nigra of C57/Bl6 mice were carried out. As shown in **Figure 34**, t-toxin expression was detected in dopaminergic neurons of stereotactically injected mice after one week of treatment with DOX (2 g/l) in the drinking water, beginning the day after surgery. To demonstrate that expression of the toxin is reversible, mice treated in the same manner (lentivirus injection followed by DOX treatment for one week) were kept for an additional week in which they did not receive DOX, and then processed for immunocytochemistry. Upon discontinuation of DOX treatment, mice did not show t-toxin immunofluorescence (**Fig.34**), thereby demonstrating the ability of this inducible system to control expression and activity of tethered toxins *in vivo*.
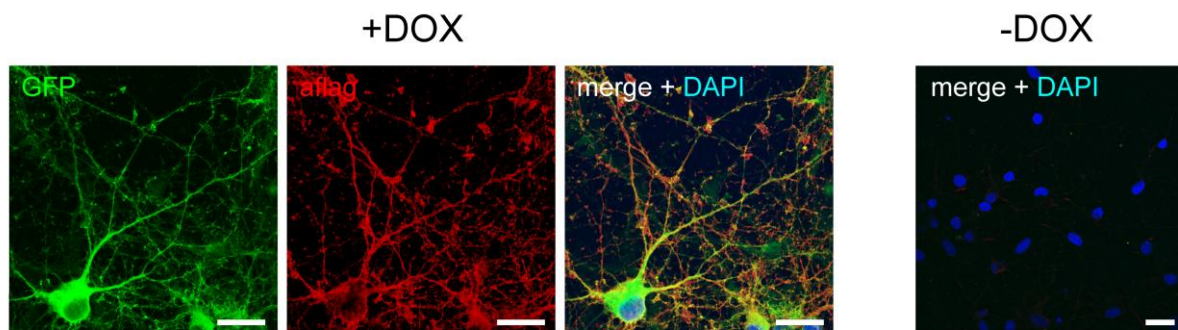
Figure 32. Expression analyses of iMVIIA-PE in rat hippocampal neurons.

Transduced neurons show bright EGFP fluorescence and anti-flag immunostaining after 5 days of doxycycline (DOX) treatment (1 µg/ml). In contrast, cells infected in parallel, but not treated with DOX (right image) displayed no EGFP fluorescence or anti-flag staining, suggesting a very tight regulation of MVIIA-PE expression without obvious leakiness. Scale bars, 25 µm.
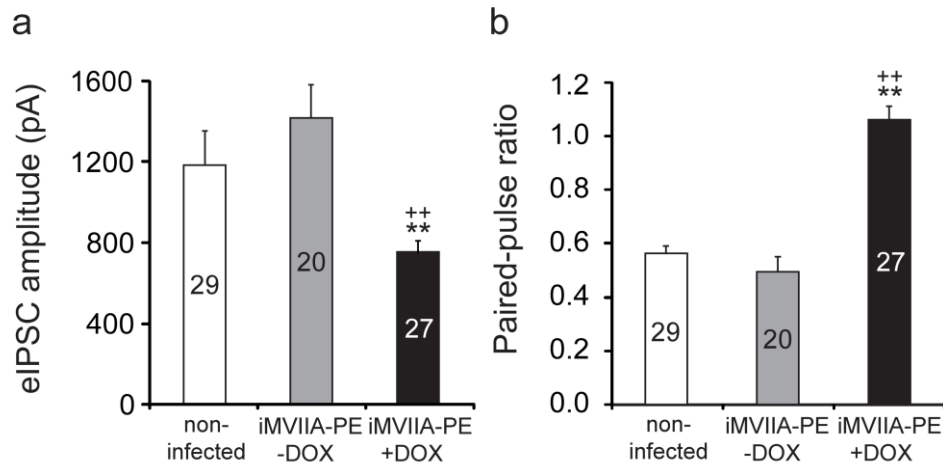
Figure 33. Electrophysiological analysis of iMVIIA-PE in neurons of rat hippocampus culture.

Functional activity of iMVIIA-PE was evaluated by paired-pulse recordings in cultured hippocampal neurons. Voltage-gated calcium currents showed significantly (**a**) reduced amplitudes of the first postsynaptic currents and (**b**) increased paired-pulse ratios only after DOX administration. **/++P ≤ 0.005; * compared to non-infected control; + compared to corresponding t-toxin infection. Number of recorded cells is shown in/above columns.
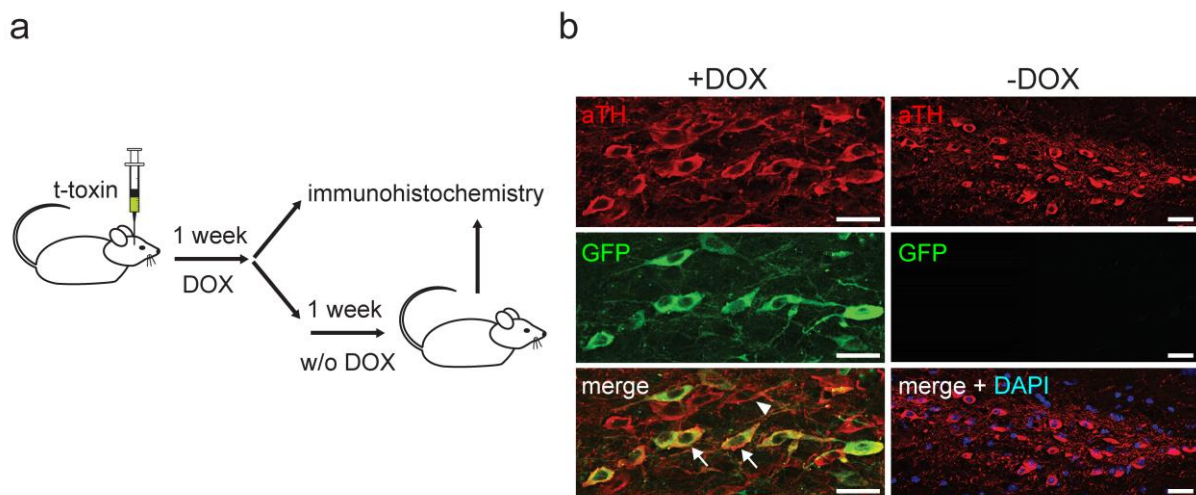
Figure 34. Doxycycline induced expression of iMVIIa-PE *in vivo*.

(**a**) Mice were stereotactically injected with iMVIIa-PE lentivirus in the substantia nigra and received DOX in the drinking water (2 g/l) for one week, beginning the day after injection. A control group of mice was treated in the same manner, but kept for one additional week without DOX to show reversibility of expression. (**b**) iMVIIa-PE expression (green) is shown in dopaminergic neurons (TH immunostaining, red) in mice treated with DOX (left column, arrows: GFP[+]/TH^{+} cells, arrowhead: non-infected TH[+] neuron). No green fluorescence could be detected in the control mice with discontinued DOX treatment (right column, blue represents nuclear DAPI staining). These findings indicate efficient DOX regulated expression of iMVIIa-PE *in vivo*. Scale bars, 25 µm.

### 3.2.7   Analyses of Cre-dependent t-toxin constructs

One of the important advantages of the t-toxin strategy versus systemic application of soluble toxins is the possibility to achieve cell-autonomous effects in specific cell-populations within circuits. Since there are very few available vectors using cell-specific promoters for lentivirus-mediated gene expression, a Cre recombinase (Cre) mediated approach to express t-toxins only in Cre expressing cells was used. Thus, a *lox*P cassette flanking DsRed (Miething C., Duyster J., in preparation) was subcloned in front of the green fluorescent t-toxin (designated cMVIIA-PE; **Fig.35**). In conditions without Cre-recombinase, solely DsRed is expressed and generation of functional t-toxin is inhibited by an introduced frameshift in the DNA reading frame after DsRed, which generates several translational stop codons throughout the t-toxin sequence. Thus, the expression of functional t-toxin is possible only after successful excision of the *lox*P cassette by Cre-recombinase.
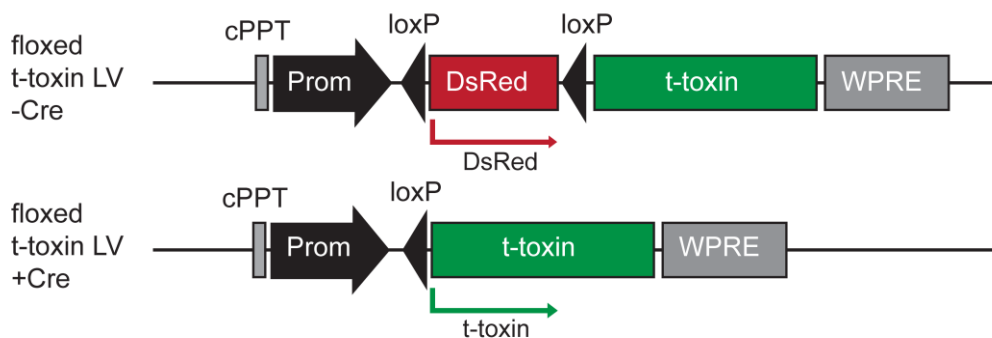
Figure 35. Schematic of the Cre-dependent lentiviral vector cMVIIA-PE.
DsRed, flanked by two loxP sites was inserted between Ubiquitin C promoter and t-toxin. After integration into the genome, DsRed is expressed (upper lane) in cells without Cre recombinase. Only in cells containing Cre recombinase, DsRed is excised and t-toxin gets expressed (lower lane).

Bright green fluorescent signal, indicative of efficient Cre-excision, was detected in cMVIIA-PE transduced HEK293T cells only upon delivery of Cre recombinase, by addition of the recombinant Tat-Cre fusion protein[103] (**Fig.36a**). Furthermore, quantification by FACS analysis demonstrated high levels of green fluorescence and elimination of red fluorescence upon Cre excision of the DsRed cassette in transduced HEK293T cells after co-infection with LV-Cre-SD, a self deleting lentivirus expressing Cre recombinase[104] (**Fig.36b**).
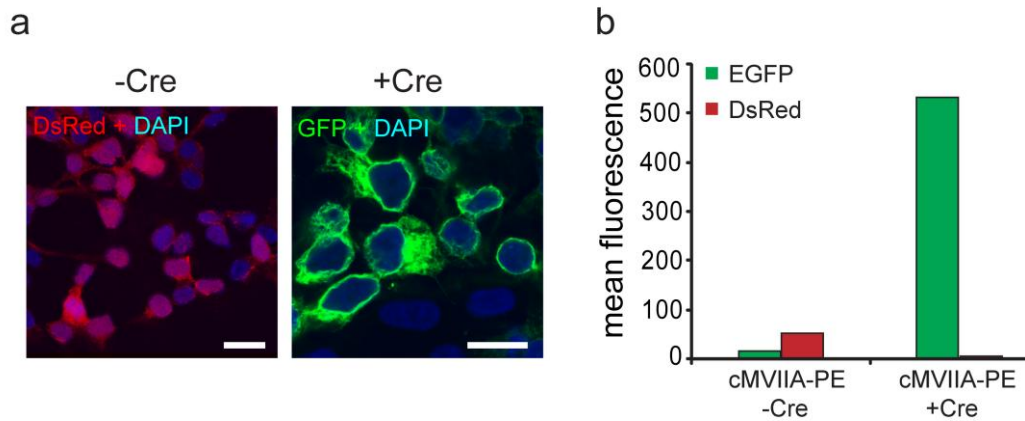
**Figure 36. Expression analyses of cMVIIA-PE in HEK293 cells**

(**a**) Merged images of HEK293 cells transduced with cMVIIA-PE showing DsRed but no t-toxin expression in conditions without Cre recombinase (left image), and robust t-toxin (green) expression with loss of DsRed fluorescence after addition of tat-Cre protein (right image). Scale bars, 20 µm (left image) and 15 µm (right image). (**b**) FACS analysis of cMVIIA-PE transduced HEK293 cells before, and 5 days after co-infection with LV-Cre-SD shows marked increase in EGFP fluorescence and complete loss of DsRed fluorescence in + Cre conditions. This indicates a robust Cre-dependent expression control of cMVIIA-PE.

For functional analysis of cMVIIA-PE, paired-pulse recordings in rat hippocampus culture were carried out. Here, inhibition of presynaptic calcium currents occurred only in cMVIIA-PE transduced cells, co-infected with LV-Cre-SD[104], as shown by decrease of eIPSCs first amplitudes (**Fig.37a**) and increase in PPR in these cells (**Fig.37b**). To validate the cell specific expression of floxed t-toxins with Cre levels expressed in Cre-transgenic mice, Brn4 Cre transgenic mice were used[105]. Transduction of cortical cultures prepared from these mice with cMVIIA-PE revealed discrete expression of the green fluorescent t-toxin in a subset of neurons and red fluorescence in Cre-negative cells (**Fig.38**). These data indicate a tight, Cre-dependent regulation of functional MVIIA-PE expression upon cMVIIA-PE transduction of mammalian cells and neurons. Thus, Cre-dependent constructs seem to be a promising extension of the tethered toxin approach to further broaden the possible applications of t-toxins.
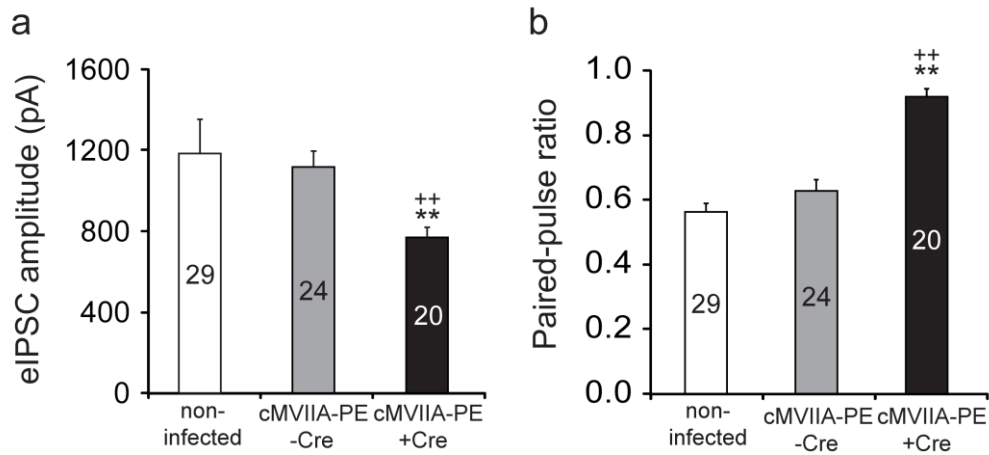
Figure 37. Electrophysiological analysis of cMVIIA-PE in cultured rat hippocampal neurons.

Functional analysis by paired-pulse recordings in cMVIIA-PE transduced hippocampal neurons shows (**a**) reduced postsynaptic responses and (**b**) increased PPR only in cells co-infected with LV-Cre-SD. $**/++P \leq 0.005$; * compared to non-infected control; + compared to corresponding t-toxin infection. Number of recorded cells is shown in/above columns.
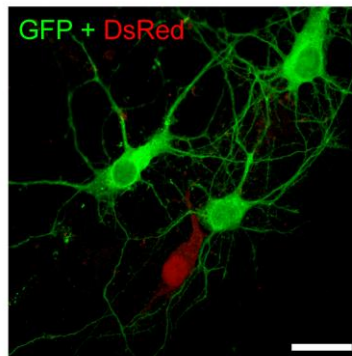

Figure 38. Expression analysis in cortex culture of transgenic Cre mice.

Transduced cortical neurons from Brn4-Cre transgenic mice show cMVIIA-PE expression in Cre positive neurons (green) and DsRed fluorescence in Cre negative cells (red). Scale bar, 20 µm.

3.2.8 Functional *in vivo* analyses

3.2.8.1 Stereotaxic injection of t-toxin lentivirus in mice

To demonstrate the applicability of lentiviral t-toxins to silence synaptic transmission *in vivo,* a variation of the nigro-striatal pathway lesioning experiments[82,83] was used to test whether t-toxin mediated inactivation of $Ca_v2.1$ and $Ca_v2.2$ channels could impair dopamine release from dopaminergic neurons onto striatal medium spiny neurons. Mice received a unilateral stereotactic injection into the substantia nigra pars compacta (SNpc) with either the control lentivirus (no toxin-PE) or with a virus suspension containing both t-toxins MVIIA-PE and AgaIVA-VG in a 1:1 ratio. Between two to three weeks after virus injection, animals were injected intraperitoneally (i.p.) with saline and two hours later with apomorphine (0.5 mg/kg) and rotational behaviors were scored in an open field box (**Fig.39**). Locomotor trajectories (**Fig.40**) were recorded on videotape and the number of net turns was counted during a period of 15 minutes after saline or apomorphine treatment, respectively. Mice injected with the control virus displayed very mild or no circling behavior under both conditions (saline: -1 ± 1 turns, apomorphine: 0 ± 1 turns, n=7), while all mice injected with the double t-toxin virus suspension showed stereotyped contralateral circling behavior after saline (11 turns ± 2, n=12), that reversed direction upon apomorphine treatment (10 turns ± 3, n=12) (**Fig.40**). These results suggest a unilateral impairment of the nigro-striatal pathway due to inhibition of dopamine release in the striatum, by MVIIA-PE and AgaIVA-VG mediated $Ca_v2.1$ and $Ca_v2.2$ channel block..
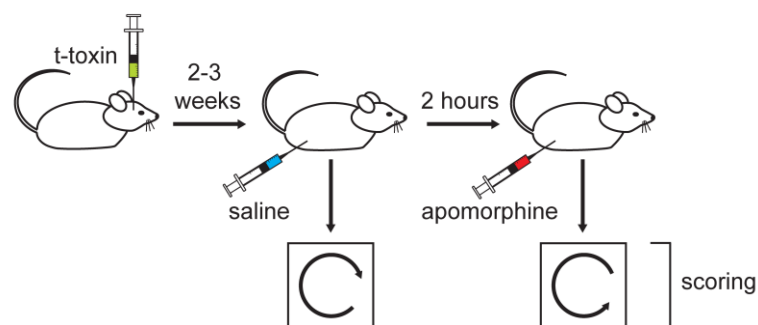

Figure 39. Scheme of the rotational behavior analyses in stereotactically injected mice.

Between two to three weeks after stereotactic injection of double t-toxin lentivirus mix (MVIIA-PE + AgaIVA-VG) or control no toxin-PE lentivirus, mice were administered saline (i.p.) and rotational behavior was measured. Two hours later, apomorphine (0.5 mg/kg) was injected (i.p.) and rotational behavior was scored again.

3.2.8.2   Behavioral analysis
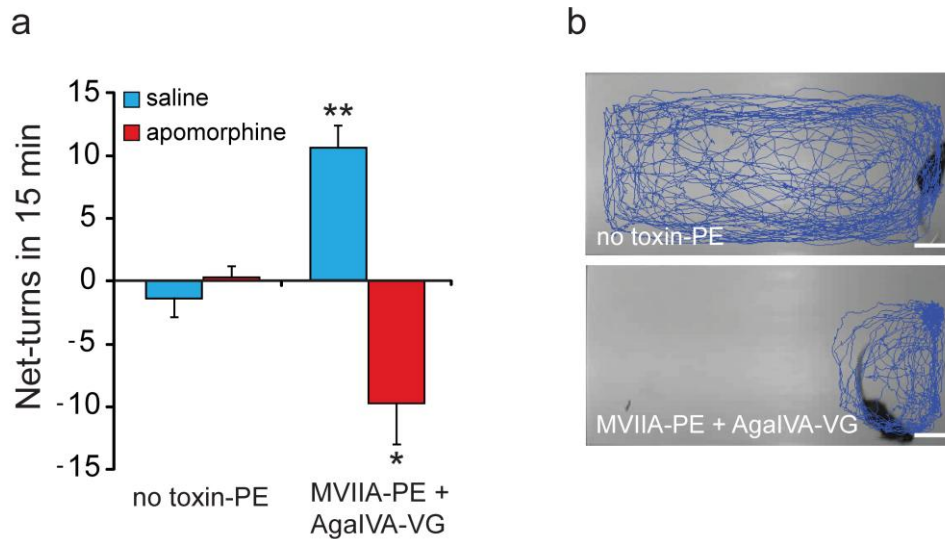
Figure 40. *In vivo* inhibition of dopaminergic neurotransmission in mice by t-toxins.

(**a**) Rotational behavior and reversal of direction after apomorphine administration (0.5 mg/kg) occurred only in mice, which were stereotactically injected in the SNpc with double t-toxin (MVIIA-PE + AgaIVA-VG, n=12), indicative of t-toxin interference with dopaminergic signaling in the nigro-striatal pathway. Mice injected with control lentivirus (no toxin-PE, n=7) showed no circling behavior. *P = 0.0081; **P = 0.00007. (**b**) Representative movement tracks of control and t-toxin injected mice upon administration of apomorphine. Scale bars, 5 cm.

Brain sections were prepared from the stereotactically injected mice 3 weeks to 5 months after surgery to evaluate the infection efficiency (**Fig.41**). Accurate and robust expression of the t-toxins MVIIA-PE and AgaIVA-VG (green fluorescence) was detected in neurons of the SN, mostly in the pars compacta. To confirm these results, brain sections were examined for immunoreactivity to EGFP and the dopaminergic marker tyrosine hydroxylase (TH). These immunostainings detected t-toxin expression in the cell bodies, axons and striatal terminals of dopaminergic neurons of stereotactically injected mice (**Fig.41**). Furthermore, quantification of the area occupied by t-toxin transduced cells with respect to the total area of dopaminergic positive neurons showed a high overlay and no differences to control mice infected with control lentivirus (no toxin-PE) (**Fig.42**). Although no direct measurements of $Ca_v2.1$ and $Ca_v2.2$ activities in dopaminergic neurons were performed, these data indicate, that co-expression of the two t-toxins can be used to inhibit Ca_v dependent dopamine release and disturb locomotor behavior in mice.

3.2.8.3   Immunohistochemistry
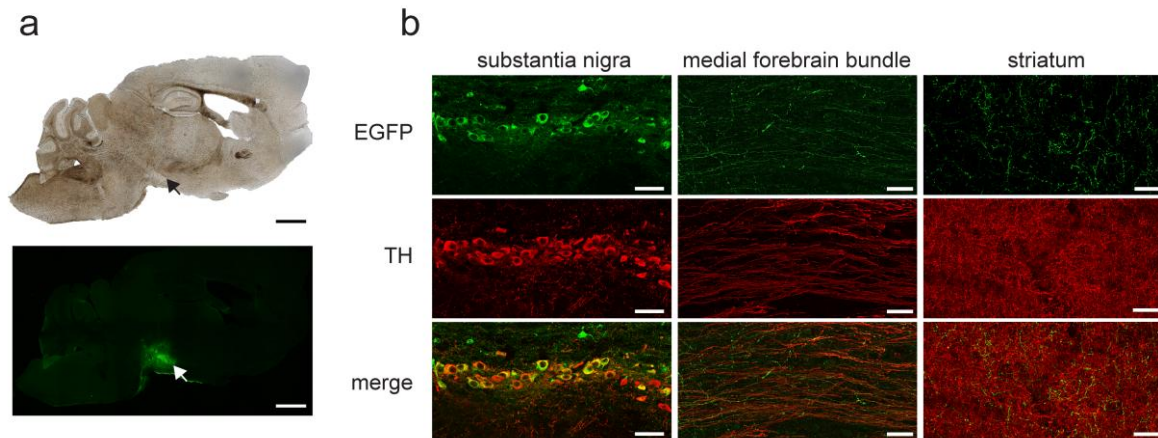
Figure 41. Analysis of t-toxin expression *in vivo*.

(**a**) Immunostainings of sagittal brain sections showing the site of MVIIA-PE + AgaIVA-VG lentivirus injection in SNpc (arrow). EGFP/Venus (green) indicates the virally transduced area and tyrosine hydroxylase staining (TH, red) labels dopaminergic (DA) neurons of the SNpc. (**b**) Confocal images of lentivirus transduced DA neurons show co-localization of EGFP and TH-labeling in neuronal cell bodies (SNpc), axons (medial forebrain bundle) and terminals (striatum). Scale bars, 25 µm.
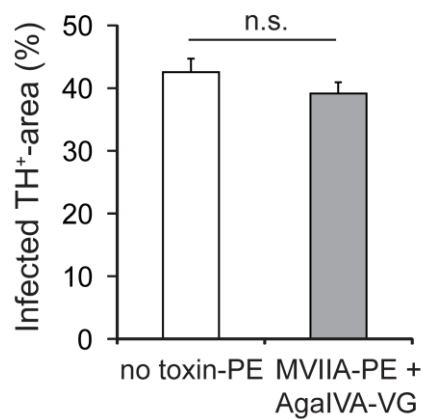
Figure 42. Quantification of TH-labeled area in SNpc showing colocalization with EGFP signal.

Immunohistochemically stained TH positive and EGFP positive areas in serial sagittal brain sections (MVIIA-PE + AgaIVA-VG: n=6 mice, no toxin-PE: n=3 mice) were analyzed and represented as percentage of TH immunopositive area which also shows EGFP staining. No difference could be observed between no toxin-PE control injections and MVIIA-PE + AgaIVA-VG co-injections. P = 0.266.

4.   Discussion

This work established the use of newly generated fluorescent membrane-tethered toxins to block $Ca_v2.1$ and $Ca_v2.2$ voltage-gated calcium channels within neuronal circuits *in vitro* and *in vivo*. The developed t-toxins combine the selectivity of conotoxin MVIIA and agatoxin IVA for $Ca_v2.1$ and $Ca_v2.2$ channels and the ability to restrict their action to targeted cells by membrane tethering, Cre-dependence and Tet-inducibility. The specificity and efficiency of these t-toxins was demonstrated *in vitro* in HEK293-$Ca_v2.2$ cells and rat hippocampal neurons. Furthermore, we could show the functional interference of these t-toxins with the central nigro-striatal dopaminergic pathway *in vivo* in mice upon stereotaxic injection of t-toxin harboring lentivirus. These data illustrate the general applicability of the t-toxin strategy as a straightforward method that can be used to block calcium currents mediated through $Ca_v2.1$ and $Ca_v2.2$ channels, resulting in cell-specific and cell-autonomous silencing of neurotransmission. Furthermore, different t-toxins incorporating the conotoxin GID were shown to block α7 and α3β4 nicotinic acetylcholine receptors without affecting α4β2 subunit combinations in *X. laevis* oocytes.

4.1   Influence of linker length on t-toxin activity

One important aspect for conotoxin GID containing t-toxin functionality was found to be the length of the chosen linker sequence between the toxin and membrane anchor/TM domain. In the tested constructs, linkers of 10 and 23 amino acids resulted in highest toxin activity, while longer linkers (46 and 69 aa, respectively) caused gradual decrease of toxin functionality, most probably by preventing the toxin to bind to the target site. This effect could be due to the formation of undesired secondary structures of linkers with increasing length or masking of the binding sites of either the toxin or, less likely, the channel by the linker. Alternatively, another explanation would be that by using longer linkers, the physical distance between toxin and channel becomes too large and the linker flexibility is not sufficient to allow proper binding. This hypothesis is supported by the finding that the increase in linker length leads to a proportional loss in toxin activity, whereas for the first mentioned explanations a non-gradual loss of functionality would be expected. Thus, despite the linking region was designed to consist primarily of glycine and asparagines residues in order to allow toxin binding to the target site by ensuring rotational freedom and flexibility of the linker, this proposed flexibility is obviously not sufficient in constructs with linkers of more than ~30 residues.

4.2   Comparison of soluble GID and t-toxin GID activity

The soluble form of α-conotoxin GID was reported to selectively inhibit the α7, α3β2 and α4β2 subtypes of the neuronal nAChR with IC_{50} values of 4.5, 3.1 and 152 nm, respectively[28]. In comparison, the potency of GID on other subunit combinations, like α3β4, α4β4 and muscle nAChRs was reported to be at least 1000-fold lower[28]. However, when tested as tethered toxin version (t-GID) in this work, the constructs showed block of α7 and α3β4 nAChRs, while α4β2 nicotine-induced currents were not altered, irrespective of the linker length. Most probably, the substitution of the non-proteinogenic γ-carboxyglutamic acid with glutamic acid (γ4E) in t-GID could account for the selective loss of activity on α4β2 nAChRs. This hypothesis is supported by the finding that deletion of the N-terminal four residues of GID (GIDΔ1–4) leads to ~4 fold decrease in activity at the α4β2 receptor, without affecting the functionality at α3β2 and α7 nAChRs[28]. Furthermore, a lack of tolerance to sequence variation in this region for α4β2 interaction has been reported recently[29], highlighting the importance of these residues for the activity of GID, and indicating a tightly defined binding site on α4β2 receptors. However, this unexpected finding provides the possibility of using t-GID to modulate α7, α3β4 and α3β2 without affecting α4β2 subunit combinations. As α7 and α4β2 receptors are the two most abundant nAChRs in the brain[56], t-GID could be applied to further analyze and define the function and contribution of α7, α3β4 and α3β2 nAChRs to specific circuits in the brain, by selective targeting of cells and brain regions with viral vectors and mouse transgenesis.

4.3   The paired-pulse ratio as a measure of neurotransmission

The inhibition of $Ca_v2.1$ and $Ca_v2.2$ calcium currents by t-toxins was electrophysiologically quantified by paired-pulse recordings, i.e. a presynaptic neuron was stimulated consecutively with two short pulses and the amplitudes of the first ($eIPSC_1$) and second postsynaptic responses ($eIPSC_2$) were recorded in a coupled postsynaptic neuron. The calculated paired-pulse ratio (PPR: $eIPSC_2/eIPSC_1$) was used as a measure of presynaptic neurotransmitter release[102]. Depending on the type of synapse, either paired-pulse depression (PPD: PPR <1.0), or paired-pulse facilitation (PPF: PPR >1.0) can be detected[81]. In general, the smaller the probability of NT release is for the first pulse, the more facilitated is the response to the second pulse. This PPF is accounted for by the residual calcium hypothesis, according to which a small fraction of calcium entering the terminal after the first pulse increases the probability of NT release to a second action potential, leading to an increase in PPR[106]. In

contrast, PPD can be largely attributed to depletion of a readily releasable pool of NT vesicles[81,107]. However, other mechanisms, such as intrinsic presynaptic calcium channel inactivation[108], negative feedback through inhibitory autoreceptors[109] or receptor desensitization[81,110] cannot be ruled out.

In our hippocampus cultures, both $Ca_v2.1$ and $Ca_v2.2$ calcium channels were involved in synaptic neurotransmission, as was shown by inhibition of individual currents by soluble toxins and t-toxins. The typical response of native neurons was found to be PPD (PPR < 0.6), whereas t-toxin transduced neurons had increased PPR (MVIIA-PE: PPR ~ 0.9) or showed PPF (AgaIVA-VG: PPR ~1.1). An explanation for this change towards PPF, which is in accordance with the residual calcium hypothesis, would be that the Ca^{2+} influx of the remaining unblocked calcium channel is not sufficient to elicit normal NT release and only reaches the necessary Ca^{2+} concentration threshold with the second stimulation. Thus, this would result in bigger second amplitudes compared to the first amplitudes and cause PPF. An even more pronounced PPR with dramatically decreased amplitudes was seen in co-infections with both t-toxins. These findings support the hypothesis that in single infections most of the remaining response is caused by the unblocked calcium channel. Indeed, it could be demonstrated that the paired-pulse response could be completely abolished in co-infections by a 3-fold increase of the virus load per cell. Therefore it can be speculated that in double-infections where a response could still be obtained, not every neuron had been infected by both t-toxin lentiviruses, thus resulting in cells with incomplete inhibition. Considering that the amount of t-toxin induced block in single infections was comparable to soluble toxins, this indicates that the silencing of neurotransmission is more a question of infectivity and construct delivery to every targeted cell and not of t-toxin efficiency.

4.4   Lack of functionality in multi-target t-toxins

Inhibition of $Ca_v2.1$ and $Ca_v2.2$ with a single toxin would have the great advantage of only requiring one infection event per cell. Therefore, the multi-target peptide toxins AgaIIIA and MVIIC were used to generate t-toxins. ω-Agatoxin IIIA is known to possess a broad spectrum of activity, blocking all known neuronal high threshold calcium channels, including L- (Ca_v1), N- ($Ca_v2.2$), P/Q- ($Ca_v2.1$), and R-type ($Ca_v2.3$) channels[36], but in contrast to AgaIVA, the block induced by AgaIIIA is only partial[37,39]. However, when expressed as t-toxin AgaIIIA-VG, no blocking activity in HEK293-$Ca_v2.2$ cells could be detected and the increase in PPR

in rat hippocampal neurons was only modest (0.75 ± 0.04). It was concluded that this toxin, at least in the chosen construct design, is not suited for specific, high-affinity block of calcium channels. The most probable reason may be indeed that the native AgaIIIA can only achieve partial block of the targeted calcium channels.

Also ω-conotoxin MVIIC was used in this work to generate MVIIC-PE t-toxin, as the native MVIIC was reported to block both $Ca_v2.1$ (low affinity) and $Ca_v2.2$ (high affinity)[34]. However, no inhibitory effect of MVIIC-PE on calcium channels could be detected in HEK293-$Ca_v2.2$ cells, as well as in rat hippocampal neurons. This is surprising, because MVIIA and MVIIC are both pore-blockers, do not contain modified amino acids, have similar sizes and share the same disulfide-backbone. Thus, it may only be speculated, that the lower affinity of MVIIC compared to both MVIIA and AgaIVA[32,111], as well as possible hindrances in the construct design, like additional disulfide bridges could account for this lack of activity. It was reported that replacement of the N-terminal half of MVIIC with that of MVIIA significantly increased the affinity for N-type calcium channels[112]. Furthermore, reverse mutation from Lys7 to Pro7 decreased the affinity for both P/Q- and N-type channels, whereas that from Leu11 to Thr11 increased the affinity for P/Q-type channels and decreased the affinity for N-type channels[113]. These findings indicate that in principle, it could be possible to engineer a recombinant toxin with high affinity for both $Ca_v2.1$ and $Ca_v2.2$. As long as this is not available, the only alternative appears to be the combined use of the best single blockers of $Ca_v2.1$ and $Ca_v2.2$, namely AgaIVA and MVIIA, respectively.

4.5   Inducible and Cre-recombinase dependent expression

In order to broaden the range of possible applications of t-toxins, we investigated lentiviral vectors that allow the doxycycline or Cre-recombinase dependent expression of transgenes. The inducible construct iMVIIA-PE was based on the vector pLVUT-tTR-KRAB[50], which uses the repression activity of a tTR-KRAB fusion protein. When tethered to DNA, KRAB recruits a multiprotein complex that induces heterochromatin formation extending over 2–3 kilobases[50]. This process can be reversibly controlled by the antibiotic doxycycline.

The expression properties of iMVIIA-PE in this vector was in agreement with the reported properties of this vector[50]. For instance, in both cases the time for full expression and full repression was in the range of 5-6 days after doxycycline addition or removal, respectively.

When compared to constitutive expression, the fluorescence of cells was slightly lower when MVIIA-PE was expressed in the inducible vector. Furthermore, the reduction of the first amplitude in eIPSC recordings in rat hippocampal neurons was decreased by ~38 % compared to the constitutive version. However, the PPR upon iMVIIA-PE infection was slightly higher than with the constitutive version. These differences might partially be explained with variations in the hippocampus cell culture or lentiviral preparations and infection procedures. It can also be speculated, that a longer incubation time with doxycycline before measurements, than the applied 5 days, might help to further increase the expression levels and thereby achieve increased block of eIPSC amplitudes. In continuation of this work, the detailed functional analysis of DOX-inducible t-toxins, also *in vivo*, and the combined use of both MVIIA-PE and AgaIVA-VG inducible variants will help to further develop this regulated approach of specific ion channel inhibition.

For the Cre-recombinase-dependent expression of t-toxins, we generated the lentiviral vector pFU-cMVIIA-PE, which allows expression of MVIIA-PE only in Cre recombinase positive cells. Analyses of the expression and functionality with this vector revealed a very tight Cre-dependent regulation, with complete absence of detectable expression or activity in conditions without Cre recombinase. After Cre-excision, eIPSC recordings in rat hippocampal neurons showed ~35 % less reduction of the first amplitude compared to constitutive expression, which is comparable to the DOX-induced iMVIIA-PE discussed above. The obtained PPR by expression of cMVIIA-PE corresponded well to the constitutively expressed MVIIA-PE, indicating functional active cMVIIA-PE.

Considering the fact that both inducible and Cre-recombinase dependent lentiviral vectors were less efficient in blocking the first amplitudes, while reaching the same or even slightly higher PPRs than constitutively expressed MVIIA-PE, the question remains what is causing this reduced levels of current block. It might well be that the overall infection and expression levels were not high enough to reach the same effects as with constitutive vectors. This hypothesis is supported by the finding that co-transduction of MVIIA-PE and AgaIVA-VG with a MOI of 2.5 led to reductions of amplitudes, while an increased MOI of 7.5 resulted in complete silencing of neurotransmission. Thus, as mentioned above, increased expression times for both constructs, as well as higher infection levels might help to achieve a greater reduction of the amplitudes.

4.6   Inhibition of dopamine release in the nigro-striatal pathway by t-toxins

The *in vivo* functionality of $Ca_v2.1$ and $Ca_v2.2$ calcium channel specific t-toxins MVIIA-PE and AgaIVA-VG to silence dopaminergic synaptic transmission was demonstrated in this work in mice by unilateral injection of lentivirus into the substantia nigra pars compacta (SNpc), inducing stereotyped circling behavior. Recently, the contribution of VGCCs to dopaminergic (DA) neurotransmission in the striatum was shown by *in vivo* microdialysis of calcium channel peptide toxins AgaIVA, MVIIC and GVIA[114]. These studies revealed that AgaIVA and MVIIC reduced K^+-evoked DA release, while the $Ca_v2.2$ specific GVIA strongly blocked the Ca^{2+} evoked and basal DA release, suggesting that DA neurotransmission in the striatum is mainly regulated by $Ca_v2.2$ but not by $Ca_v2.1$ cannels[114]. Nevertheless, in this work, both t-toxins MVIIA-PE and AgaIVA-VG were co-injected in order to achieve block of both $Ca_v2.1$ and $Ca_v2.2$ channels to prevent potential compensatory mechanisms.

T-toxin injected mice showed an ipsilateral rotational phenotype, which could be reversed to contralateral circling by administration of the dopamine (DA) agonist apomorphine. These findings were in accordance to reported phenotypes in studies of drug-induced lesions of DA neurons in SNpc[82,83,85,115], as well as to GVIA induced inhibition of DA neurotransmission in the striatum by application of the toxin with osmotic pumps in rats[116]. In these reports, the number of DA neurons remaining in the lesioned SNpc was correlated with the number of rotations induced by apomorphine. Typically, only animals in which the lesioned SNpc contained 20 % or fewer DA neurons than the intact side rotated after administration of apomorphine (~0.05 mg/kg). However, when the concentration of apomorphine was increased to ~0.5 mg/kg, contralateral circling could be observed in mice in which DA was depleted only by ~61 %[83]. In t-toxin expressing mice generated in this work, no obvious loss of DA neurons or change of morphology could be detected, and the proportion of DA neurons which were EGFP positive was not altered in t-toxin injected mice compared to no toxin-PE injected control mice. Thus, as the number of DA cells was not changed, the rotational behavior of t-toxin mice most likely indicates inhibition of DA transmission in the striatum. The number of turns in 15 min (saline: 11 turns +/- 2, APO: 10 turns +/- 3; n=12), was found to be lower than in 6-OHDA lesion studies (no drug: ~11-50 turns, depending on the lesion size)[82,83]. This difference could possibly be explained with the greater efficiency of 6-OHDA uptake by DA

neurons, and the bigger spread of 6-OHDA by diffusion, whereas lentiviral particles are limited in their tissue penetration capacity. It may be speculated that by increasing the number of injection sites, or using the smaller adeno-associated virus for delivery, the spread of the t-toxin expression, and thus the number of rotations may be increased.

4.7 Advantages of t-toxins over other approaches

Conventional methods to study ion channel function include pharmacological manipulations of cells with soluble peptide toxins or synthetic reagents, which have been extensively used to determine the structure and functions of ion channels and receptors[10,32,117]. The advantage of direct treatment with agonists or antagonists is an instant effect of the applied drug and the ease of application without additional preparation steps in advance. However, due to diffusion and degradation, the activity of soluble modulators is limited in time and targeting of specific cells is not possible. Moreover, *in vivo* application is only achieved by constant administration through osmotic pumps or similar devices.

In contrast, the t-toxin approach described in this work provides a constant replenishment of the antagonist by cell-autonomous expression, enabling long-term effects. Furthermore, it enhances the working concentration of the blocker peptide by tethering peptide toxins close to their point of activity in the cell plasma membrane. In addition, the cell-autonomy allows selective targeting of specific cell populations, and the modular composition of t-toxins permits the engineering of a large variety of constructs, e.g. using different fluorescent markers, linkers, viral vectors and point mutation variants.

An alternative to the t-toxin approach of blocking $Ca_v2.1$ and $Ca_v2.2$ is the knock-out of the alpha subunits Cacna1a of $Ca_v2.1$ and Cacna1b of $Ca_v2.2$ in transgenic mice. However, in Cacna1a and Cacna1b null mutant mice, changes in calcium channel expression have been shown to occur, and $Ca_v2.2$ channels were found to functionally compensate for the absence of $Ca_v2.1$ channels[74,99,118]. This effect is most probably due to the mechanism of calcium channel sorting and trafficking, where $Ca_v2.1$ and $Ca_v2.2$ compete for specific slots in the molecular machinery that regulates the final localization of channels at the presynaptic active zone. Thus, if one channel is underrepresented, the other one is processed more efficiently and thereby compensates for the loss. Sequences in the cytoplasmic II–III loop of Ca_v2 voltage-gated calcium channels, termed the synaptic protein interaction (synprint) site, together with

other, yet undefined targeting mechanisms are responsible for this incorporation of presynaptic calcium channels into the synaptic vesicle fusion apparatus[119]. Thus, an advantage of the t-toxin strategy described in this work is the targeting of channels without any signs of functional compensation under the tested conditions, thus preventing the problems that occur in null mutant mice.

One could also think of conditional mutagenesis of the pore subunit genes Cacna1a of $Ca_v2.1$[120] and Cacna1b of $Ca_v2.2$ channels to avoid compensatory effects. This would require both conditional alleles for each channel subunit gene, and Cre driver lines expressing Cre recombinase in the cells of interest. However, no conditional alleles for Cacna1b have been reported so far. Also the expression of dominant negative calcium channel subunits has been reported to block Ca^{2+} currents *in vitro*[100,121]. Nevertheless, this method can result in accumulation of protein complexes in the ER, raising concerns that the manipulated cells may suffer from constitutive ER stress[121].

The siRNA or shRNA approach is also widely used to downregulate gene expression by using cellular systems to destroy the mRNA of target genes[122,123]. However, in most cases, downregulation is not complete and siRNAs/shRNAs can induce non-specific alterations in gene expression. Using gene expression profiling, it was shown that some siRNAs can induce silencing of off-target genes containing as few as 11 nucleotides identical to the siRNA[124]. The off-target gene regulation was often equally as sensitive to the siRNA as target silencing, indicating that this effect was not simply an artefact of high siRNA concentrations. Furthermore, it has been reported that siRNAs and shRNAs can induce a partial interferon response[125,126]. Finally, downregulation of $Ca_v2.1$ or $Ca_v2.2$ with the RNA interference approach could probably lead to the same compensatory effects described in Cacna1a knock-out mice (discussed above), due to more efficient processing of the non-targeted calcium channels.

In contrast to optogenetic methods, which have been most often used for short-time dynamic activation of neurons by light[127], the t-toxin approach described here is particularly well suited for genetic regulation of neurotransmission over relatively longer time frames. Moreover, optogenetic approaches require the direct accessibility of target areas, making it difficult to manipulate neurotransmission in deeper brain regions[128,129], and may result in alteration of the physiology of the neuron due to the hyperpolarization of the plasma membrane.

Importantly, no effect on neuronal survival, passive membrane properties and neuronal firing were observed in neurons in which $Ca_v2.1$ and $Ca_v2.2$ calcium currents were blocked individually or simultaneously by t-toxins. Furthermore, no differences in the number or general morphology of t-toxin expressing dopaminergic neurons compared to non-infected controls could be seen even after five months post-infection. The absence of obvious signs of toxicity, the demonstration that t-toxin expression can be regulated over the period of days or weeks using the tetracycline regulatory system, and the development of the Cre dependent t-toxin viruses described here, suggest that this strategy can be productively used as a valuable new tool to study the contributions of specific neurons to normal or abnormal behaviors, such as those that occur under conditions of long-term stress or drug abuse.

4.8 Possible applications of t-toxins

4.8.1 T-toxins in research

T-toxins have already been successfully used in zebrafish to block muscle nAChRs[89], in chick to inhibit nAChRs[95] and in Drosophila to modulate voltage-gated sodium channels[93]. In this work, the newly generated t-toxins incorporating ω-conotoxin MVIIA and ω-Agatoxin IVA were shown to efficiently block $Ca_v2.1$ and $Ca_v2.2$ mediated calcium currents *in vitro* and *in vivo*, resulting in cell-specific and cell-autonomous silencing of neurotransmission. The fact that both toxins are well-characterized and established tools for dissecting $Ca_v2.1$ from $Ca_v2.2$ calcium currents in many species indicates that also the lentiviral t-toxins could be used for circuitry studies in various animal models. Thus, MVIIA and AgaIVA tethered toxins could potentially be broadly applied to inhibit $Ca_v2.1$ and $Ca_v2.2$ calcium currents individually or simultaneously for characterization of the channel contribution to physiological functions and circuit analyses in a wide variety of species.

4.8.2 Therapeutic potential of t-toxins

The tethered toxin strategy also represents a potential new avenue for the development of genetic therapies for chronic diseases caused by malfunction of ion channels and peptide ligand receptors. Several human disorders that affect nervous system functions have been traced to mutations in genes encoding ion channels or regulatory proteins[130]. These disorders, referred to as channelopathies, could potentially be targeted by the t-toxin strategy when the

disorder is caused by ion channel hyperactivity. For instance, conotoxin MVIIA (commercialized as Prialt[®]) is already used to treat severe chronic pain in humans[17-19]. However, its use requires the implantation of intrathecal microinfusion pumps, which allow constant administration of the soluble drug to minimize the still substantial side effects due to block of CNS channels. In our group we have genetically targeted t-MVIIA to nociceptive neurons and shown that transgenic mice are protected from inflammatory and neuropathic pain, suggesting that this strategy could be a viable alternative therapy to avoid uncontrolled diffusion of the injected toxin and the necessity for repetitive treatments[131]. Further examples of hyperactive disorders include gain-of-function mutations in $Ca_v2.1$ calcium channels, linked to familial hemiplegic migraine type 1 (FHM-1)[132,133], and mutations in neuronal nAChRs associated to autosomal dominant nocturnal frontal lobe epilepsy (ADNFLE)[134,135]. Here, one potential application would be to use t-toxins in corresponding mouse mutant models to dissect the circuitry of the diseases in a cell-specific manner.

Conversely, activation of receptors with peptide agonists, expressed as t-peptide ligands could possibly be used to selectively regulate G-protein coupled receptors (GPCRs). For instance, isoforms of glucagon-like and calcitonin-gene-related peptides are presently being used to regulate insulin release and bone remodeling in diabetes[136] and osteoporosis[137], respectively. Similarly, neuropeptides involved in feeding-regulation such as orexin or ghrelin[138] could be targeted to circuits controlling appetite control, or tethered opioid peptides could be directed to nociceptive neurons.

Importantly, only a small percentage of existing peptide toxins has been characterized so far. It is estimated that there are around 500 species of cone snails, each producing 50 to 200 different conotoxins[1,23,27]. With a similar number of peptide toxins derived from snakes, spiders, sea anemones, scorpions and other venomous animals[27,36,139], it is estimated that thousands of compounds could be available to target different ion channels, receptors, and other signaling molecules. For example, genetically encoded t-toxins specific for Ca_v1, $Ca_v2.3$ and Ca_v3 mediated calcium currents, could be used to manipulate hormone secretion and muscle contraction. With ever-growing interest and technical possibilities to identify the potential of naturally occurring venom peptide toxins[2,4,5], an increasing number of peptide based treatments could be possible. Furthermore, simultaneous progress of the safety of viral delivery methods for human gene therapy will increase the number of diseases to which the t-toxin/t-peptide strategy could be applicable.

4.8.3 Application of t-toxins for drug discovery

Ion channels and receptors belong to the most important molecular drug targets, but still remain underexploited in drug discovery. Peptide toxins, which are effective modulators of ion channels and receptors, offer an intriguing opportunity for increasing the drug development pipeline. A major limitation to the universal usage of peptide toxins in the development of therapeutics has been the low efficiency of venom retrieval from life animals. To circumvent this, most toxins are synthesized chemically, but this too has significant limitations, one of them is to obtain the correct disulfide scaffold with *in vitro* folding. To overcome these synthesis problems, several structural strategies and characterization methods have been developed[4,140-143]. However, even when the toxin is successfully synthesized, soluble toxins cannot be directed to single cell populations, are expensive, and have a limited time of application that makes their use *in vivo* problematic. The t-toxin strategy overcomes these limitations with the ability to recombinantly express the toxins in the cell itself, together with the receptor or channel to be screened. Another advantage would be that point mutations could easily be introduced. Recent reports use the t-peptide technology to characterize point mutants of peptide hormones against class B1 GPCRs[144]. In a similar manner, the t-peptide technology could be applied to screen gene libraries of t-peptides against specific membrane proteins by co-expression in the same cell. T-peptides with activating or blocking capabilities could be monitored with functional assays, i.e. calcium influx quantifications. This type of screen could be beneficial to block channels that are hyperactive in certain diseases, such as TRPP2[145], for which no natural toxins have yet been identified. These features make the t-peptide genetic approach a promising strategy for drug discovery and development of targeted therapeutics.

4.9   Possible further optimizations of t-toxins

In neurons which were co-infected with MVIIA-PE and AgaIVA-VG in this work, it was shown that silencing of neurotransmission could potentially be further optimized by ensuring the virus delivery of both constructs to all target cells, and not by higher efficiency of the single t-toxin, as this was found to be sufficient to inhibit all target channels in a cell. Therefore, it would be beneficial to have a single t-toxin for the inhibition of both $Ca_v2.1$ and $Ca_v2.2$, requiring only one infection event per cell. This would greatly enhance the targeting of cells, and the generation, as well as the administration of two virus preparations would be unnecessary. Unfortunately, as discussed above, the attempts to use AgaIIIA and MVIIC as t-toxins for simultaneous block of several calcium channels with a single toxin failed. Hence, ongoing work in the lab is now dedicated to develop a functional t-toxin construct carrying both MVIIA and AgaIVA.

Furthermore, intracellular targeting would offer a possibility of dissecting the functions of somato-dendritic versus presynaptic nAChR and calcium channels. Thus, in current studies of our group, t-toxins are fused with different intracellular targeting signals and proteins in order to achieve specific localization of t-toxins.

It may also be possible to include several other functional domains into the t-toxins, like protease cleavage sites for rapid inactivation, light- or chemical sensitive linkers for fast activation/inactivation or additional ligands and motifs for increased binding to the target channel. In this way, t-toxins could be 'tailor-made' according to their specific application.

5.   Conclusions

Based on the structural homology of the endogenous prototoxin lynx1 with the snake α-bungarotoxin, our lab has recently developed the tethered toxin (t-toxin) strategy for recombinant expression of functionally active, membrane-bound toxins, by using the biological scaffold of lynx1 (secretory signal and GPI signal).

The work presented here expands the t-toxin approach and establishes for the first time the utility of t-toxins to specifically inhibit calcium currents *in-vivo* in mice. This has been accomplished by the integration of new modules and peptide toxins to generate novel t-toxins, and by using lentiviral vectors for gene delivery to targeted cells. The optimized constructs were generated by incorporation of several well-characterized peptide toxins, to achieve cell-specific and autonomous blockade of voltage gated calcium channels ($Ca_v2.1$ and $Ca_v2.2$; toxins: AgaIIIA, AgaIVA, MVIIA and MVIIC), as well as of nicotinic acetylcholine receptors (nAChRs; toxin: GID). In addition, fluorescent reporter proteins (EGFP, Venus and mCherry) were integrated to enable constant monitoring of the expression and subcellular localization. Furthermore, to achieve efficient insertion of t-toxins into the plasma membrane, the PDGF-receptor transmembrane domain or a glycophosphatidylinositol (GPI) anchor were attached.

We show here that expression of calcium channel specific t-toxins by constitutive, inducible, as well as Cre-recombinase dependent lentiviral constructs can be efficiently used to inhibit $Ca_v2.1$ and $Ca_v2.2$ ionic currents *in vitro* in rat hippocampal neurons. Moreover, complete silencing of neurotransmission was achieved by simultaneous blockade of $Ca_v2.1$ and $Ca_v2.2$ by t-toxin co-transduction in these neurons. And importantly, the *in vivo* efficacy of this approach to block neurotransmission could be demonstrated by inhibition of dopaminergic signaling in the nigro-striatal pathway in lentivirus injected mice. In addition to calcium-channel t-toxins, the functionality of nAChR specific constructs was demonstrated in this work by inhibition of α7 and α3β4 nAChRs in *Xenopus laevis* oocytes.

In conclusion, the optimized t-toxins generated in this work provide a straightforward new method to inhibit $Ca_v2.1$ and $Ca_v2.2$ voltage-gated calcium channels and nicotinic acetylcholine receptors (nAChRs) on long-term scale by recombinant and cell-autonomous expression in targeted cells.

Given the extreme diversity of natural peptide venoms, membrane-tethered toxins are promising new tools for long-term modulation of neurotransmission by inhibition of specific ionic currents, and for characterization of the contribution of very diverse channels and receptors to physiological functions in a wide variety of species.

5. Zusammenfassung

Basierend auf der strukturellen Ähnlichkeit des endogenen Prototoxins lynx1 mit dem Schlangengift α-Bungarotoxin hat unsere Arbeitsgruppe die sogenannte „tethered-toxin" (T-Toxin) Methode entwickelt, bei welcher die Grundsequenz von lynx1, bestehend aus einem Sekretionssignal und einem Glycophosphatidylinositol (GPI)-Membrananker genutzt wird, um funktionale Peptidtoxine als Fusionsproteine membranständig zu exprimieren.

In der vorliegenden Arbeit wurde diese Methode weiterentwickelt und die Funktionalität von T-Toxinen zur Inhibierung von Kalzium-Kanälen konnte zum ersten Mal *in-vivo* im Mausmodell demonstriert werden. Dies wurde zum einen durch die Integration neuer Module und Peptidtoxine, als auch durch die Verwendung lentiviraler Vektoren zum Gentransport in die Zielzellen ermöglicht. Der Einbau von genau charakterisierten Neurotoxinen ermöglicht die zell-spezifische und zell-autonome Inhibierung von Kalzium-Kanälen (Ca$_v$2.1 und Ca$_v$2.2; Toxine: AgaIIIA, AgaIVA, MVIIA und MVIIC), als auch von nikotinischen Azetylcholinrezeptoren (nAChR; toxin: GID). Zusätzlich wurden erstmals Fluoreszenzmarker integriert (EGFP, Venus und mCherry), welche eine ständige Expressions- und Lokalisationsanalyse der Fusionsproteine erlauben. Um die Membranständigkeit der Kostrukte zu gewährleisten wurde die Transmembrandomäne des PDGF-Rezeptors oder ein GPI-Membrananker verwendet.

Wir konnten zeigen, dass die Inhibierung der Kalzium-Kanäle Ca$_v$2.1 und Ca$_v$2.2 duch spezifische T-Toxine von konstitutiven, induzierbaren und Cre-rekombinase abhängigen lentiviralen Vektoren zu einer Beeinflussung der Neurotransmission in kultivierten Hippocampus Neuronen führt. Zudem wurde eine vollständige Blockierung der Neurotransmission durch die gleichzeitige Inhibierung beider Kanäle nach Ko-Transduktion der T-Toxine erzielt. Bedeutenderweise konnte die Funktionalität dieser Konstrukte auch *in vivo,* durch Blockierung der Dopaminausschüttung im nigro-striatalen Signalübertragungsweg in Lentivirus-injizierten Mäusen gezeigt werden. Desweiteren wurde die Funktionalität von nAChR-spezifischen T-Toxinen durch Inhibierung von α7 und α3β4 nACh-Rezeptoren in *Xenopus laevis* Oocyten nachgewiesen.

Die aus dieser Arbeit hervorgegangenen T-Toxine stellen eine Erweiterung der vorhandenen rekombinanten und pharmakologischen Methoden zur Untersuchung der physiologischen Funktionen von Ionenkanälen und Rezeptoren dar. Sie erlauben deren zell-spezifische und zell-autonome Langzeit-Inhibierung und können damit für die genauere Charakterisierung dieser Ionenkanäle und Rezeptoren in verschiedensten Tiermodellen verwendet werden.

6. Appendix

6.1 Abbreviations

AgaIIIA	Agatoxin III A
AgaIVA	Agatoxin IVA
6-OHDA	6-Hydroxydopamine
BSA	Bovine serum albumin
$Ca_v2.1$	P/Q-type voltage-gated calcium channel
$Ca_v2.2$	N-type voltage-gated calcium channel
$Ca_v2.3$	R-type voltage-gated calcium channel
cDNA	Complementary DNA
CNS	Central nervous system
DA	Dopamine
DAPI	4′,6-Diamidino-2-phenylindol
DIV	Days in vitro
DMEM	Dulbecco's modified Eagle's medium
DMSO	Dimethyl sulfoxide
DNA	Deoxyribonucleic acid
dNTP	Deoxynucleotidetriphosphate
DTT	Dithiothreitol
EDTA	Ethylenediaminetetraacetic acid
eEPSC	Evoked excitatory postsynaptic current
EGFP	Enhanced green fluorescent protein
eIPSC	Evoked inhibitory postsynaptic current
FBS	Fetal bovine serum
GABA	γ-aminobutyric acid
GPCR	G-protein coupled receptor
GPI	Glycosylphosphatidylinositol
HCl	Hydrochloric acid
i.p.	intraperitoneal
K_d	Dissociation constant
LV	Lentivirus
MFB	Medial forebrain bundle
MOI	Multiplicity of infection (virus particles/cell)
MQ	Type-I ultrapure water (from Barnstead E-pure system)
mRNA	Messenger ribonucleic acid
nAChR	Nicotinic acetylcholine receptor

NaCl	Sodium chloride
NaOH	Sodium hydroxide
OD	Optical density
o/n	Over night
PBS	Phosphate-buffered saline
PBT	PBS-Tween-20
PCR	Polymerase chain reaction
PDGF-R	Platelet-derived growth factor receptor
PDGF-R-TM	Platelet-derived growth factor receptor transmembrane domain
PFA	Paraformaldehyde
pH	Potentium hydrogenii
PI-PLC	Phosphatidylinositol-specific phospholipase C
PNS	Peripheral nervous system
PPR	Paired-pulse recordings
RHC	Rat hippocampus culture
RNase	Ribonuclease
rpm	Revolutions per minute
RT	Room temperature
SDS	Sodium dodecyl sulphate
TTX	Tetrodotoxin
TM	Transmembrane domain
TU	Transducing unit
s.e.m	Standard error of the mean
SD	Standard deviation
SNpc	Substantia nigra pars compacta
SNpr	Substantia nigra pars reticulata
SSC	Sodiumchloride-sodiumcitrate
STI	Stereotaxic injection
TAE	Tris-acetate EDTA
TE	Tris-EDTA
TH	Tyrosine hydroxylase
t-toxin	Membrane tethered toxin
Tris	Tris-(hydroxymethyl-) aminoethane
t-RNA	Transfer ribonucleic acid
VGCC	Voltage-gated calcium channel
VGSC	Voltage-gated sodium channel
VTA	Ventral tegmental area

Units

bp	base pairs
°C	Degrees Celsius
d	Days
g	Gram
h	Hour
kb	Kilobase
kDa	Kilodalton
l	Liter
M	Molar
mg	Milligram
min	Minute
ml	Milliliter
mM	Millimolar
nA	Nanoampere
ng	Nanogram
pA	Picoampere
µg	Microgram
s	Second
U	Unit (for enzyme activity)

6.2 Plasmid maps
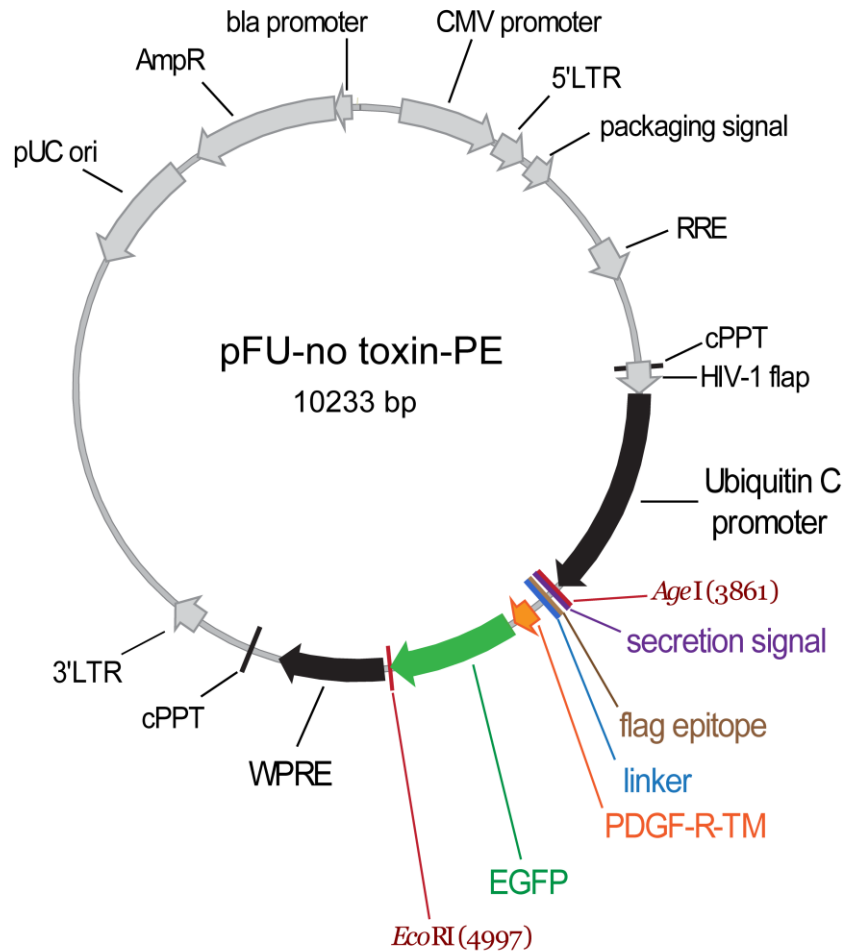
atgtctgcacttctgatcctagctcttgttggagctgcagttgctatcgattacaaagacgatgacgacaagcttgcggccgctggtaacg
gaaatggcaacgggaatggtaacggaaacggcaacgggggatggtactcgagttgctgtgggccaggacacgcaggaggtcatcgt
ggtgccacactccttgcccttttaaggtggtggtgatctcagccatcctggccctggtggtgctcaccatcatctcccttatcatcctcatcat
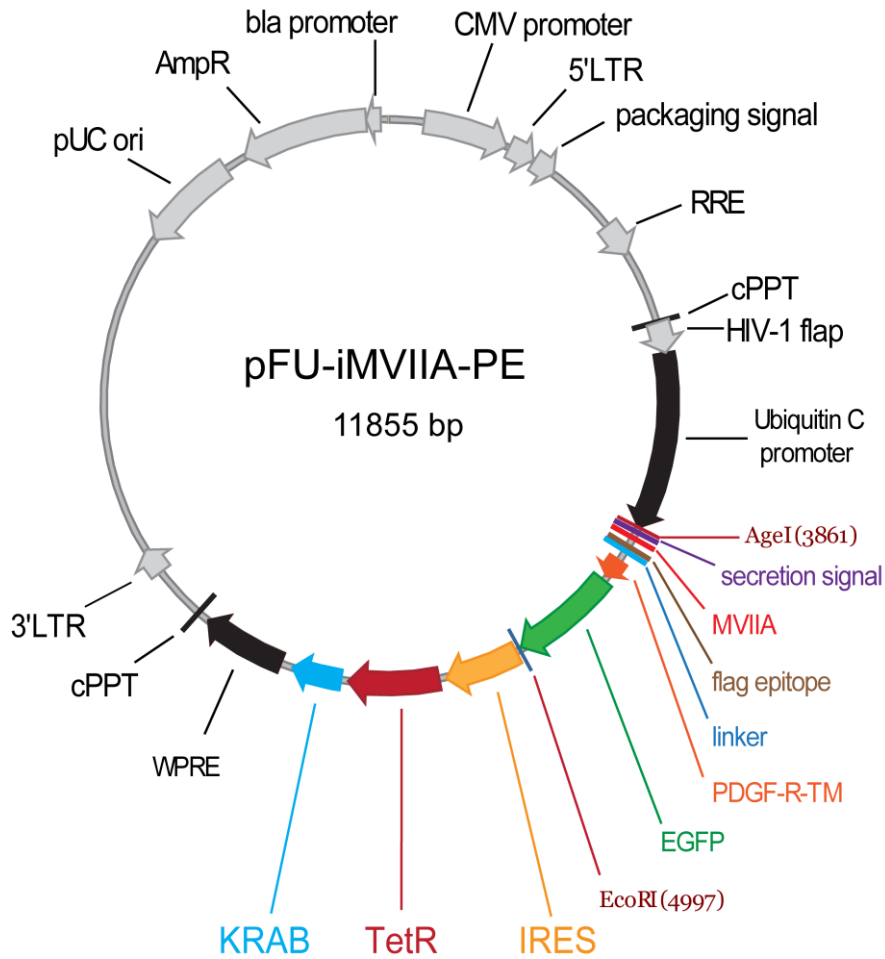gctttggcagaagaaaccacgtaggatccaccggccggtcgccaccatggtgagcaagggcgaggagctgttcaccggggtggtg
cccatcctggtcgagctggacggcgacgtaaacggccacaagttcagcgtgtccggcgagggcgagggcgatgccacctacggca
agctgaccctgaagttcatctgcaccaccggcaagctgcccgtgccctggcccacgcctcgtgaccaccctgacctacggcgtgcagt
gcttcagccgctaccccgaccacatgaagcagcacgacttcttcaagtccgccatgcccgaaggctacgtccaggagcgcaccatctt
cttcaaggacgacggcaactacaagacccgcgccgaggtgaagttcgagggcgacaccctggtgaaccgcatcgagctgaagggc
atcgacttcaaggaggacggcaacatcctggggcacaagctggagtacaactacaacagccacaacgtctatatcatggccgacaag
cagaagaacggcatcaaggtgaacttcaagatccgccacaacatcgaggacggcagcgtgcagctcgccgaccactaccagcaga
acacccccatcggcgacggccccgtgctgctgcccgacaaccactacctgagcacccagtccgccctgagcaaagaccccaacga
gaagcgcgatcacatggtcctgctggagttcgtgaccgccgccgggatcactctcggcatggacgagctgtacaagtaa

Figure 43. Plasmid map and sequence of negative control construct no toxin-PE in lentiviral vector pFUGW.
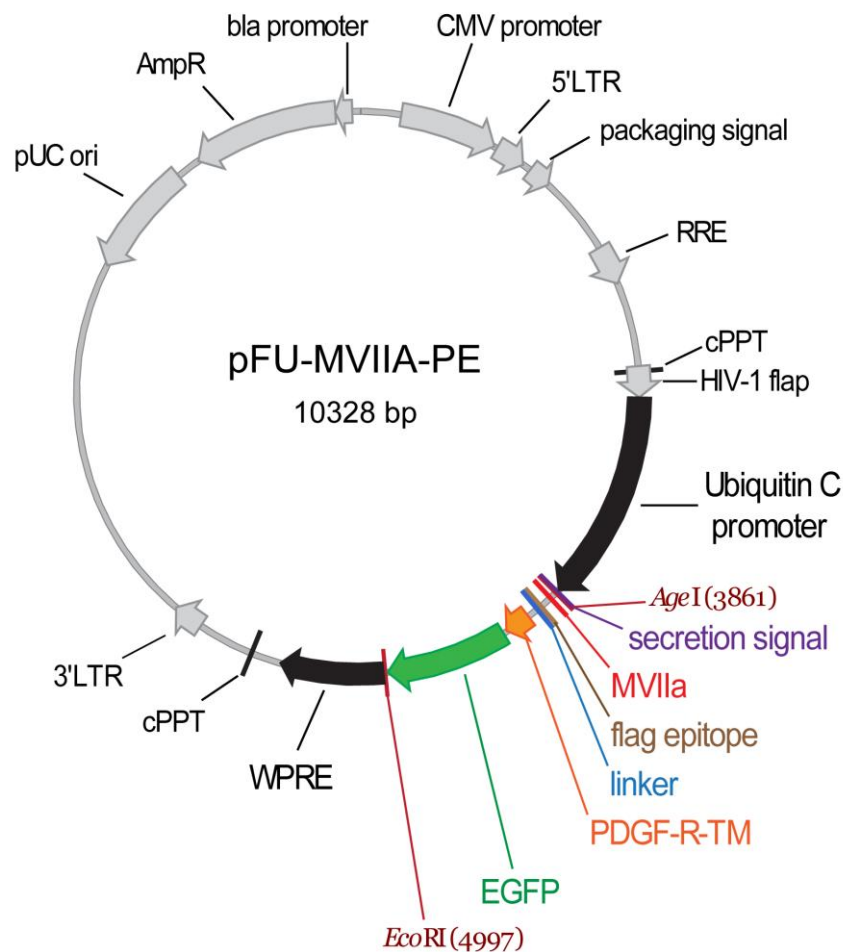
atgtctgcacttctgatcctagctcttgttggagctgcagttgcttgcaaaggcaagggcgcgaagtgctcccgcctcatgtatgactgtt
gcaccggatcgtgtaggtccggtaagtgcatcgattacaaagacgatgacgacaagcttgcggccgctggtaacggaaatggcaacg
ggaatggtaacggaaacggcaacggggatggtactcgagttgctgtgggccaggacacgcaggaggtcatcgtggtgccacactcc
ttgccctttaaggtggtggtgatctcagccatcctggccctggtggtgctcaccatcatctcccttatcatcctcatcatgctttggcagaag
aaaccacgtaggatccaccggccggtcgccaccatggtgagcaagggcgaggagctgttcaccggggtggtgcccatcctggtcga
gctggacggcgacgtaaacggccacaagttcagcgtgtccggcgagggcgagggcgatgccacctacggcaagctgaccctgaa
gttcatctgcaccaccggcaagctgcccgtgccctggcccaccctcgtgaccaccctgacctacggcgtgcagtgcttcagccgctac
cccgaccacatgaagcagcacgacttcttcaagtccgccatgcccgaaggctacgtccaggagcgcaccatcttcttcaaggacgac
ggcaactacaagacccgcgccgaggtgaagttcgagggcgacaccctggtgaaccgcatcgagctgaagggcatcgacttcaagg
aggacggcaacatcctggggcacaagctggagtacaactacaacagccacaacgtctatatcatggccgacaagcagaagaacggc
atcaaggtgaacttcaagatccgccacaacatcgaggacggcagcgtgcagctcgccgaccactaccagcagaacacccccatcgg
cgacggccccgtgctgctgcccgacaaccactacctgagcacccagtccgccctgagcaaagaccccaacgagaagcgcgatcac
atggtcctgctggagttcgtgaccgccgccgggatcactctcggcatggacgagctgtacaagtaa

Figure 44. Plasmid map and sequence of tethered toxin MVIIA-PE in lentiviral vector pFUGW.
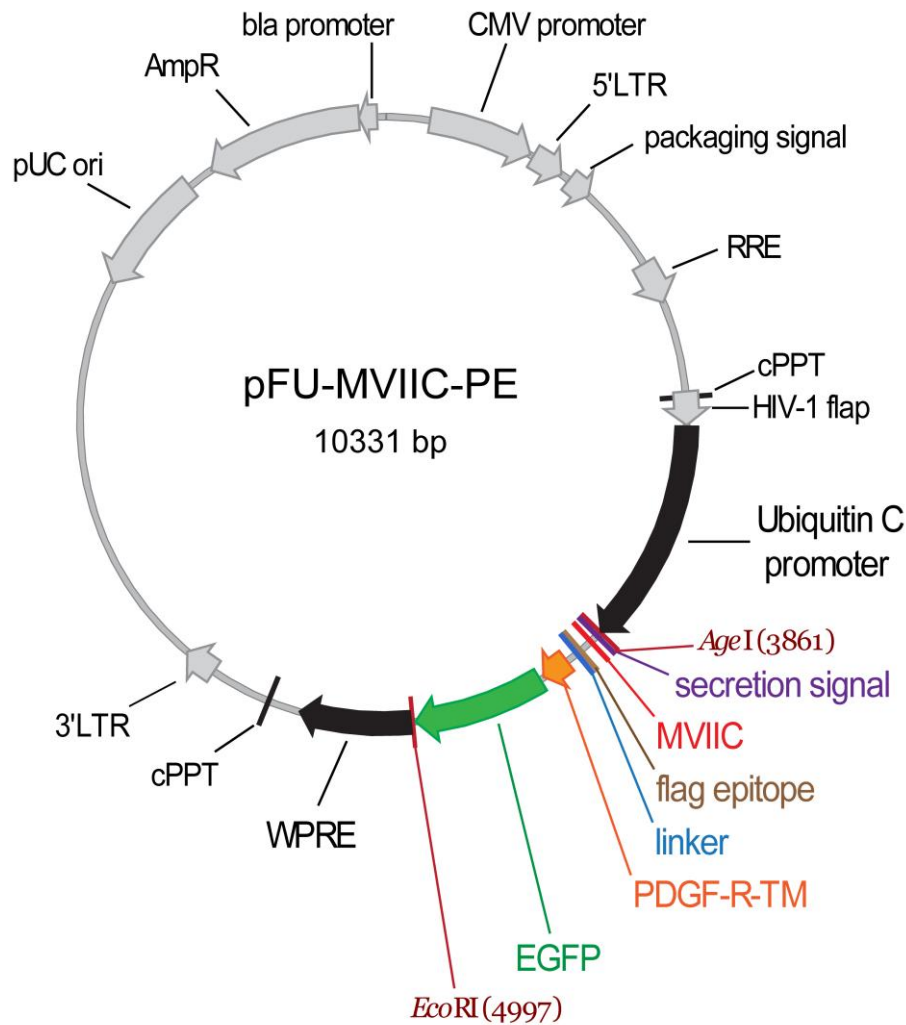
atgtctgcacttctgatcctagctcttgttggagctgcagttgtaaaggaaaaggggcgccatgtaggaaaactatgtatgactgttgttct
gggtcttgcggaaggcgaggcaagtgtatcgattacaaagacgatgacgacaagcttgcggccgctggtaacggaaatggcaacgg
gaatggtaacggaaacggcaacggggatggtactcgagttgctgtgggccaggacacgcaggaggtcatcgtggtgccacactcctt
gccctttaaggtggtggtgatctcagccatcctggccctggtggtgctcaccatcatctcccttatcatcctcatcatgctttggcagaaga
aaccacgtaggatccaccggccggtcgccaccatggtgagcaagggcgaggagctgttcaccggggtggtgcccatcctggtcgag
ctggacggcgacgtaaacggccacaagttcagcgtgtccggcgagggcgagggcgatgccacctacggcaagctgaccctgaagt
tcatctgcaccaccggcaagctgcccgtgccctggcccaccctcgtgaccaccctgacctacggcgtgcagtgcttcagccgctaccc
cgaccacatgaagcagcacgacttcttcaagtccgccatgcccgaaggctacgtccaggagcgcaccatcttcttcaaggacgacgg
caactacaagacccgcgccgaggtgaagttcgagggcgacaccctggtgaaccgcatcgagctgaagggcatcgacttcaaggag
gacggcaacatcctggggcacaagctggagtacaactacaacagccacaacgtctatatcatggccgacaagcagaagaacggcat
caaggtgaacttcaagatccgccacaacatcgaggacggcagcgtgcagctcgccgaccactaccagcagaacacccccatcggc
gacggccccgtgctgctgcccgacaaccactacctgagcacccagtccgccctgagcaaagaccccaacgagaagcgcgatcacat
ggtcctgctggagttcgtgaccgccgccgggatcactctcggcatggacgagctgtacaagtaa

Figure 45. Plasmid map and sequence of tethered toxin MVIIC-PE in lentiviral vector pFUGW.
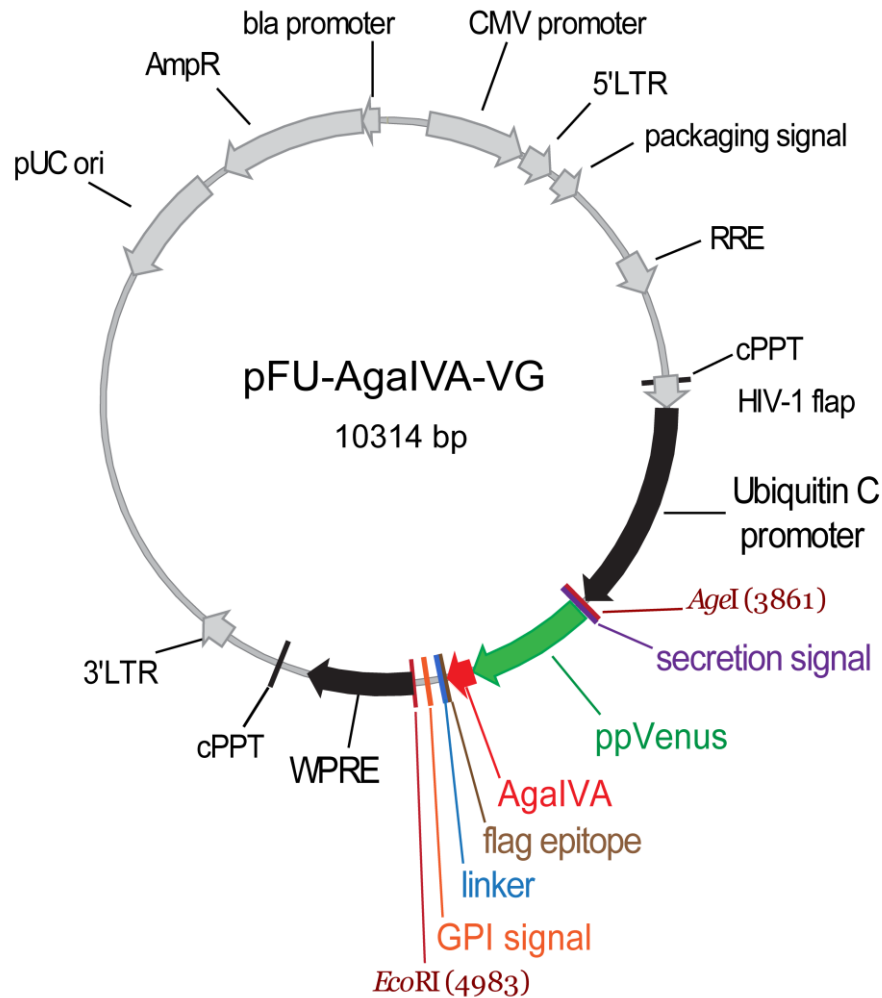
gccaccatgtctgcacttctgatcctagctcttgttggagctgcagttgctgtgagcaagggcgaggagctgttcaccggggtggtgcc
catcctggtcgagctggacggcgacgtaaacggccacaagttcagcgtgtccggcgagggcgagggcgatgccacctacggcaag
ctgaccctgaagctgatctgcaccaccggcaagctgcccgtgcccctggcccaccctcgtgaccaccctgggctacggcctgcagtgc
ttcgcccgctaccccgaccacatgaagcagcacgacttcttcaagtccgccatgcccgaaggctacgtccaggagcgcaccatcttctt
caaggacgacggcaactacaagacccgcgccgaggtgaagttcgagggcgacaccctggtgaaccgcatcgagctgaagggcat
cgacttcaaggaggacggcaacatcctggggcacaagctggagtacaactacaacagccacaacgtctatatcaccgccgacaagc
agaagaacggcatcaaggccaacttcaagatccgccacaacatcgaggacggcggcgtgcagctcgccgaccactaccagcagaa
cacccccatcggcgacggccccgtgctgctgcccgacaaccactatctgagctaccagtccgccctgagcaaagaccccaacgaga
agcgcgatcacatggtcctgctggagttcgtgaccgccgccgggatcactctcggcatggacgagctgtacaagtccggccggactc
agatcttaaagaagaagtgcatcgccaaggactacggcaggtgcaagtggggcggcacccccctgctgtaggggcaggggctgcatc
tgtagcatcatgggcaccaactgcgagtgcaagcccaggctgatcatggagggcctgggcctggccatcgattacaaagacgatgac
gacaagcttgcggccgctggtaacggaaatggcaacgggaatggtaacggaaacggcaacggggatggtaatggaggtgcactct
gcaacggtgctggctttgctaccccggtgaccttggccctggtcccagcactcctagctaccttctggagcttgctgtaa

Figure 46. Plasmid map and sequence of tethered toxin AgaIVA-VG in lentiviral vector pFUGW.

Figure 47. Plasmid map and sequence of tethered toxin AgaIIIA-VG in lentiviral vector pFUGW.

Figure 48. Plasmid map of doxyxcyline inducible MVIIA-PE in lentiviral vector pFU-iMVIIA-PE.
Genetic code shows IRES, TetR and KRAB coding sequences.
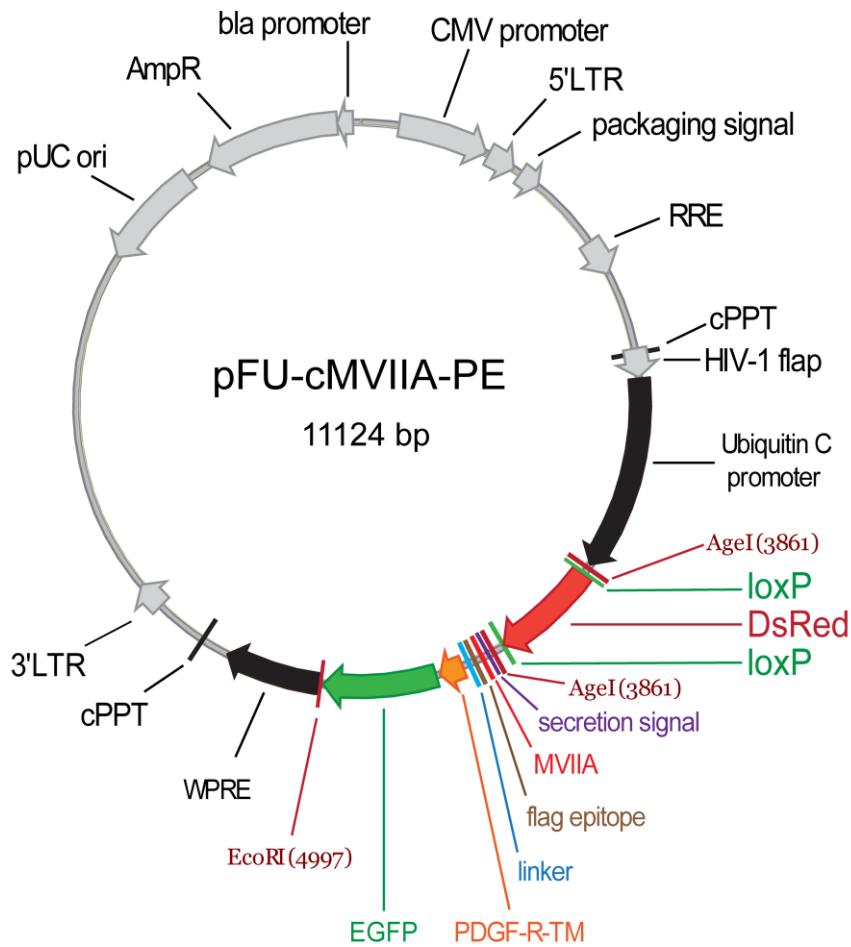
ataacttcgtatagcatacattatacgaagttattctagacacaaccatggcctcctccgagaacgtcatcaccgagttcatgcgcttcaag
gtgcgcatggagggcaccgtgaacggccacgagttcgagatcgagggcgagggcgagggccgcccctacgagggccacaacac
cgtgaagctgaaggtgaccaagggcggcccccctgcccttcgcctgggacatcctgtcccccccagttccagtacggctccaaggtgta
cgtgaagcaccccgccgacatccccgactacaagaagctgtccttccccgagggcttcaagtgggagcgcgtgatgaacttcgagga
cggcggcgtggcgaccgtgacccaggactcctccctgcaggacggctgcttcatctacaaggtgaagttcatcggcgtgaacttcccc
tccgacggcccccgtgatgcagaagaagaccatgggctgggaggcctccaccgagcgcctgtaccccgcgacggcgtgctgaagg
gcgagacccacaaggccctgaagctgaaggacggcggccactacctggtggagttcaagtccatctacatggccaagaagcccgtg
cagctgcccggctactactacgtggacgccaagctggacatcacctcccacaacaaggactacaccatcgtggagcagtacgagcg
caccgagggccgccaccacctgttcctgtagagctcgcgactctagactgagtgagtgacataacttcgtatagcatacattatacgaa
gttat

Figure 49. Plasmid map of Cre-recombinase dependent MVIIA-PE in lentiviral vector pFU-cMVIIA-PE. Genetic code shows loxP and DsRed coding sequences.

6.3   Index of figures

6.4   Index of tables

Erklärung

Hiermit versichere ich, Sebastian Auer, dass ich die vorgelegte Dissertation mit dem Titel ‚Development of new membrane-tethered toxins as genetic tools for *in vitro* and *in vivo* silencing of ion channels' selbstständig, ohne unerlaubte Hilfe angefertigt habe.

16.02.2010
Ort, Datum   Unterschrift

6.5   Publication and presentation list

Publications

Auer S, Sturzebecher A S, Juttner R, Santos-Torres J, Hanack C, Frahm S, Liehl B, and Ibanez-Tallon I (2010). Silencing neurotransmission with membrane-tethered toxins. *Nat Meth* (*advance online publication*). Available at: http://dx.doi.org/10.1038/nmeth.1425.

Stürzebecher A, Hu J, Smith E S J, Frahm S, Santos-Torres J, Kampfrath B, **Auer S**, Lewin G R, Ibanez-Tallon I (accepted Feb. 2010). An *in vivo* tethered toxin approach for the cell-autonomous inactivation of voltage-gated sodium channel currents in nociceptors. *J Physiol*.

Holford M, **Auer S**, Laqua M, Ibañez-Tallon I (2009). Manipulating neuronal circuits with endogenous and recombinant cell-surface tethered modulators. *Front Mol Neurosci* 2:21.

Oral presentations

"Silencing neurotransmission with membrane-tethered toxins." MDC Neuro Retreat 2009. Hotel Hubertusstock, Joachimsthal, 30. Sept.-01. Oct. 2009.

"Silencing neurotransmission with membrane-tethered toxins." Berlin Brain Days. MDC.C, 10.-12. Dec. 2008, (awarded 2nd prize).

"Development of genetic tools for selective and reversible silencing of ion channels using natural toxins." PhD-Retreat of MDC/FMP 2008. Hotel Döllnsee-Schorfheide, Templin, 18.-20. Aug. 2008.

Poster presentations

Auer S, Stürzebecher A, Jüttner R, Santos-Torres J, Hanack C, Frahm S, Ibañez-Tallon I. "Silencing neurotransmission with membrane-tethered toxins." SfN Neuroscience Meeting 2009. McCormick Place Convention Center, Chicago, USA. 17.-21. Oct. 2009.

Auer S, Stürzebecher A, Jüttner R, Santos-Torres J, Hanack C, Frahm S, Ibañez-Tallon I. "Silencing neurotransmission with membrane-tethered toxins." PhD-Retreat of MDC/FMP 2009. Hotel Sommerfeld, Kremmen, Germany. 03.-05. Sept. 2009.

Auer S, Jüttner R, Santos-Torres J, Ibañez-Tallon I. "Optimization of venom peptide tethered toxins for cell-autonomous inactivation of calcium ion channels." Integrative approaches to brain complexity. Joint Cold Spring Harbour/Wellcome Trust Conference, Hinxton, United Kingdom. 01.-05. Oct. 2008.

Auer S, Jüttner R, Santos-Torres J, Ibañez-Tallon I. "Development of genetic tools for selective and reversible silencing of ion channels using natural toxins." Berlin Neuroscience Forum 2008. Congress Hotel Preußischer Hof, Liebenwalde, Germany. 05.-07. June 2008.

Auer S, Jüttner R, Santos-Torres J, Ibañez-Tallon I. "Development of genetic tools for selective and reversible silencing of ion channels using natural toxins." Development and function of somatosensation and pain. MDC, Berlin, Germany. 14.-17. May 2008.

6.6 Curriculum Vitae

For reasons of data protection,
the curriculum vitae is not included in the online version

For reasons of data protection,
the curriculum vitae is not included in the online version

7.   References

1.   Terlau, H. & Olivera, B.M. Conus Venoms: A Rich Source of Novel Ion Channel-Targeted Peptides. *Physiol. Rev.* **84**, 41-68 (2004).
2.   Blumenthal, K.M. & Seibert, A.L. Voltage-gated sodium channel toxins: poisons, probes, and future promise. *Cell Biochem Biophys* **38**, 215-238 (2003).
3.   Lynch, S.S., Cheng, C.M. & Yee, J.L. Intrathecal ziconotide for refractory chronic pain. *Ann Pharmacother* **40**, 1293-1300 (2006).
4.   Han, T.S., Teichert, R.W., Olivera, B.M. & Bulaj, G. Conus venoms - a rich source of peptide-based therapeutics. *Curr Pharm Des* **14**, 2462-2479 (2008).
5.   Twede, V.D., Miljanich, G., Olivera, B.M. & Bulaj, G. Neuroprotective and cardioprotective conopeptides: an emerging class of drug leads. *Curr Opin Drug Di De* **12**, 231-239 (2009).
6.   Phui Yee, J.S.*, et al.* Snake postsynaptic neurotoxins: gene structure, phylogeny and applications in research and therapy. *Biochimie* **86**, 137-149 (2004).
7.   Catterall, W.A. Molecular Properties of Voltage-Sensitive Sodium Channels. *Annu Rev Biochem* **55**, 953-985 (1986).
8.   Tsetlin, V. Snake venom alpha-neurotoxins and other 'three-finger' proteins. *Eur J Biochem* **264**, 281-286 (1999).
9.   Norton, R.S. & Olivera, B.M. Conotoxins down under. *Toxicon* **48**, 780-798 (2006).
10.   Narahashi, T. Tetrodotoxin: a brief history. *Proc Jpn Acad Ser B Phys Biol Sci* **84**, 147-154 (2008).
11.   Llewellyn, L.E. Saxitoxin, a toxic marine natural product that targets a multitude of receptors. *Nat Prod Rep* **23**, 200-222 (2006).
12.   Hucho, F., Tsetlin, V.I. & Machold, J. The emerging three-dimensional structure of a receptor. The nicotinic acetylcholine receptor. *Eur J Biochem* **239**, 539-557 (1996).
13.   Léna, C. & Changeux, J.P. Allosteric nicotinic receptors, human pathologies. *J Physiol* **92**, 63-74 (1998).
14.   Endo, T. & Tamiya, N. Structure-function relationship of postsynaptic neurotoxins from snake venoms. *Snake Toxins (Harvey, A.L., ed.)*, Pergamon Press, New York. 165-222.-Pergamon Press, New York. 165-222. (1991).
15.   Zuo, X.-P. & Ji, Y.-H. Molecular mechanism of scorpion neurotoxins acting on sodium channels: insight into their diverse selectivity. *Mol Neurobiol* **30**, 265-278 (2004).
16.   Bosmans, F. & Tytgat, J. Voltage-gated sodium channel modulation by scorpion alpha-toxins. *Toxicon* **49**, 142-158 (2007).
17.   Zamponi, G.W., Lewis, R.J., Todorovic, S.M., Arneric, S.P. & Snutch, T.P. Role of voltage-gated calcium channels in ascending pain pathways. *Brain Res Rev* **60**, 84-89 (2009).
18.   Miljanich, G.P. Ziconotide: neuronal calcium channel blocker for treating severe chronic pain. *Curr Med Chem* **11**, 3029-3040 (2004).
19.   Staats, P.S.*, et al.* Intrathecal ziconotide in the treatment of refractory pain in patients with cancer or AIDS: a randomized controlled trial. *J Am Med Assoc* **291**, 63-70 (2004).
20.   Nirthanan, S.*, et al.* Candoxin, a novel toxin from Bungarus candidus, is a reversible antagonist of muscle (alphabetagammadelta) but a poorly reversible antagonist of neuronal alpha 7 nicotinic acetylcholine receptors. *J Biol Chem* **277**, 17811-17820 (2002).
21.   Drachman, D.B. The biology of myasthenia gravis. *Annu Rev Neurosci* **4**, 195-225 (1981).

22. Mebs, D. Snake venoms: toolbox of the neurobiologist. *Endeavour* **13**, 157-161 (1989).
23. Olivera, B.M. & Teichert, R.W. Diversity of the neurotoxic Conus peptides: a model for concerted pharmacological discovery. *Mol Interv* **7**, 251-260 (2007).
24. Bulaj, G. & Olivera, B.M. Folding of conotoxins: formation of the native disulfide bridges during chemical synthesis and biosynthesis of Conus peptides. *Antioxid Redox Sign* **10**, 141-155 (2008).
25. Ekberg, J., Craik, D.J. & Adams, D.J. Conotoxin modulation of voltage-gated sodium channels. *Int J Biochem Cell Biol* **40**, 2363-2368 (2008).
26. Olivera, B.M. E.E. Just Lecture, 1996. Conus venom peptides, receptor and ion channel targets, and drug design: 50 million years of neuropharmacology. *Mol Biol Cell* **8**, 2101-2109 (1997).
27. Lewis, R.J. & Garcia, M.L. Therapeutic potential of venom peptides. *Nat Rev Drug Discov* **2**, 790-802 (2003).
28. Nicke, A.*, et al.* Isolation, structure, and activity of GID, a novel alpha 4/7-conotoxin with an extended N-terminal sequence. *J Biol Chem* **278**, 3137-3144 (2003).
29. Millard, E.L.*, et al.* Inhibition of neuronal nicotinic acetylcholine receptor subtypes by alpha-Conotoxin GID and analogues. *J Biol Chem* **284**, 4944-4951 (2009).
30. Olivera, B.M.*, et al.* Neuronal calcium channel antagonists. Discrimination between calcium channel subtypes using omega-conotoxin from Conus magus venom. *Biochemistry* **26**, 2086-2090 (1987).
31. Kim, J.I., Takahashi, M., Ohtake, A., Wakamiya, A. & Sato, K. Tyr13 is essential for the activity of omega-conotoxin MVIIA and GVIA, specific N-type calcium channel blockers. *Biochem Biophys Res Commun* **206**, 449-454 (1995).
32. Olivera, B.M., Miljanich, G.P., Ramachandran, J. & Adams, M.E. Calcium channel diversity and neurotransmitter release: the omega-conotoxins and omega-agatoxins. *Annu Rev Biochem* **63**, 823-867 (1994).
33. Kohno, T.*, et al.* Three-dimensional structure in solution of the calcium channel blocker omega-conotoxin MVIIA. *Biochemistry* **34**, 10256-10265 (1995).
34. McDonough, S.I., Swartz, K.J., Mintz, I.M., Boland, L.M. & Bean, B.P. Inhibition of calcium channels in rat central and peripheral neurons by omega-conotoxin MVIIC. *J Neurosci* **16**, 2612-2623 (1996).
35. Farr-Jones, S., Miljanich, G.P., Nadasdi, L., Ramachandran, J. & Basus, V.J. Solution structure of omega-conotoxin MVIIC, a high affinity ligand of P-type calcium channels, using 1H NMR spectroscopy and complete relaxation matrix analysis. *J Mol Biol* **248**, 106-124 (1995).
36. Adams, M.E. Agatoxins: ion channel specific toxins from the American funnel web spider, Agelenopsis aperta. *Toxicon* **43**, 509-525 (2004).
37. Venema, V.J., Swiderek, K.M., Lee, T.D., Hathaway, G.M. & Adams, M.E. Antagonism of synaptosomal calcium channels by subtypes of omega- agatoxins. *J. Biol. Chem.* **267**, 2610-2615 (1992).
38. Reily, M.D., Holub, K.E., Gray, W.R., Norris, T.M. & Adams, M.E. Structure-activity relationships for P-type calcium channel-selective omega-agatoxins. *Nat Struct Biol* **1**, 853-856 (1994).
39. Mintz, I.M.*, et al.* P-type calcium channels blocked by the spider toxin [omega]-Aga-IVA. *Nature* **355**, 827-829 (1992).
40. Randall, A. & Tsien, R.W. Pharmacological dissection of multiple types of Ca2+ channel currents in rat cerebellar granule neurons. *J Neurosci* **15**, 2995-3012 (1995).
41. Mintz, I.M., Adams, M.E. & Bean, B.P. P-type calcium channels in rat central and peripheral neurons. *Neuron* **9**, 85-95 (1992).

42.   Winterfield, J.R. & Swartz, K.J. A hot spot for the interaction of gating modifier toxins with voltage-dependent ion channels. *J Gen Physiol* **116**, 637-644 (2000).

43.   Delenda, C. Lentiviral vectors: optimization of packaging, transduction and gene expression. *J Gene Med* **6** S125-138 (2004).

44.   Naldini, L.*, et al.* In vivo gene delivery and stable transduction of nondividing cells by a lentiviral vector. *Science* **272**, 263-267 (1996).

45.   Cockrell, A.S. & Kafri, T. Gene delivery by lentivirus vectors. *Mol Biotechnol* **36**, 184-204 (2007).

46.   Zufferey, R., Donello, J.E., Trono, D. & Hope, T.J. Woodchuck hepatitis virus posttranscriptional regulatory element enhances expression of transgenes delivered by retroviral vectors. *J Virol* **73**, 2886-2892 (1999).

47.   Akkina, R.K.*, et al.* High-efficiency gene transfer into CD34+ cells with a human immunodeficiency virus type 1-based retroviral vector pseudotyped with vesicular stomatitis virus envelope glycoprotein G. *J Virol* **70**, 2581-2585 (1996).

48.   Aiken, C. Pseudotyping human immunodeficiency virus type 1 (HIV-1) by the glycoprotein of vesicular stomatitis virus targets HIV-1 entry to an endocytic pathway and suppresses both the requirement for Nef and the sensitivity to cyclosporin A. *J Virol* **71**, 5871-5877 (1997).

49.   Lois, C., Hong, E.J., Pease, S., Brown, E.J. & Baltimore, D. Germline transmission and tissue-specific expression of transgenes delivered by lentiviral vectors. *Science* **295**, 868-872 (2002).

50.   Szulc, J., Wiznerowicz, M., Sauvain, M.-O., Trono, D. & Aebischer, P. A versatile tool for conditional gene expression and knockdown. *Nat Meth* **3**, 109-116 (2006).

51.   Nagy, A. Cre recombinase: the universal reagent for genome tailoring. *Genesis* **26**, 99-109 (2000).

52.   Hamilton, D.L. & Abremski, K. Site-specific recombination by the bacteriophage P1 lox-Cre system. Cre-mediated synapsis of two lox sites. *J Mol Biol* **178**, 481-486 (1984).

53.   Wang, X. Cre transgenic mouse lines. *Methods Mol Biol* **561**, 265-273 (2009).

54.   Karlin, A. Emerging structure of the nicotinic acetylcholine receptors. *Nat Rev Neurosci* **3**, 102-114 (2002).

55.   Paterson, D. & Nordberg, A. Neuronal nicotinic receptors in the human brain. *Prog Neurobiol* **61**, 75-111 (2000).

56.   Dani, J.A. & Bertrand, D. Nicotinic acetylcholine receptors and nicotinic cholinergic mechanisms of the central nervous system. *Annu Rev Pharmacol* **47**, 699-729 (2007).

57.   Dani, J.A. Overview of nicotinic receptors and their roles in the central nervous system. *Biol Psychiat* **49**, 166-174 (2001).

58.   Fabian-Fine, R.*, et al.* Ultrastructural distribution of the alpha7 nicotinic acetylcholine receptor subunit in rat hippocampus. *J Neurosci* **21**, 7993-8003 (2001).

59.   Taly, A., Corringer, P.J., Guedin, D., Lestage, P. & Changeux, J.P. Nicotinic receptors: allosteric transitions and therapeutic targets in the nervous system. *Nat Rev Drug Discov* **8**, 733-750 (2009).

60.   Changeux, J.P. & Edelstein, S.J. Allosteric receptors after 30 years. *Neuron* **21**, 959-980 (1998).

61.   Dutertre, S.b. & Lewis, R.J. Toxin insights into nicotinic acetylcholine receptors. *Biochem Pharmacol* **72**, 661-670 (2006).

62.   Giniatullin, R., Nistri, A. & Yakel, J.L. Desensitization of nicotinic ACh receptors: shaping cholinergic signaling. *Trends Neurosci* **28**, 371-378 (2005).

63.   Albuquerque, E.X.*, et al.* Properties of Neuronal Nicotinic Acetylcholine Receptors: Pharmacological Characterization and Modulation of Synaptic Function. *J Pharmacol Exp Ther* **280**, 1117-1136 (1997).

64. Gotti, C. & Clementi, F. Neuronal nicotinic receptors: from structure to pathology. *Prog Neurobiol* **74**, 363-396 (2004).

65. Lindstrom, J.M. Nicotinic acetylcholine receptors of muscles and nerves: comparison of their structures, functional roles, and vulnerability to pathology. *Ann N Y Acad Sci* **998**, 41-52 (2003).

66. Conti-Tronconi, B.M., McLane, K.E., Raftery, M.A., Grando, S.A. & Protti, M.P. The nicotinic acetylcholine receptor: structure and autoimmune pathology. *Crit Rev Biochem Mol Biol* **29**, 69-123 (1994).

67. Berg, D.K. & Conroy, W.G. Nicotinic alpha 7 receptors: synaptic options and downstream signaling in neurons. *J Neurobiol* **53**, 512-523 (2002).

68. Bertrand, D., Galzi, J.L., Devillers-Thiery, A., Bertrand, S. & Changeux, J.P. Mutations at two distinct sites within the channel domain M2 alter calcium permeability of neuronal alpha 7 nicotinic receptor. *Proc Natl Acad Sci U S A* **90**, 6971-6975 (1993).

69. Gray, R., Rajan, A.S., Radcliffe, K.A., Yakehiro, M. & Dani, J.A. Hippocampal synaptic transmission enhanced by low concentrations of nicotine. *Nature* **383**, 713-716 (1996).

70. Alkondon, M., Pereira, E.F., Wonnacott, S. & Albuquerque, E.X. Blockade of nicotinic currents in hippocampal neurons defines methyllycaconitine as a potent and specific receptor antagonist. *Mol Pharmacol* **41**, 802-808 (1992).

71. Castro, N.G. & Albuquerque, E.X. alpha-Bungarotoxin-sensitive hippocampal nicotinic receptor channel has a high calcium permeability. *Biophys J* **68**, 516–524-516–524 (1995).

72. Catterall, W.A., Perez-Reyes, E., Snutch, T.P. & Striessnig, J. International Union of Pharmacology. XLVIII. Nomenclature and structure-function relationships of voltage-gated calcium channels. *Pharmacol Rev* **57**, 411-425 (2005).

73. Yu, F.H. & Catterall, W.A. The VGL-chanome: a protein superfamily specialized for electrical signaling and ionic homeostasis. *Sci STKE* **2004**, re15 (2004).

74. Catterall, W.A. & Few, A.P. Calcium channel regulation and presynaptic plasticity. *Neuron* **59**, 882-901 (2008).

75. Mori, Y.*, et al.* Molecular pharmacology of voltage-dependent calcium channels. *Jpn J Pharmacol* **72**, 83-109 (1996).

76. Lacinova, L. Voltage-dependent calcium channels. *Gen Physiol Biophys* **24 Suppl 1**, 1-78 (2005).

77. Hofmann, F., Biel, M. & Flockerzi, V. Molecular basis for Ca2+ channel diversity. *Annu Rev Neurosci* **17**, 399-418 (1994).

78. Nowycky, M.C., Fox, A.P. & Tsien, R.W. Three types of neuronal calcium channel with different calcium agonist sensitivity. *Nature* **316**, 440-443 (1985).

79. Llinas, R., Sugimori, M., Lin, J.W. & Cherksey, B. Blocking and isolation of a calcium channel from neurons in mammals and cephalopods utilizing a toxin fraction (FTX) from funnel-web spider poison. *Proc Natl Acad Sci U S A* **86**, 1689-1693 (1989).

80. Bourinet, E.*, et al.* Splicing of alpha 1A subunit gene generates phenotypic variants of P- and Q-type calcium channels. *Nat Neurosci* **2**, 407-415 (1999).

81. Zucker, R.S. & Regehr, W.G. Short-term synaptic plasticity. *Annu Rev Physiol* **64**, 355-405 (2002).

82. Ungerstedt, U. & Arbuthnott, G.W. Quantitative recording of rotational behavior in rats after 6-hydroxy-dopamine lesions of the nigrostriatal dopamine system. *Brain Res* **24**, 485-493 (1970).

83. Schwarting, R.K.W. & Huston, J.P. The unilateral 6-hydroxydopamine lesion model in behavioral brain research. Analysis of functional deficits, recovery and treatments. *Prog Neurobiol* **50**, 275-331 (1996).

84. Da Cunha, C.*, et al.* Hemiparkinsonian rats rotate toward the side with the weaker dopaminergic neurotransmission. *Behav Brain Res* **189**, 364-372 (2008).

85. Deumens, R., Blokland, A. & Prickaerts, J. Modeling Parkinson's disease in rats: an evaluation of 6-OHDA lesions of the nigrostriatal pathway. *Exp Neurol* **175**, 303-317 (2002).

86. Mink, J.W. The Basal Ganglia: Focused selection and inhibition of competing motor programs. *Prog Neurobiol* **50**, 381-425 (1996).

87. Groenewegen, H.J. The basal ganglia and motor control. *Neural Plast* **10**, 107-120 (2003).

88. Takakusaki, K., Saitoh, K., Harada, H. & Kashiwayanagi, M. Role of basal ganglia-brainstem pathways in the control of motor behaviors. *Neurosci Res* **50**, 137-151 (2004).

89. Ibañez-Tallon, I.*, et al.* Tethering naturally occurring peptide toxins for cell-autonomous modulation of ion channels and receptors in vivo. *Neuron* **43**, 305-311 (2004).

90. Miwa, J.M.*, et al.* lynx1, an endogenous toxin-like modulator of nicotinic acetylcholine receptors in the mammalian CNS. *Neuron* **23**, 105-114 (1999).

91. Ibañez-Tallon, I.*, et al.* Novel modulation of neuronal nicotinic acetylcholine receptors by association with the endogenous prototoxin lynx1. *Neuron* **33**, 893-903 (2002).

92. Hruska, M., Ibañez-Tallon, I. & Nishi, R. Cell-autonomous inhibition of alpha 7-containing nicotinic acetylcholine receptors prevents death of parasympathetic neurons during development. *J Neurosci* **27**, 11501-11509 (2007).

93. Wu, Y., Cao, G., Pavlicek, B., Luo, X. & Nitabach, M.N. Phase Coupling of a Circadian Neuropeptide With Rest/Activity Rhythms Detected Using a Membrane-Tethered Spider Toxin. *PLoS biology* **6**, e273 (2008).

94. Holford, M., Auer, S., Laqua, M. & Ibañez-Tallon, I. Manipulating neuronal circuits with endogenous and recombinant cell-surface tethered modulators. *Front Mol Neurosci* **2**, 21 (2009).

95. Hruska, M. & Nishi, R. Cell-autonomous inhibition of alpha 7-containing nicotinic acetylcholine receptors prevents death of parasympathetic neurons during development. *J Neurosci* **27**, 11501-11509 (2007).

96. Dudanova, I.*, et al.* Important Contribution of {alpha}-Neurexins to Ca2+-Triggered Exocytosis of Secretory Granules. *J. Neurosci.* **26**, 10599-10613 (2006).

97. Hillyard, D.R.*, et al.* A new Conus peptide ligand for mammalian presynaptic Ca2+ channels. *Neuron* **9**, 69-77 (1992).

98. Mintz, I.M., Venema, V.J., Adams, M.E. & Bean, B.P. Inhibition of N- and L-type Ca2+ channels by the spider venom toxin omega-Aga-IIIA. *Proc Natl Acad Sci U S A* **88**, 6628-6631 (1991).

99. Cao, Y.-Q.*, et al.* Presynaptic Ca2+ Channels Compete for Channel Type-Preferring Slots in Altered Neurotransmission Arising from Ca2+ Channelopathy. *Neuron* **43**, 387-400 (2004).

100. Cao, Y.Q. & Tsien, R.W. Effects of familial hemiplegic migraine type 1 mutations on neuronal P/Q-type Ca2+ channel activity and inhibitory synaptic transmission. *Proc Natl Acad Sci U S A* **102**, 2590-2595 (2005).

101. Poncer, J.C., McKinney, R.A., Gahwiler, B.H. & Thompson, S.M. Either N- or P-type calcium channels mediate GABA release at distinct hippocampal inhibitory synapses. *Neuron* **18**, 463-472 (1997).

102.   Dobrunz, L.E. & Stevens, C.F. Heterogeneity of release probability, facilitation, and depletion at central synapses. *Neuron* **18**, 995-1008 (1997).

103.   Peitz, M., Pfannkuche, K., Rajewsky, K. & Edenhofer, F. Ability of the hydrophobic FGF and basic TAT peptides to promote cellular uptake of recombinant Cre recombinase: A tool for efficient genetic engineering of mammalian genomes. *Proc Natl Acad Sci U S A* **99**, 4489-4494 (2002).

104.   Pfeifer, A., Brandon, E.P., Kootstra, N., Gage, F.H. & Verma, I.M. Delivery of the Cre recombinase by a self-deleting lentiviral vector: Efficient gene targeting in vivo. *Proc Natl Acad Sci U S A* **98**, 11450-11455 (2001).

105.   Ahn, K., Mishina, Y., Hanks, M.C., Behringer, R.R. & Crenshaw, E.B., 3rd. BMPR-IA signaling is required for the formation of the apical ectodermal ridge and dorsal-ventral patterning of the limb. *Development* **128**, 4449-4461 (2001).

106.   Zucker, R.S. Short-term synaptic plasticity. *Annu Rev Neurosci* **12**, 13-31 (1989).

107.   Wang, L.Y. & Kaczmarek, L.K. High-frequency firing helps replenish the readily releasable pool of synaptic vesicles. *Nature* **394**, 384-388 (1998).

108.   Gingrich, K.J. & Byrne, J.H. Simulation of synaptic depression, posttetanic potentiation, and presynaptic facilitation of synaptic potentials from sensory neurons mediating gill-withdrawal reflex in Aplysia. *J Neurophysiol* **53**, 652-669 (1985).

109.   Forsythe, I.D. & Clements, J.D. Presynaptic glutamate receptors depress excitatory monosynaptic transmission between mouse hippocampal neurones. *J Physiol* **429**, 1-16 (1990).

110.   Neher, E. & Sakaba, T. Combining deconvolution and noise analysis for the estimation of transmitter release rates at the calyx of held. *J Neurosci* **21**, 444-461 (2001).

111.   Minami, K.*, et al.* Role of Thr(11) in the binding of omega-conotoxin MVIIC to N-type Ca2+ channels. *FEBS Lett* **491**, 127-130 (2001).

112.   Sato, K.*, et al.* Binding of chimeric analogs of omega-conotoxin MVIIA and MVIIC to the N- and P/Q-type calcium channels. *FEBS Lett* **414**, 480-484 (1997).

113.   Sato, K.*, et al.* Binding of six chimeric analogs of omega-conotoxin MVIIA and MVIIC to N- and P/Q-type calcium channels. *Biochem Biophys Res Commun* **269**, 254-256 (2000).

114.   Okada, M.*, et al.* Effects of Ca2+ channel antagonists on striatal dopamine and DOPA release, studied by in vivo microdialysis. *Br J Pharmacol* **123**, 805-814 (1998).

115.   Gancher, S., Mayer, A. & Youngman, S. Changes in apomorphine pharmacodynamics following repeated treatment in 6-hydroxydopamine-lesioned rats. *Brain Res* **729**, 190-196 (1996).

116.   Haubrich, C.*, et al.* N-type calcium channel blockers -- tools for modulation of cerebral functional units? *Brain Res* **855**, 225-234 (2000).

117.   Chang, C.C. Looking back on the discovery of alpha-bungarotoxin. *J Biomed Sci* **6**, 368-375 (1999).

118.   Inchauspe, C.G., Martini, F.J., Forsythe, I.D. & Uchitel, O.D. Functional Compensation of P/Q by N-Type Channels Blocks Short-Term Plasticity at the Calyx of Held Presynaptic Terminal. *J. Neurosci.* **24**, 10379-10383 (2004).

119.   Szabo, Z., Obermair, G.J., Cooper, C.B., Zamponi, G.W. & Flucher, B.E. Role of the synprint site in presynaptic targeting of the calcium channel Cav2.2 in hippocampal neurons. *Eur J Neurosci* **24**, 709-718 (2006).

120.   Todorov, B.*, et al.* Conditional inactivation of the Cacna1a gene in transgenic mice. *Genesis* **44**, 589-594 (2006).

121.   Jeng, C.J., Sun, M.C., Chen, Y.W. & Tang, C.Y. Dominant-negative effects of episodic ataxia type 2 mutations involve disruption of membrane trafficking of human P/Q-type Ca2+ channels. *J Cell Physiol* **214**, 422-433 (2008).

122. Hannon, G.J. RNA interference. *Nature* **418**, 244-251 (2002).
123. Mello, C.C. & Conte, D., Jr. Revealing the world of RNA interference. *Nature* **431**, 338-342 (2004).
124. Jackson, A.L.*, et al.* Expression profiling reveals off-target gene regulation by RNAi. *Nat Biotechnol* **21**, 635-637 (2003).
125. Sledz, C.A., Holko, M., de Veer, M.J., Silverman, R.H. & Williams, B.R. Activation of the interferon system by short-interfering RNAs. *Nat Cell Biol* **5**, 834-839 (2003).
126. Bridge, A.J., Pebernard, S., Ducraux, A., Nicoulaz, A.L. & Iggo, R. Induction of an interferon response by RNAi vectors in mammalian cells. *Nat Genet* **34**, 263-264 (2003).
127. Airan, R.D.*, et al.* Integration of light-controlled neuronal firing and fast circuit imaging. *Curr Opin Neurobiol* **17**, 587-592 (2007).
128. Lechner, H.A., Lein, E.S. & Callaway, E.M. A genetic method for selective and quickly reversible silencing of Mammalian neurons. *J Neurosci* **22**, 5287-5290 (2002).
129. Lerchner, W.*, et al.* Reversible silencing of neuronal excitability in behaving mice by a genetically targeted, ivermectin-gated Cl- channel. *Neuron* **54**, 35-49 (2007).
130. George, A.L. Inherited disorders of voltage-gated sodium channels. *J Clin Invest* **115**, 1990-1999 (2005).
131. Auer, S.*, et al.* Silencing neurotransmission with membrane-tethered toxins. *Nat Methods* (2010).
132. Ophoff, R.A.*, et al.* Familial hemiplegic migraine and episodic ataxia type-2 are caused by mutations in the Ca2+ channel gene CACNL1A4. *Cell* **87**, 543-552 (1996).
133. Tottene, A.*, et al.* Enhanced excitatory transmission at cortical synapses as the basis for facilitated spreading depression in Ca(v)2.1 knockin migraine mice. *Neuron* **61**, 762-773 (2009).
134. Steinlein, O.K.*, et al.* A missense mutation in the neuronal nicotinic acetylcholine receptor alpha 4 subunit is associated with autosomal dominant nocturnal frontal lobe epilepsy. *Nat Genet* **11**, 201-203 (1995).
135. Klaassen, A.*, et al.* Seizures and enhanced cortical GABAergic inhibition in two mouse models of human autosomal dominant nocturnal frontal lobe epilepsy. *Proc Natl Acad Sci U S A* **103**, 19152-19157 (2006).
136. Green, B.D. & Flatt, P.R. Incretin hormone mimetics and analogues in diabetes therapeutics. *Best Prac Res Cl En* **21**, 497-516 (2007).
137. Hoare, S.R.J. Mechanisms of peptide and nonpeptide ligand binding to Class B G-protein-coupled receptors. *Drug Discov Today* **10**, 417-427 (2005).
138. Shioda, S.*, et al.* Neural networks of several novel neuropeptides involved in feeding regulation. *Nutrition* **24**, 848-853 (2008).
139. Marris, E. Marine natural products: drugs from the deep. *Nature* **443**, 904-905 (2006).
140. Munson, M.C. & Barany, G. Synthesis of .alpha.-conotoxin SI, a bicyclic tridecapeptide amide with two disulfide bridges: illustration of novel protection schemes and oxidation strategies. *J Am Chem Soc* **115**, 10203-10210 (1993).
141. Cuthbertson, A. & Indrevoll, B.r. A method for the one-pot regioselective formation of the two disulfide bonds of [alpha]-conotoxin SI. *Tetrahedron Lett* **41**, 3661-3663 (2000).
142. Walewska, A.*, et al.* Integrated oxidative folding of cysteine/selenocysteine containing peptides: improving chemical synthesis of conotoxins. *Angew Chem Int Edit* **48**, 2221-2224 (2009).
143. Ueberheide, B.M., Fenyö, D., Alewood, P.F. & Chait, B.T. Rapid sensitive analysis of cysteine rich peptide venom components. *Proc Natl Acad Sci U S A* **106**, 6910-6915 (2009).

144. Fortin, J.-P.*, et al.* Membrane-tethered ligands are effective probes for exploring class B1 G protein-coupled receptor function. *Proc Natl Acad Sci U S A* **106**, 8049-8054 (2009).

145. Torres, V.E. & Harris, P.C. Autosomal dominant polycystic kidney disease: the last 3 years. *Kidney Int* **76**, 149-168 (2009).